NASA CONTRACTOR REPORT

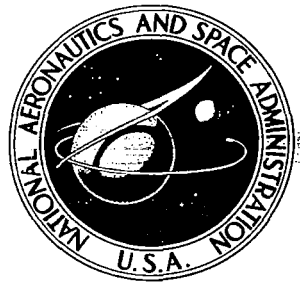

NASA CR-2019

PILOT DYNAMICS FOR INSTRUMENT APPROACH TASKS: FULL PANEL MULTILOOP AND FLIGHT DIRECTOR OPERATIONS

by David H. Weir and Duane T. McRuer

Prepared by
SYSTEMS TECHNOLOGY, INC.
Hawthorne, Calif.
for Ames Research Center

NATIONAL AERONAUTICS AND SPACE ADMINISTRATION • WASHINGTON, D. C. • MAY 1972

1. Report No.	2. Government Accession No.	3. Recipie
NASA CR-2019		

4. Title and Subtitle	5. Report Date
Pilot Dynamics for Instrument Approach Tasks: Full Panel Multiloop and Flight Director Operations	May 1972
	6. Performing Organization Code

7. Author(s)	8. Performing Organization Report No.
David H. Weir and Duane T. McRuer	
	10. Work Unit No.

9. Performing Organization Name and Address	11. Contract or Grant No.
Systems Technology, Inc. Hawthorne, California	NAS 2-5690
	13. Type of Report and Period Covered
12. Sponsoring Agency Name and Address	Contractor Report
National Aeronautics & Space Administration Washington, D.C.	14. Sponsoring Agency Code

15. Supplementary Notes

16. Abstract

Measurements and interpretations of single and multiloop pilot response properties during simulated instrument approach are presented. Pilot subjects flew Category II-like ILS approaches in a fixed base DC-8 simulator at the Ames Research Center. A conventional instrument panel and controls were used, with simulated vertical gust and glide slope beam bend forcing functions. Reduced and interpreted pilot describing functions and remnant are given for pitch attitude, flight director, and multiloop (longitudinal) control tasks. The response data are correlated with simultaneously recorded eye scanning statistics, previously reported in NASA CR-1535. The resulting combined response and scanning data and their interpretations provide a basis for validating and extending the theory of manual control displays.

17. Key Words (Suggested by Author(s))	18. Distribution Statement
Pilot Dynamics Instrument Approach Flight Directors Manual Control Displays	UNCLASSIFIED-UNLIMITED

19. Security Classif. (of this report)	20. Security Classif. (of this page)	21. No. of Pages	22. Price*
UNCLASSIFIED	UNCLASSIFIED	106	3.00

*For sale by the National Technical Information Service, Springfield, Virginia 22151

1. Instrument landing systems
2. Display systems
3. Flight simulation
4. Landing simulation

FOREWORD

This report summarizes experimental research accomplished as one part of an overall program arrived at developing models and methods for the analysis and design of manual control displays. It presents the results of the second phase of a two phase effort to measure and correlate pilot control actions and eye movements during instrument approach tasks. The first phase results comprising the eye scanning data were published in NASA CR-1535.

This research was conducted for the Man-Machine Integration Branch of the NASA Ames Research Center under Contract NAS2-5690. The NASA project monitors were M. Sadoff and W. D. Chase. The STI Technical Director was D. T. McRuer and the Project Engineer was D. H. Weir.

The authors acknowledge the fine and careful work of R. H. Klein in executing much of the experimental operation. In addition, the authors would like to thank Messrs. H. R. Jex, W. F. Clement, and R. E. Magdaleno of STI for their helpful comments through the course of this program. The project was materially aided by the interest and cooperation of the pilot subjects. Finally, the care and diligence of the STI Production Staff in preparing the final report draft is gratefully acknowledged.

ABSTRACT

Measurements and interpretations of single and multiloop pilot response properties during simulated instrument approach are presented. Pilot subjects flew Category II-like ILS approaches in a fixed base DC-8 simulator at the Ames Research Center. A conventional instrument panel and controls were used, with simulated vertical gust and glide slope beam bend forcing functions. Reduced and interpreted pilot describing functions and remnant are given for pitch attitude, flight director, and multiloop (longitudinal) control tasks. The response data are correlated with simultaneously recorded eye scanning statistics, previously reported in NASA CR-1535. The resulting combined response and scanning data and their interpretations provide a basis for validating and extending the theory of manual control displays.

CONTENTS

FIGURES

TABLES

SECTION I

INTRODUCTION

A. OBJECTIVES

During the past few years several interrelated research programs have been directed toward developing a theory of manual control displays useful in the analysis and design of pilot/vehicle dynamic control systems. This theory combines servoanalysis techniques, multiloop pilot response models, and scanning and sampling perceptual models, as evolved and described in Refs. 1-5.

Further development and validation of this manual control display theory required measurement and interpretation of simultaneous eye movement and pilot response data in flight control tasks under realistic instrument conditions. The overall objective of the program of which this report is a part was to accomplish this measurement and interpretation effort for a range of pilot subjects and instrument approach tasks.

This report presents the reduced single and multiloop pilot response data. A previous phase of the program produced a companion report (Ref. 6) which details the reduced eye scanning traffic and statistics. A third result of this most recent program was the preparation of an archival digital Master Data Tape which contains the basic pilot response and eye movement data for the 31 experimental runs analyzed. Described in Ref. 7, this Master Data Tape is available to other research organizations for analyses, modelling, and data interpretation activities.

The specific objectives of the phase of the study reported herein were to:

- Select a representative set of single and multiloop data runs for analysis and interpretation
- Compute pilot describing functions
- Compute remnant spectra and linear correlations
- Compute performance measures and statistical distributions of the response variables

- Analyze, interpret, and model the pilot response data
- Correlate pilot response properties with the corresponding scanning traffic

The result is a new base of reduced and interpreted data, suitable for validating and extending the overall manual control display theory.

B. PREVIEW OF THE REPORT

This report emphasizes the experimental results and their analysis. Accordingly, Sections II and III begin with the pilot describing function measurements and interpretations. Section II includes data for two single loop tasks: pitch attitude control with a single instrument and flight director control with a conventional instrument approach panel layout. The multiloop data in Section III are for longitudinal-only (with lateral autopilot) and all-axis glide slope beam following tasks; with response measurements made in the longitudinal pilot/vehicle control loops. In Sections II and III the response data are modelled and interpreted both as pilot-alone describing functions, and as combined pilot/vehicle describing functions from a crossover model viewpoint.

The single and multiloop pilot remnant spectra are given in Section IV. Normalized open-loop and closed-loop forms are available for the single loop tasks. Closed-loop remnant spectra are given for the multiloop control configurations.

The connections between the response data in this report and the eye scanning results from Ref. 6 are given in Section V. This includes correlation of scanning properties and both crossover frequency and remnant levels.

The conclusions and interpretations are drawn together in Section VI.

Details of the experiments, the basic data, and the data reduction procedures are provided in the appendices. Appendix A describes those features of the simulator and experimental task variables which are pertinent to dynamic response data interpretation. Other details related mainly to the eye scanning traffic are provided in Ref. 6, and they have not been repeated here.

SECTION II

SINGLE LOOP RESPONSE DATA

Single loop pilot/vehicle control implies the presence of only one feedback cue to which the pilot responds. Two such tasks were used in these experiments. Configuration A involved pitch attitude control with a single, artificial horizon-type attitude instrument on the panel. Configuration E was a longitudinal flight director control task, with the instrument mounted as part of a conventional instrument approach panel layout. The more complete flight director task, plus the other instruments, resulted in some status scanning. The dynamic response data for these two tasks are presented and interpreted in this section.

A. PITCH ATTITUDE CONTROL

The pilot/vehicle system model for quasilinear describing function data reduction and interpretation is shown in Fig. 1. The controlled

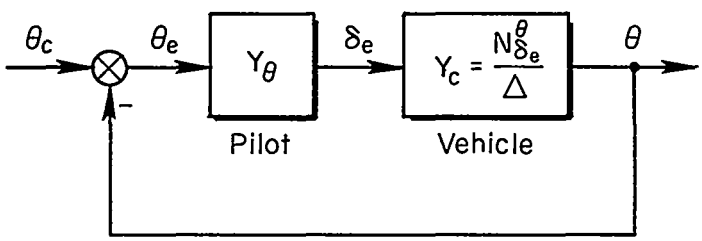

Figure 1. Pitch Attitude Control Task, Configuration A

element dynamics corresponded to a DC-8 in landing approach configuration. The simulated vehicle pitch response was subtracted from the random-appearing forcing function (θ_c) to obtain the pitch attitude error (θ_e) displayed on the attitude instrument. The experimental subjects were current, experienced airline pilots. A detailed description of the simulation and the task variables is given in Appendix A.

The system response variables were Fourier analyzed, and the values at the forcing function component frequencies were used to form spectral ratios. These spectral ratios were combined to obtain the pilot describing function (Y_θ)

at the forcing function frequencies, as described in Appendix B. All the resulting data points were used in the single loop data interpretation, because the points at forcing function frequencies had amplitudes which were well above the surrounding pilot remnant levels in the response power spectral densities. This was not always the case in the multiloop data, shown subsequently.

The open loop pilot/vehicle system describing function data are given in Fig. 2. These points were obtained directly from the following ratio of spectral ratios:

$$Y_\theta Y_c = Y_{OL} = \frac{\theta/\theta_c}{\theta_e/\theta_c} \tag{1}$$

The amplitude ratio data show the 20 dB/decade slope characteristic of the crossover model (Ref. 6), with crossover frequencies of about 0.37 and 0.9 rad/sec for Pilots 1 and 2. The phase margins are relatively large at 85 and 74 deg, respectively. The phase data show a corresponding integration plus effective pure time delay ($e^{-\tau_\theta j\omega}$) form. The time delay in the Y_{OL} data of Fig. 2 includes some lag contributions from the controlled element (Y_c), consisting of both the display and simulated vehicle dynamics. The display lag ($\tau_{D\theta}$) is about 0.1 sec, as shown in Appendix A.

The pilot-alone describing functions were computed using the spectral ratio expression

$$Y_\theta = \frac{\delta_e/\theta_c}{\theta_e/\theta_c} \tag{2}$$

The data are plotted in Fig. 3. The data for the two pilots differ primarily in gain, and the results for each pilot were fitted with the following form

$$Y_\theta = \frac{K_\theta(T_L j\omega + 1)}{(T_I j\omega + 1)} e^{-\tau_\theta j\omega} \tag{3}$$

The fits are shown on Fig. 3. The lead equalization (T_L) occurs at about the short period frequency in both cases. The lags (T_I) differ slightly, but not significantly. The phase data show a little variation about the nominal time delay (τ_θ) of 0.53 sec. This time delay includes the instrument lag increment

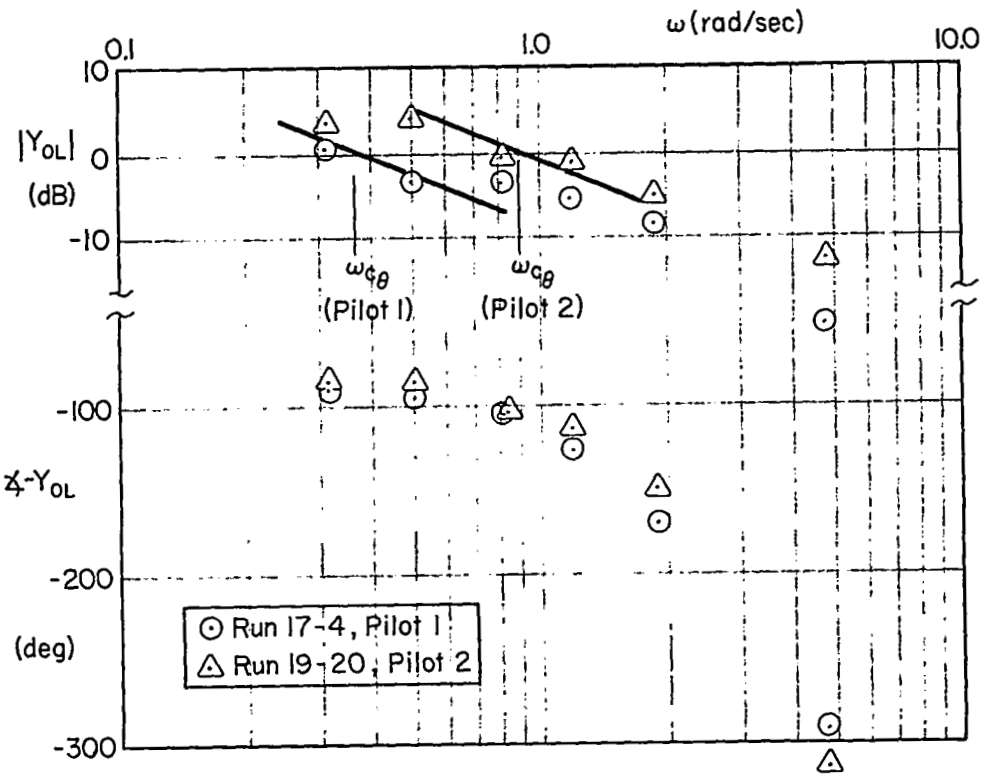

Figure 2. Open-Loop Pilot-Vehicle Describing Functions for Pitch Attitude Control

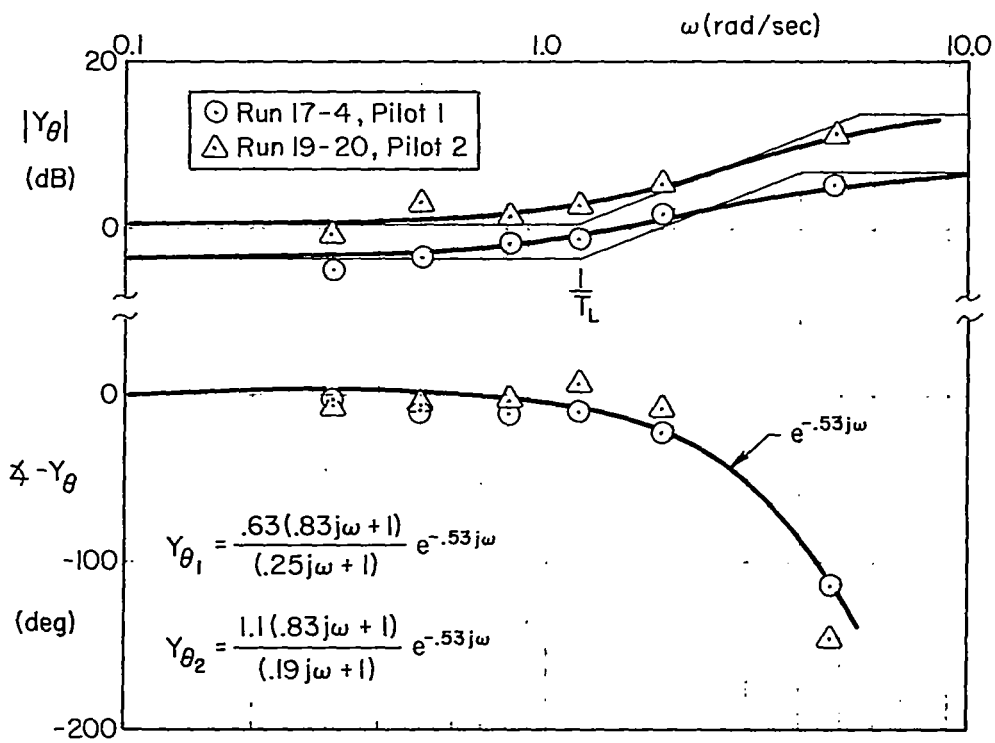

Figure 3. Pilot Describing Functions
for Pitch Attitude Control

of about 0.1 sec, and the residual (0.43 sec) is probably somewhat larger than for simple manipulators due to the dynamics of the transport-type control column. The Y_θ phase data show no low frequency phase lag (α effect) within* the measurement bandwidth.

B. FLIGHT DIRECTOR CONTROL

The pilot/vehicle system model for describing function measurements in the flight director task is given in Fig. 4. The computer equations, f(s),

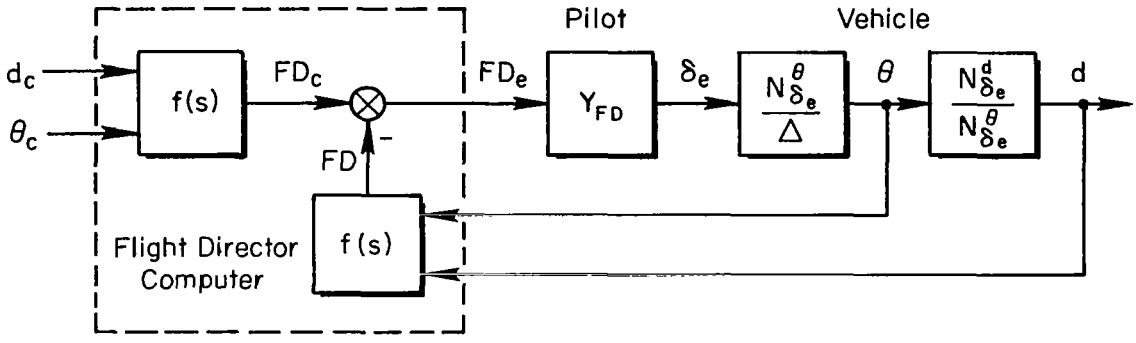

Figure 4. Flight Director Control Task, Configuration E

and resulting controlled element dynamics for the flight director (FD_e/δ_e) are given in Appendix A. Although the display gain was higher, they are quite similar in form to the dynamics of the pitch attitude control task in the mid-frequency region. The primary pilot stimulus is the displayed error (FD_e), which is the net effect of system response to both the beam deviation (d_c) and pitch attitude (θ_c) forcing functions. The other panel instruments provided response variable status information, but they were not essential to vehicle control. A more detailed description of the simulation and task variables for this experimental configuration is given in Appendix A.

---

*The so-called α effect is a low-frequency phase lag observed within the measurement bandwidth, but associated with leads and lags below measurement frequencies. As seen within the measurement frequency ranges this low-frequency phase is given approximately by α/ω, where $\alpha = \sum_i (1/T_{lag} - 1/T_{lead})_i$, where the $1/T_{lag_i}$ and $1/T_{lead_i}$ are the lags and leads less than the lowest frequency. See Ref. 12, p. 152.

Spectral ratios were computed (as described in Appendix B) to obtain the pilot describing function (Y_{FD}) and the open loop pilot/vehicle describing function ($Y_{OL} = Y_{FD} \cdot FD/\delta_e$). The response data points at both sets of input frequencies were all of good quality (correlated signal large relative to the remnant) and they were all used in the data interpretation.

The open loop pilot vehicle describing function data are given in Fig. 5. The two runs for each pilot were lumped, because the scanning and response data showed no significant differences between runs. The points were obtained directly from the spectral ratio expression

$$Y_{OL} = Y_{FD}Y_c = \frac{FD/FD_c}{FD_e/FD_c} \tag{4}$$

The amplitude ratio and phase data for Pilot 1 show little scatter, and the crossover frequency is 0.8 rad/sec with about 55 deg phase margin. The Pilot 2 data show considerable mid-frequency scatter (compared to the pitch attitude task) with a 1.2 rad/sec crossover frequency and about 45 deg phase margin. As will be shown, the mid-frequency scatter is even greater in the Pilot 2 multiloop data, and may correlate with an increase in scanning for this particular subject. Note that the phase scatter corresponds roughly to a higher order mid-frequency lead which would improve response and performance. A flight director display lag ($\tau_{D_{FD}}$) of about 0.1 sec has not been removed from the phase data.

The pilot-alone describing functions were computed as:

$$Y_{FD} = \frac{\delta_e/FD_c}{FD_e/FD_c}$$

The data are shown in Fig. 6 for Pilots 1 and 2. The data were fit with the form of Eq. 3, and the results are shown on the figures. The Pilot 2 data indicate a lower frequency lead than Pilot 1. The time delays (τ_{FD}) are about the same for both pilots, and Pilot 2 has more scatter as noted above. Both pilots show a phase lag in the lowest frequency data point. This point is below the measurement bandwidth, so it is not necessarily attributable to task differences. The data also show more mid-frequency phase lag than for pitch attitude control, and this may correlate with the increased scanning. The phase data include the 0.1 sec display lag.

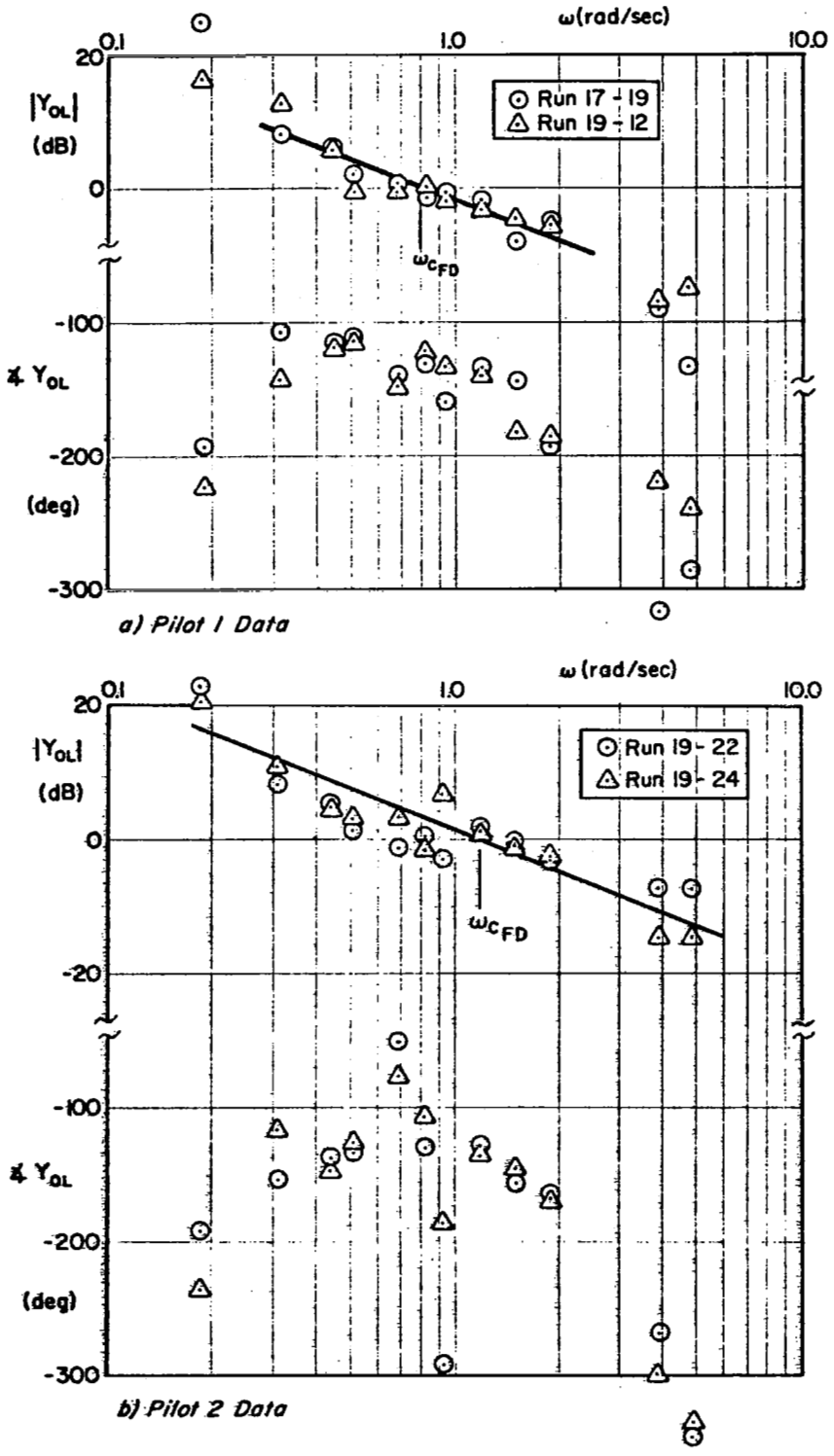

Figure 5. Open-Loop Pilot-Vehicle Describing Function for Flight Director Control

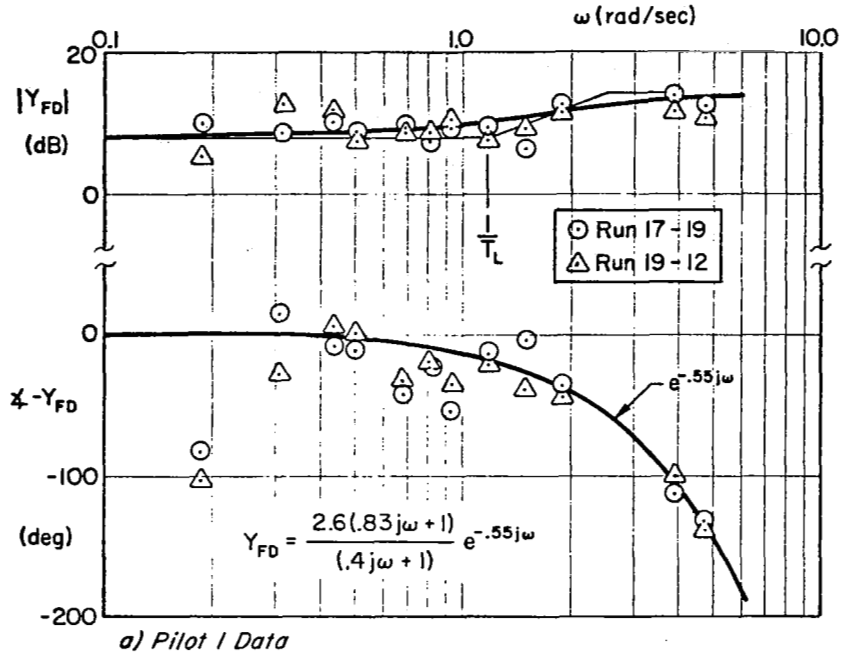

a) Pilot 1 Data

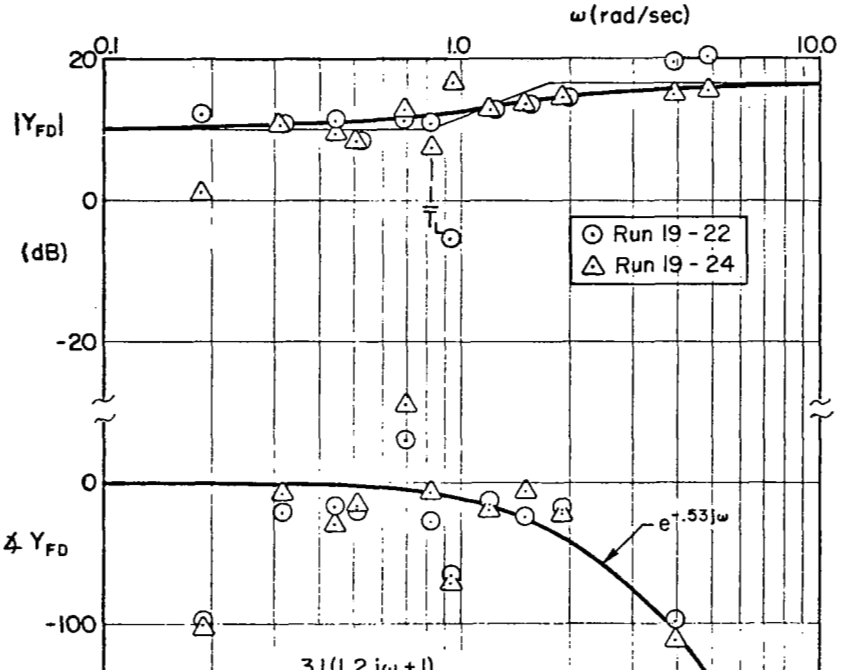

b) Pilot 2 Data

Figure 6. Pilot Describing Function for Flight Director Control

C. CORRELATION WITH PRIOR RESULTS

The single loop data can be compared with a large body of prior results. In general, both the pitch attitude and flight director response data have the simple well established crossover model form which would be expected for the tasks and controlled elements used. The pilot time delays are also consistent with prior measurements, when lag contributions due to display and manipulator dynamics are removed. However, the crossover frequencies in the present data are somewhat lower (and the stability margins are higher) than those typically reported in single axis control tasks which involve a minimum-error form of performance criterion. This difference is probably due to the following features in the experiments reported here:

- Transport-type, landing approach control task, which emphasizes performance criteria in addition to minimum error
- Airline pilot subjects, who were instructed to behave in their "normal" way for the task presented
- Realistic, low frequency forcing functions, which avoided an unusually "busy" appearance in the panel instrument displays.

The lower crossover frequencies observed, suggest that reduced performance levels should be used in manual control response estimates involving airline pilot subjects in transport tasks.

One prior study is of particular importance by way of comparison; Ref. 8, which was reported as NASA CR-1238 (hereinafter referred to as the "1238 study"). These 1238 study experiments involved a similar set of single loop and multiloop response measurements and interpretations. Pilot subjects were used, but the task definition and control criteria were oriented more towards maximum performance.

The open loop pilot/vehicle response data for the single loop pitch attitude control task in the 1238 study are shown in Fig. 7. The data for each pilot represent the average of 6 runs, and there was relatively little inter-run variability (except in the low frequency phase point). The data have the characteristic crossover model form, with crossover frequencies of 2.37 and 2.7 rad/sec and relatively small stability margins. The lowest

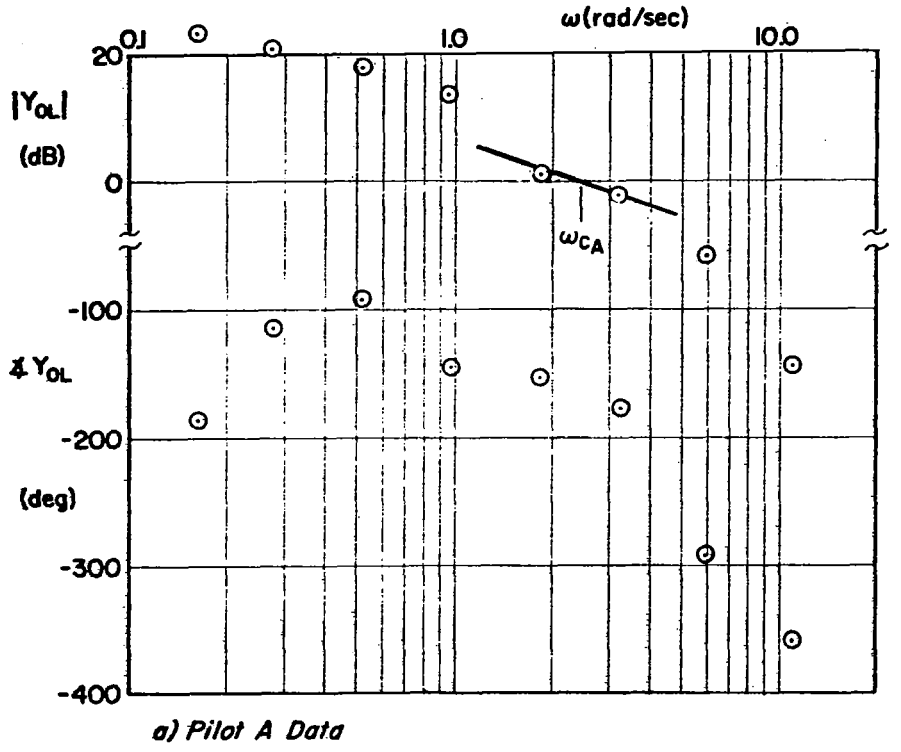

a) Pilot A Data

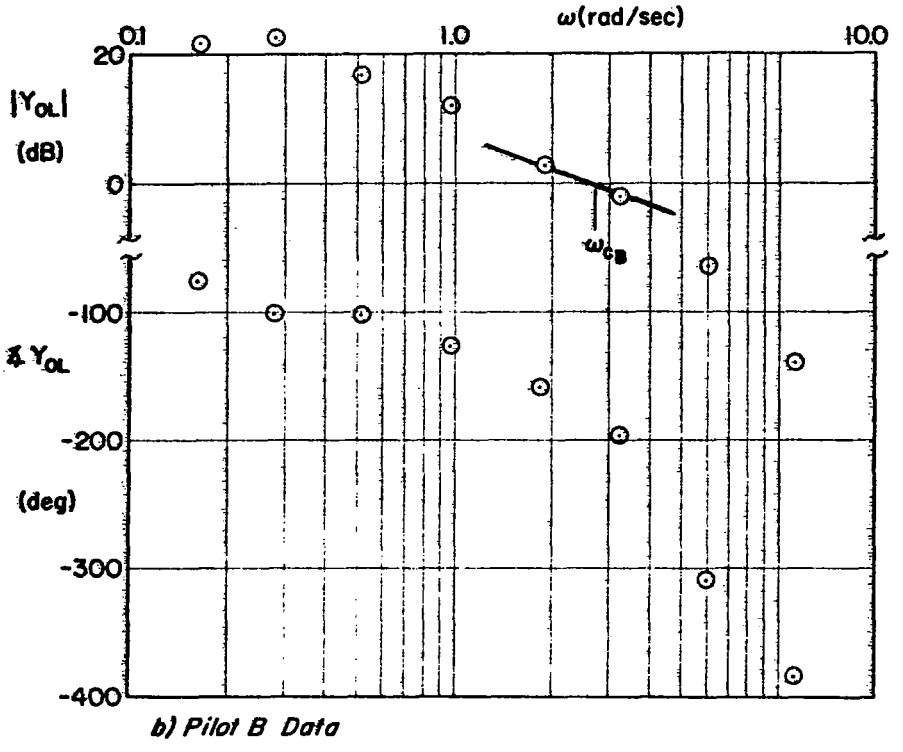

b) Pilot B Data

Figure 7. Pilot-Vehicle Describing Functions, 1238 Study

frequency data point shows some α-effect, as did the flight director results. The time delay (τ_θ) in the 1238 results is about 0.34 sec, compared to 0.43 sec observed in the new data (with instrument lag removed). The differences between the two sets of pitch attitude data may reflect largely a difference in controlled element dynamics. The two $\theta \rightarrow \delta_e$ transfer functions are compared in Fig. 8. The 1238 study used a one degree of freedom short period approximation, with natural frequency of 0.76 rad/sec and damping ratio of 0.39, while the present study had a better damped short period at about 1.2 rad/sec. The resulting mid-frequency amplitude ratio and phase lag are seen to be somewhat larger in the former case. This could account for the differences in crossover frequency and time delay.

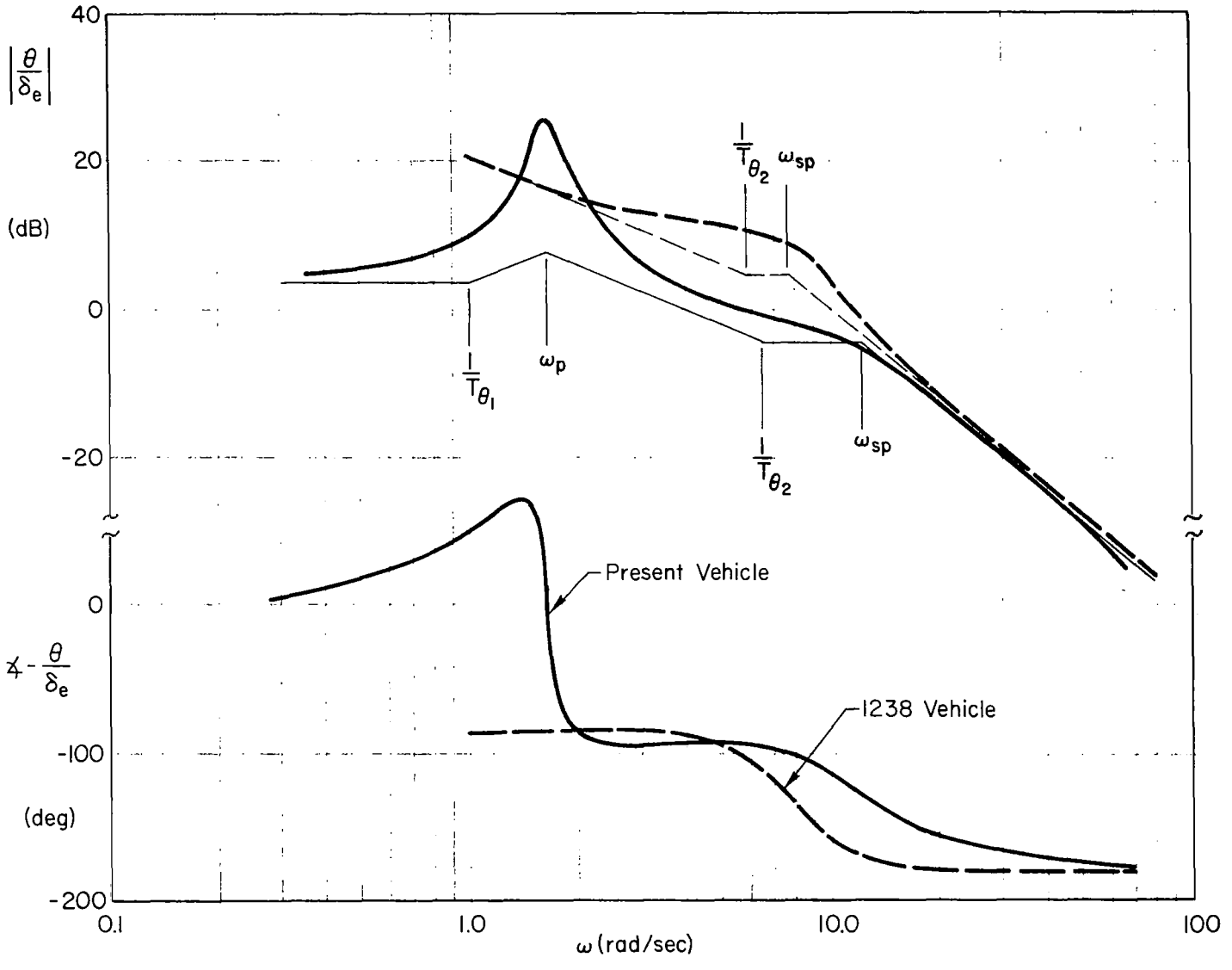

Figure 8. Comparison of Pitch Attitude to Elevator Frequency Response

SECTION III

MULTILOOP RESPONSE DATA

Multiloop pilot/vehicle control involves more than one feedback cue to the pilot, to which he responds by manipulating one or more control variables. Two multiloop tasks were used in these experiments. Configuration B involved a longitudinal-only (split axis) landing approach task; with full instrument panel, primary feedbacks of pitch attitude and glide slope beam deviation, and pilot elevator control. The lateral axes were under the control of an autopilot. The all-axis multiloop task (Configuration C) comprised primarily the same longitudinal control task as B, except that lateral vehicle motions were under human pilot control, also. Both tasks required instrument scanning. Detailed descriptions of the tasks are given in Appendix A.

The human pilot dynamic response data for these two tasks are developed, presented, and interpreted in this section. By way of development, the section begins with a summary of the guidance and control requirements on the pilot/vehicle system for either task. This is followed with a description of a longitudinal "analog" pilot, which summarizes the pre-experimental response analysis and provides one basis for data interpretation. The balance of the section concentrates on the dynamic response data for two of the pilot subjects.

A. PILOT/VEHICLE SYSTEM PROPERTIES

To accomplish the landing approach task, the pilot must provide a multiloop control structure which satisfies the guidance and control requirements. These are to establish the aircraft on the glide path, and reduce any path errors to zero in a stable, well-damped and rapid manner. In addition the skilled pilot will adopt a structure and equalization for minimum pilot effort and acceptable control "quality." This means that he will seek loop closures which require no low frequency lead equalization, and which permit a wide range of pilot gains while retaining acceptable response and performance properties. This provides for minimum pilot latency, for inattentive operation, and for maximum flexibility in gain adjustment.

To satisfy these requirements, longitudinal control in landing approach involves feedbacks of functions of pitch attitude and glide slope beam deviation (loosely equivalent to altitude). A suitable system block diagram in "series" form is shown in Fig. 9. Only pitch attitude (θ) and beam

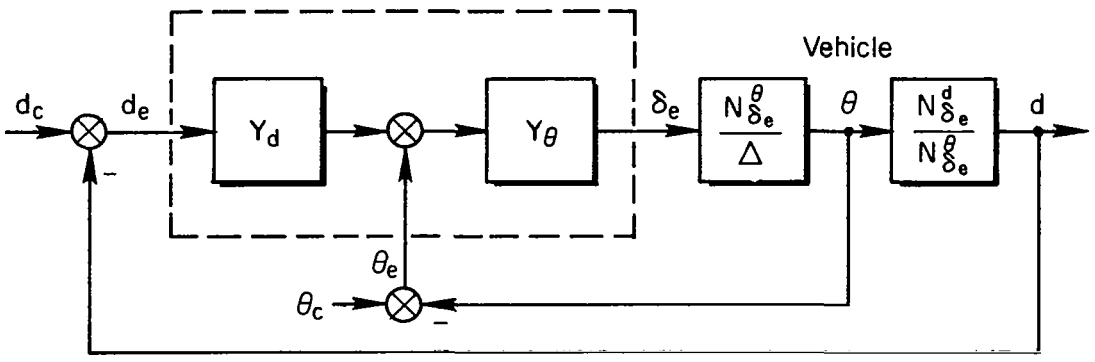

Figure 9. Multiloop System for Data Interpretation

deviation (d) feedbacks are shown, and "computation" of other functions of these variables (if needed) is implicit in the pilot describing functions Y_θ and Y_d. The series structure of Fig. 9, with Y_d providing a bias to the inner loop feedback, is only one of several alternative forms. It was selected for modelling simplicity and because there is evidence for its validity in the 1238 study (Ref. 8)*. The present data will be shown to confirm this.

B. LONGITUDINAL ANALOG PILOT

Pre-experimental estimates of pilot/vehicle response and performance were made using the series structure of Fig. 9, and the modelling rules and data available at that time. For the simulated DC-8 approach task, a simple gain plus time delay for Y_θ and a gain for Y_d were found to satisfy the guidance and control requirements and pilot-centered considerations outlined above.

*In principle either a "series" or "parallel" form is equally applicable to "explain" the data. The two forms are compared, and some of the advantages for series operation are given on p. 6 of Ref. 8.

Details of these analytical estimates and the multiloop closures are given in Appendix B. The resulting multiloop spectral ratio predictions were useful in human pilot data interpretation. The analytical model was mechanized on the simulation as an analog pilot, and the responses were recorded for a 100 sec analog pilot run. These "data" were reduced to check simulator operation and to calibrate residual error levels in the data (as shown in Appendices A and B). The analog pilot was used on-line in parallel with the human pilot to monitor performance.

C. APPROACH TO THE MULTILOOP DATA INTERPRETATION

The multiloop pilot and pilot/vehicle describing functions are derived from combinations of spectral ratios. This derivation involves selection, smoothing, interpolation, and extrapolation of the data by the analyst to obtain a compatible set of open and closed loop results for the 100 sec data runs. Unlike the simpler single loop case, the process is not determined solely by the data and there is not a unique result. The detailed spectral ratios have been included in Appendix C to illustrate the procedure and assumptions used, and to provide the starting point for possible alternate interpretations by the interested reader.

Two levels of describing function are used: pilot-alone (Y_θ and Y_q) and pilot/vehicle open-loop (Y_{OL}) estimates for the pilot times the effective controlled element. The pilot-alone describing functions involve simple model form fits and interpretations of the data. They are adjusted iteratively in some cases to bring the response resulting from successive loop closures of the open-loop model fits into correspondence with closed loop spectral ratios obtained from the data. Hence they are an interpretation of the data which emphasizes this feature. The crossover model interpretations consider the open inner and outer loop data, and attempt to achieve the best fit to the data in the region of crossover, with little emphasis on other frequency ranges of interest. Hence, there are some minor differences in the ultimate results about crossover and some differences in other frequency regions which are not "explained" by the crossover model.

The describing function data show some variability about simple model forms. This is handled for the pilot-alone describing functions by making

the open and closed-loop fits compatible with the open and closed-loop data, as noted above. For the combined pilot/vehicle data, when the best "fit" differs from the response data points near crossover, the latter are used in determining the response properties and stability margins.

Not all response data points are of good signal to noise quality. The data were screened by examining the $\Phi_{\delta_e\delta_e}$ detailed spectra and observing the amplitudes of the components at input frequencies relative to the surrounding remnant. If a component at an input frequency was at or above the remnant level, the point was considered in the spectral ratio considerations. If below the adjacent remnant, it was neglected. Points with higher signal to noise were given more weight in subsequent extrapolations and interpretations.

From the available data, results for two pilots were selected for detailed analysis based on: completeness, quality of the scanning and response data, pilot performance, and overall judgment by the experimenter/analysts. Both pilots evidenced a high degree of motivation toward performing the task in accordance with the experimental instructions. Yet the data subsequently will show that they used different response strategies; the control output of one pilot was predominantly a function of pitch angle, θ, whereas the other pilot tended to emphasize the d loop. As a result, different combinations of spectral ratios are used to estimate the inner loop describing functions. The ones used in each case are those that are dominated by the corresponding spectral ratio emphasized by that pilot. Similarly, the spectral ratios for the respective dominant loop are matched and interpreted more accurately in obtaining the describing functions.

As a final prefatory note, all the phase data in this section include the lag due to the respective panel instrument dynamics (see Appendix A).

D. LONGITUDINAL-ONLY CONTROL

One 100 sec run has been analyzed for each of the pilots in the longitudinal-only (Configuration B) task. The basic spectral ratio data are given in Appendix C.

1. Crossover Model Interpretation

Using the method summarized in Appendix B, the inner loop pilot describing function for Pilot 1 is:

$$Y_{\theta_1} = \frac{N_1}{D_2} = \frac{\delta_e/\theta_c}{d_e/d_c - \theta/\theta_c} \tag{5}$$

and for Pilot 2

$$Y_{\theta_2} = \frac{N_1}{D_1} = \frac{\delta_e/\theta_c}{\theta_e/\theta_c - d/d_c} \tag{6}$$

These were combined with the controlled element dynamics ($N^{\theta}_{\delta_e}/\Delta$) to obtain the open inner loop pilot/vehicle describing functions shown in Fig. 10.

The crossover model offers, at best, only a very poor description of the inner loop data. But, when forcibly fitted, the Pilot 1 crossover frequency is at 0.3 to 0.35 rad/sec. The steeper than 20 dB/decade amplitude ratio slope near crossover is partly due to the phugoid peak. The phase data are close to an effective time delay (τ_{θ_e}) of 1 sec, except for the low frequency lag. This low frequency phase point reduces the phase margin from 80° to 30° and implies a conditionally stable closure.

The Pilot 2 amplitude ratio (Fig. 10b) are not close to a 20 dB/decade slope, because of the mid-frequency peak. The crossover frequency occurs near 1 rad/sec with about 30 deg phase margin. The phase data are variable, yet unconventional; showing a mid-frequency dip which causes a conditionally stable system, and low frequency points which have been interpreted as a large lead. This lead is roughly compatible with the amplitude ratio peaking and it may suggest a higher order mid-frequency washout for Pilot 2. The phase point near crossover suggests an effective time delay of 1 sec.

The open outer loop pilot/vehicle describing function points were obtained directly from the cross spectral ratios

$$Y_{OL} = \frac{d/d_c}{d_e/d_c} \tag{7}$$

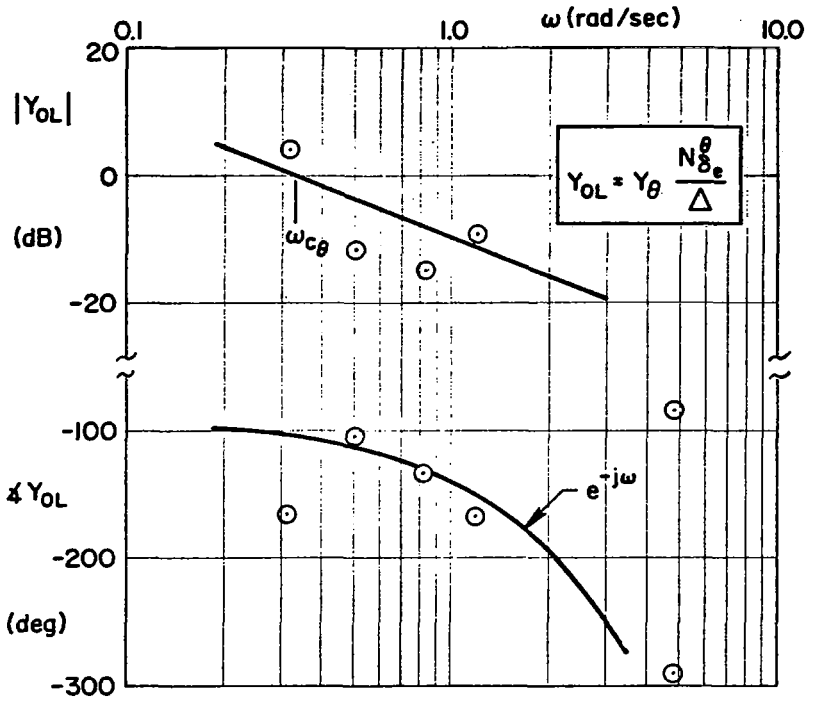

a) Pilot 1 Data, Run 19-5

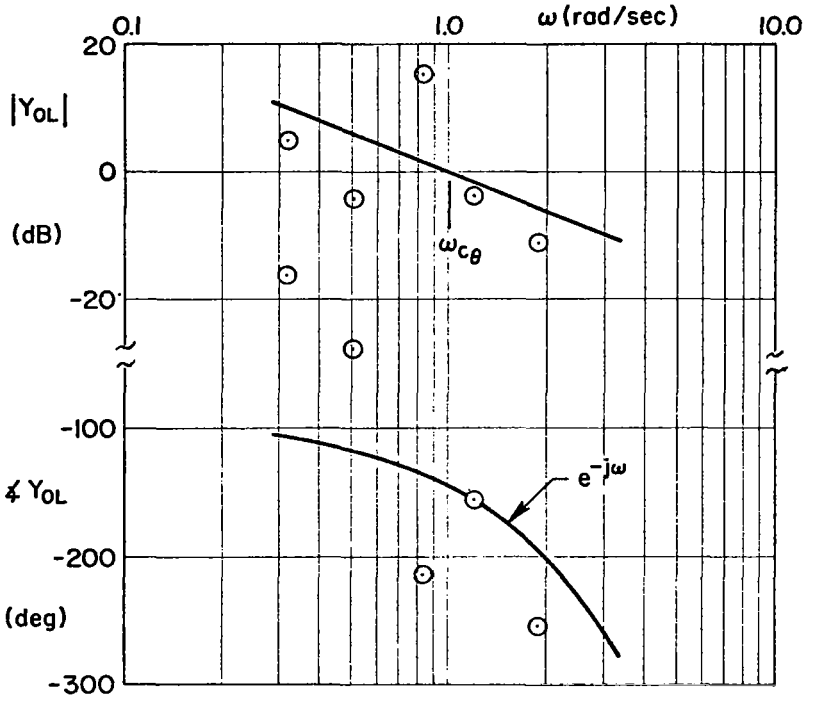

b) Pilot 2 Data, Run 19-17

Figure 10. Inner-Loop Pilot-Vehicle Describing Function for Longitudinal-Only Control

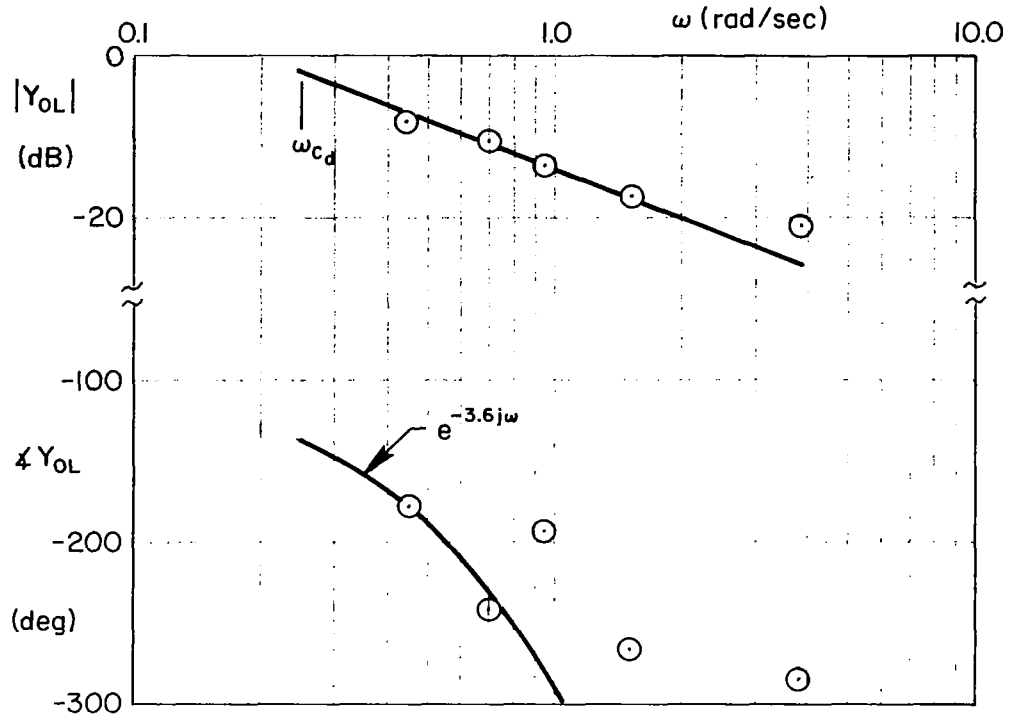

a) Pilot 1 Data, Run 19-5

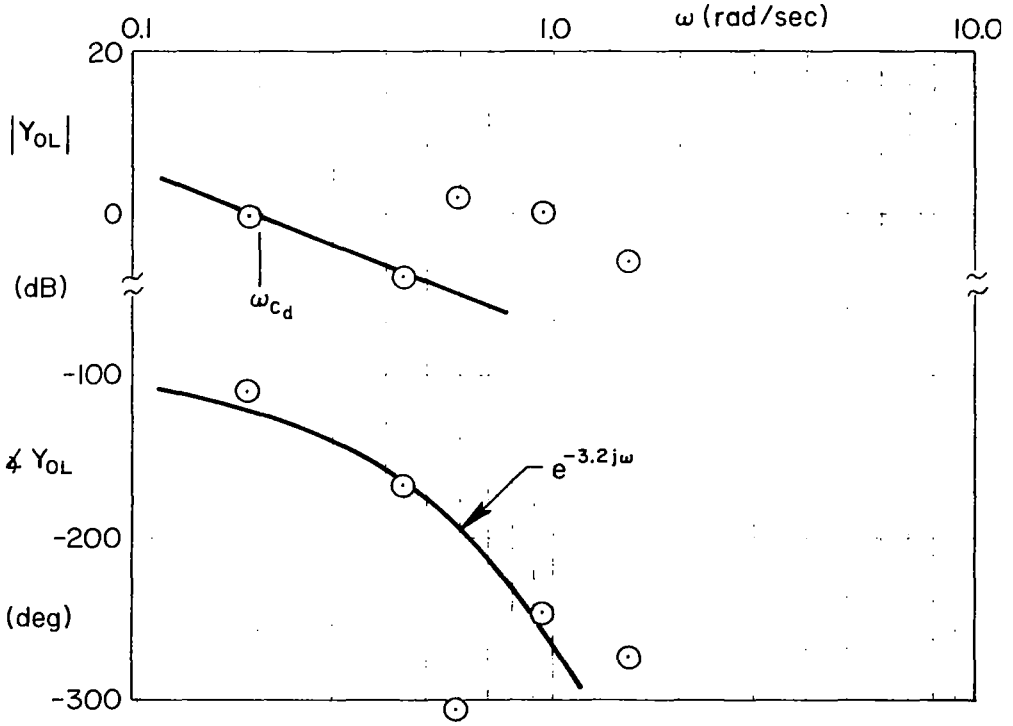

b) Pilot 2 Data, Run 19-17

Figure 11. Outer-Loop Pilot-Vehicle Describing Function for Longitudinal-Only Control

The data for Pilots 1 and 2 are shown in Fig. 11. Unlike the other data in this series, the Pilot 1 amplitude ratio data are close to a 20 dB/decade slope, so the crossover model offers an excellent interpretation. Extrapolation indicates a crossover frequency of about 0.25 rad/sec. The low frequency phase data show a time delay (τ'_{de}) of about 3.6 sec, almost entirely due to the effective outer loop controlled element lag.

The Pilot 2 data in Fig. 11b show a well defined crossover at 0.2 rad/sec, but the mid-frequency peaking makes a 20 dB/decade slope a poor fit. In fact, the mid-frequency data show an on the average instability, which must reflect data variability or nonlinear operation since the pilot did not lose control. The phase data show a time delay (τ_{de}) of about 3 sec, which is due mainly to the effective controlled element properties.

2. Pilot Describing Functions

The inner loop pilot describing function (Y_θ) for Pilot 1 was computed from the spectral ratio data in Appendix C using Eq. 5, as noted above. The Pilot 1 outer loop describing function was computed from

$$Y_d = \frac{\delta_e/d_c}{\delta_e/\theta_c} \tag{8}$$

as described in Appendix B. The data are shown in Fig. 12. The Y_θ amplitude ratio show some scatter about a simple gain fit. The phase data (including the instrument lag) are well approximated by the 0.5 sec time delay, with the low frequency point showing an α-effect. The outer loop data show some scatter about a simple gain fit. The high frequency phase lag partly reflects the glide slope instrument dynamics.

The Pilot 1 data variability in Fig. 12 makes it difficult to choose a specific gain level, so the fits in Fig. 12 were verified by iteratively closing the successive loops analytically and comparing the resulting closed-loop fits with the closed-loop spectral ratio data. A reasonably good comparison obtains, as shown in Fig. 13. The inner loop crossover frequency (ω_{c_θ}) is about 0.33 rad/sec with large stability margins, and ω_{c_d} is about 0.4 rad/sec with small stability margins. The result is a lightly damped phugoid and well damped short period, closed-loop.

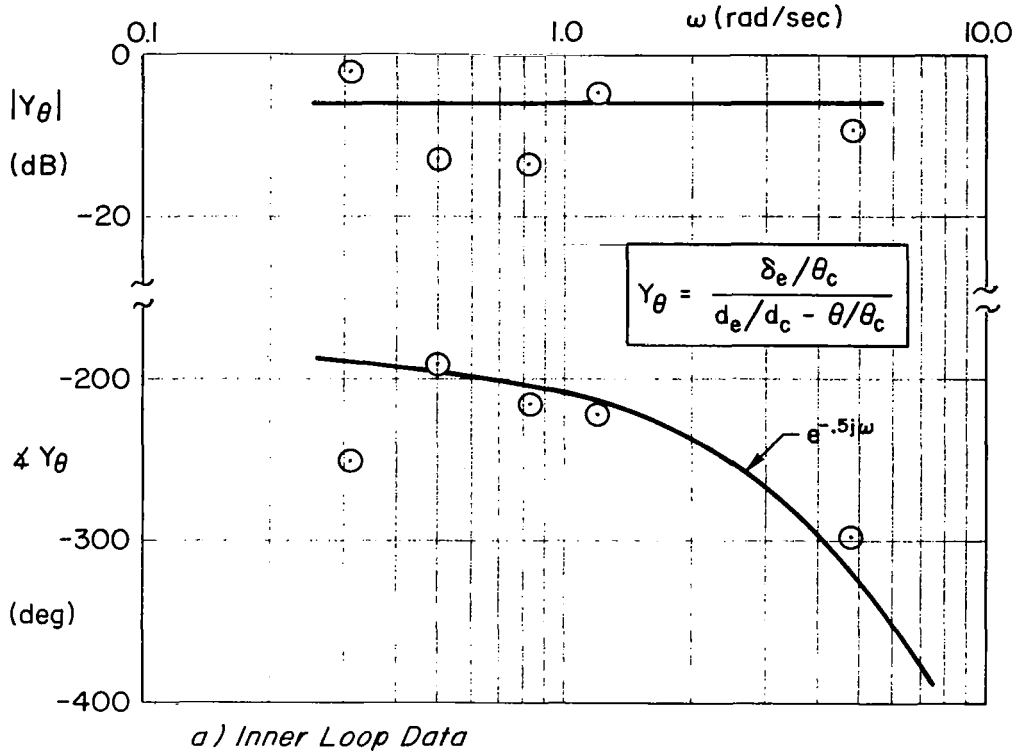

a) Inner Loop Data

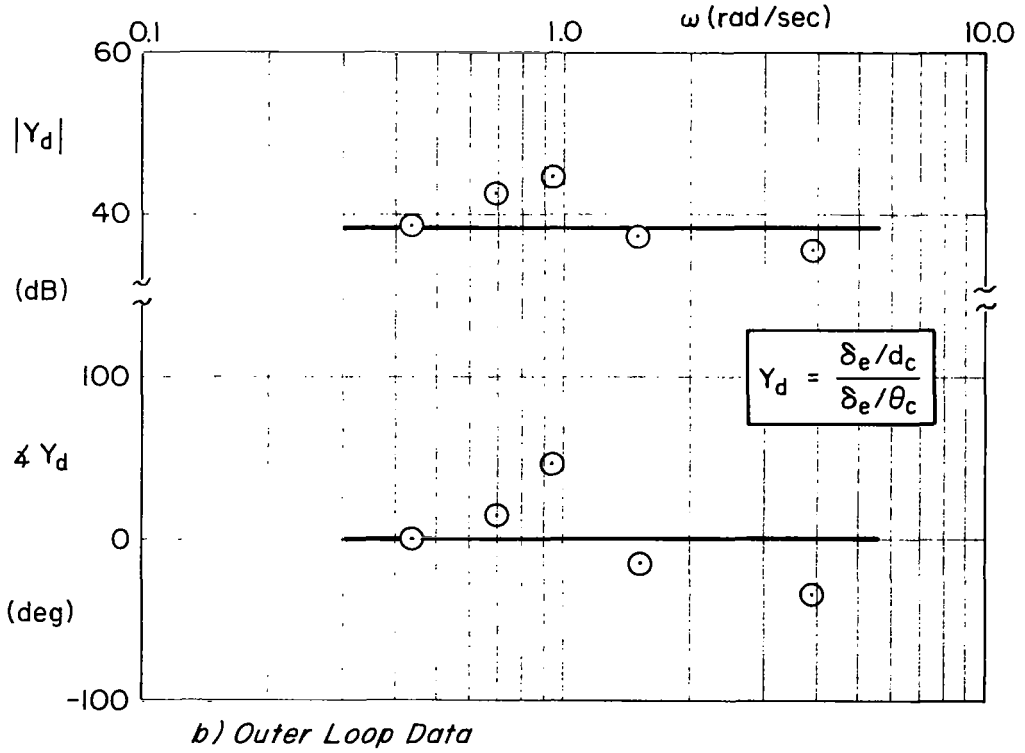

b) Outer Loop Data

Figure 12. Pilot Describing Functions for Longitudinal-Only Control; Pilot 1, Run 19-5

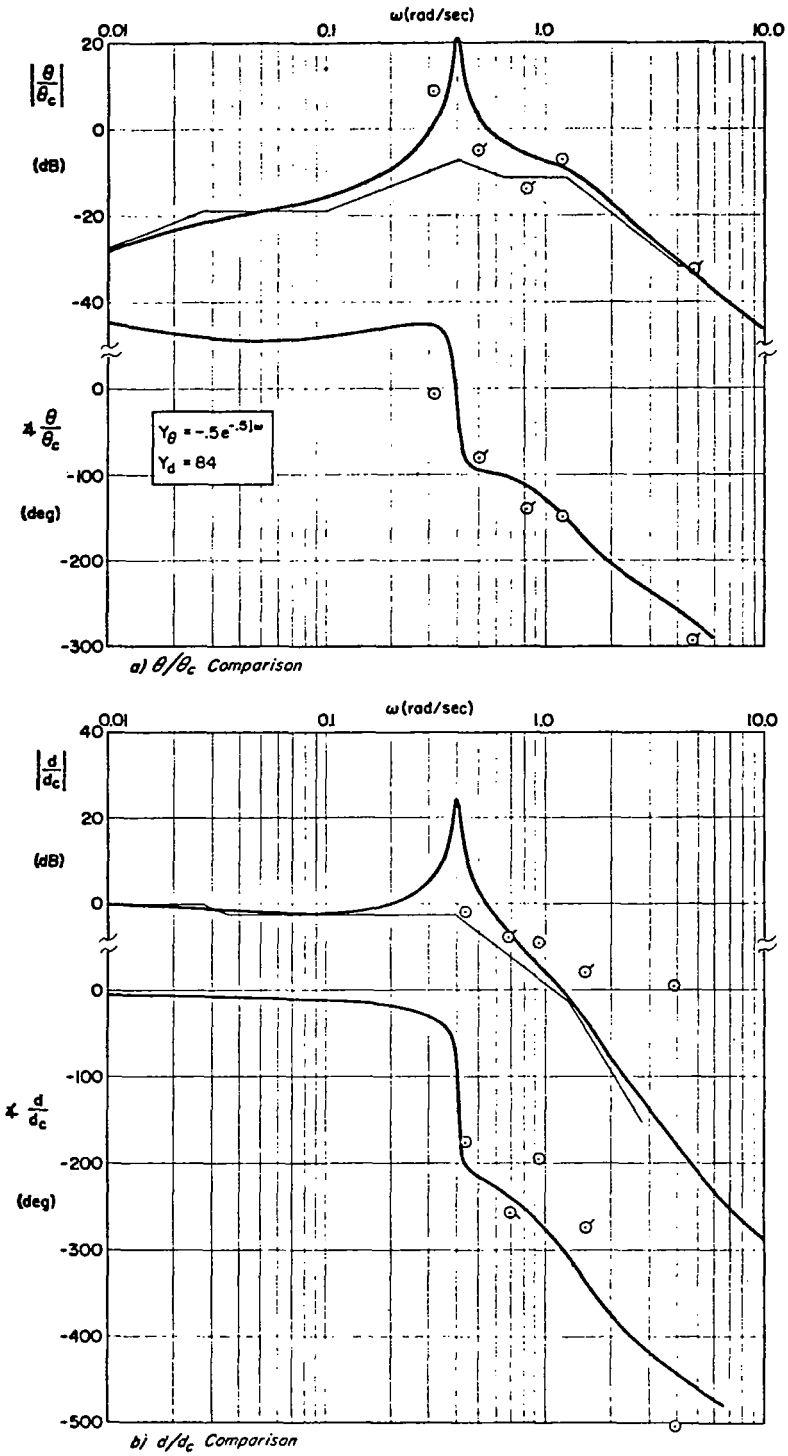

Figure 13. Closed-Loop Describing Functions for Longitudinal-Only Control; Pilot 1, Run 19-5

The inner loop describing function (Y_θ) for Pilot 2 was computed from Eq. 6, while the outer loop result (Y_d) was obtained from Eq. 8. The data are shown in Fig. 14. The Y_θ amplitude ratio show some scatter with an unusually high point at 0.82 rad/sec, as noted in the crossover model interpretation. This point is unreliable because the Y_θ denominator is the difference between two nearly equal, noisy numbers. The Y_θ phase data show a large low frequency lead. The outer loop (Y_d) amplitude ratio data have little variability about a simple gain fit. The phase data (which include the instrument dynamics) have a mid-frequency lag and a high frequency lead which have all been interpreted as scatter about a time delay of zero. Note that moving the high frequency phase point down 360° (to give a large τ_d form) is not compatible with the spectral ratio data.

The Fig. 14 fits for Pilot 2 were also adjusted and verified by making successive loop closures and comparing them with the outer closed loop spectral ratio data. The initial set of closures used $|K_\theta| \doteq 1.4$ and $K_d = 76$. This gave a lightly damped phugoid and moderately damped short period, and the closed-loop fit was a very poor match to the closed-loop data. A detailed sensitivity analysis indicated that a better outer loop match was achieved by increasing the θ-loop gain to 1.7 and decreasing the d-loop gain to 38. The results are shown in Fig. 15. The inner loop crossover (ω_{c_θ}) is then about 1.2 rad/sec with low stability margins and a lightly damped short period. The outer loop crossover (ω_{c_d}) becomes 0.25 rad/sec, and the phugoid is well damped with large phase and gain margin. Though improved, the resulting fits are still only fair; but they are about the best that can be achieved with these simple model forms for Y_θ and Y_d. Further gain adjustments only worsen the outer loop comparison, as simultaneous downward movement of the $|\theta/\theta_c|$ fit and upward shift of $|d/d_c|$ cannot be achieved.

E. ALL-AXIS CONTROL

Reduced spectral ratio data are available for two 100 sec all-axis (Configuration C) multiloop runs for each of the two pilot subjects. Since the scanning data (Ref. 6) showed no significant differences within pilots for their two respective runs, the basic spectral ratio data for each pilot were lumped prior to data interpretation. The combined basic spectral ratio data are given in Appendix C.

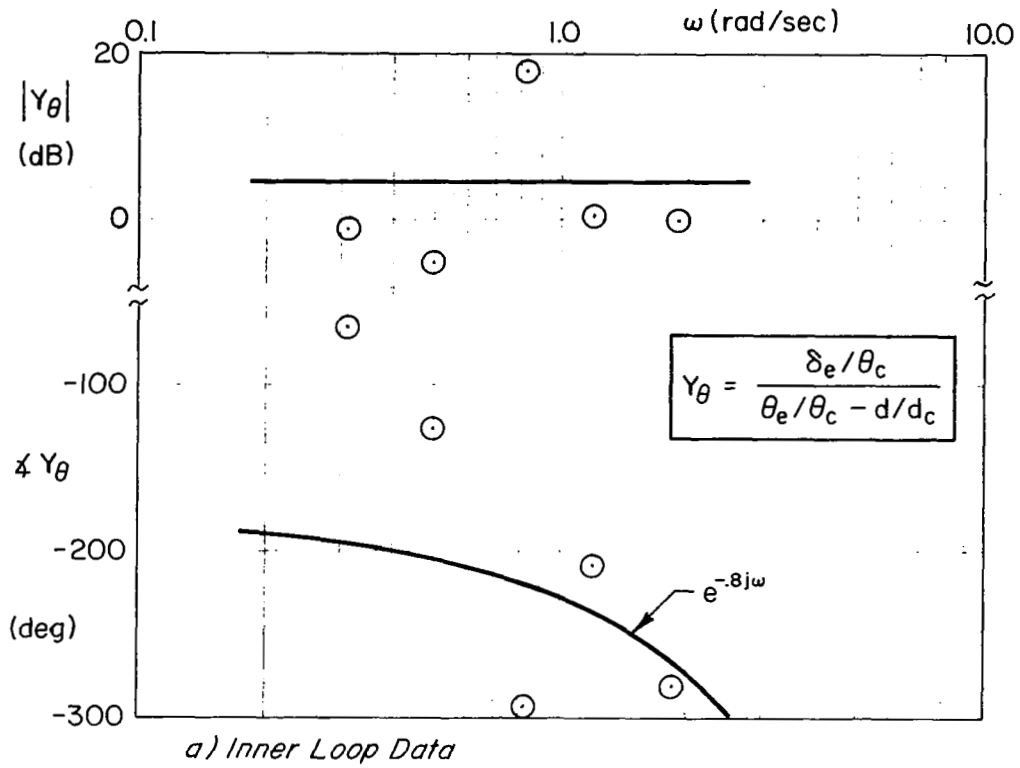

a) Inner Loop Data

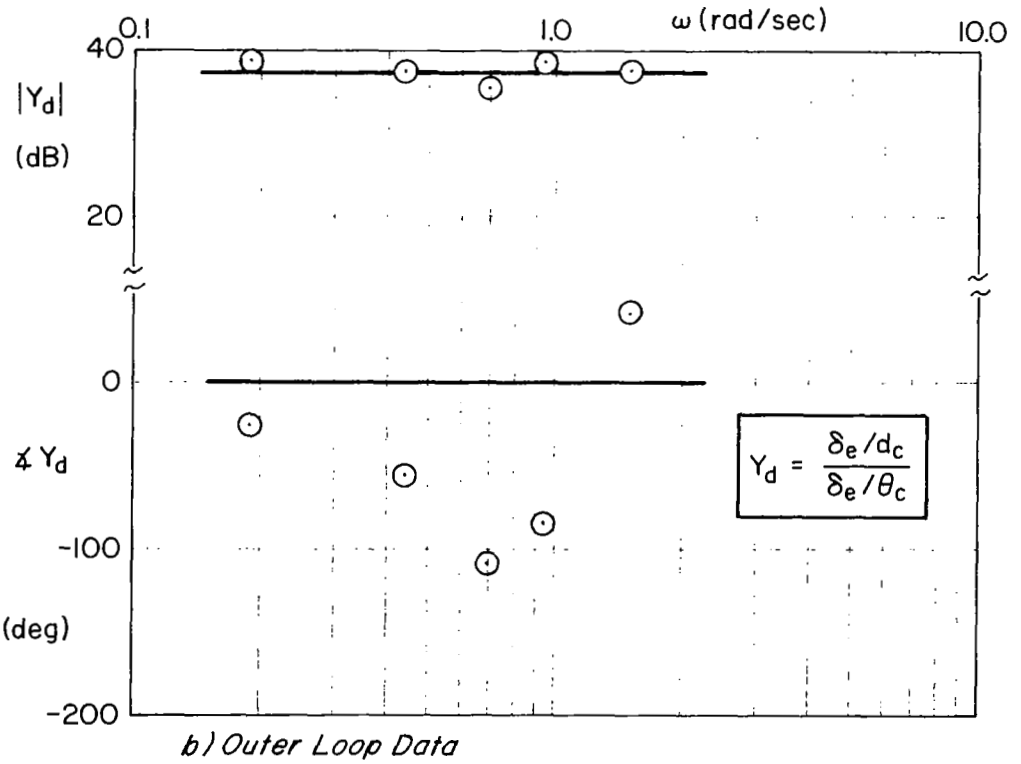

b) Outer Loop Data

Figure 14. Pilot Describing Functions for Longitudinal-Only Control; Pilot 2, Run 19-17

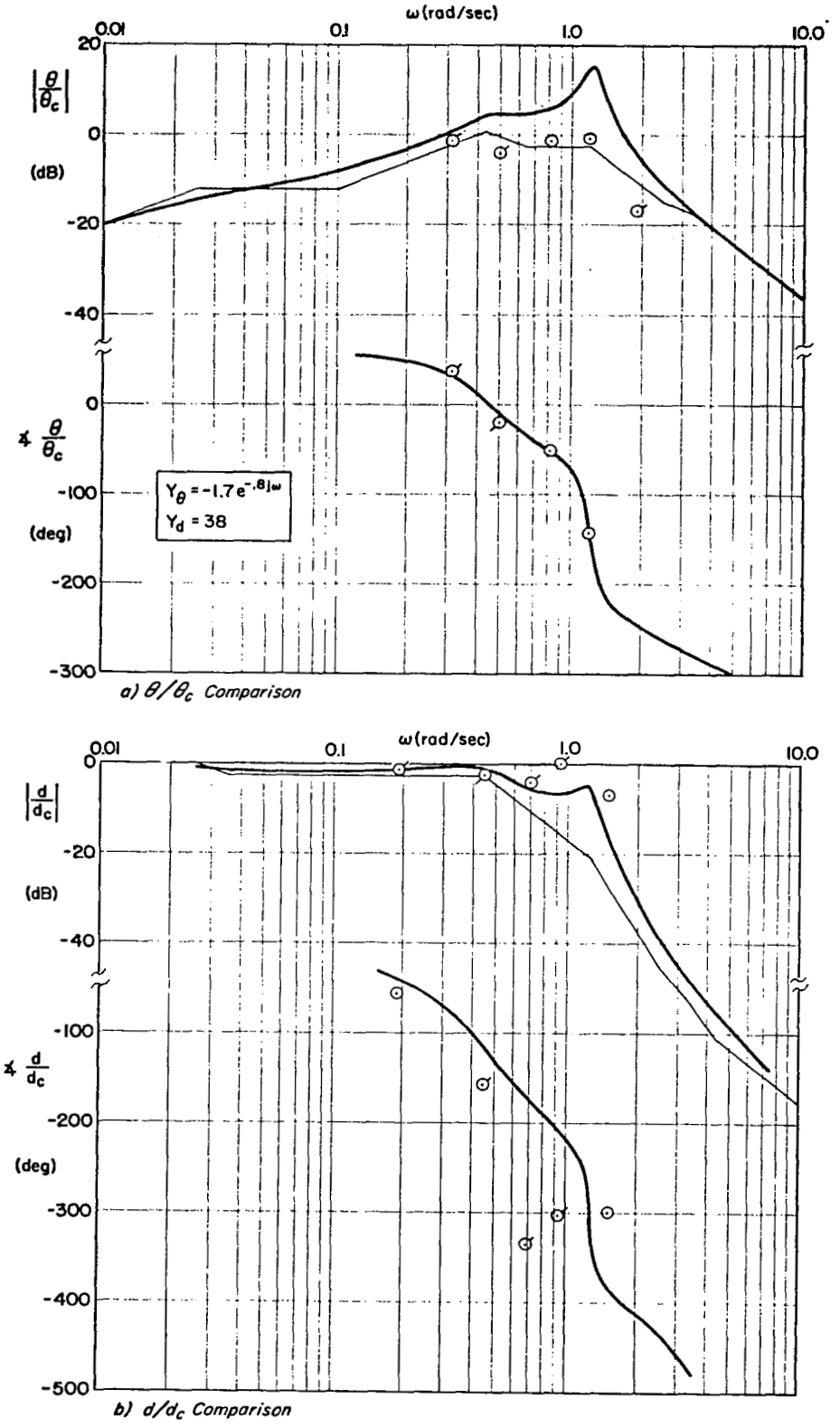

Figure 15. Closed-Loop Describing Functions for Longitudinal-Only Control; Pilot 2, Run 19-17

1. Crossover Model Interpretation

The computational forms used for the all-axis data are the same as those used in the longitudinal-only data, above, for the respective Pilot 1 and Pilot 2 results.

The open inner loop pilot/vehicle describing function data are given in Fig. 16. The pilot crossover frequency ($\omega_{c\theta}$) is well defined by the data at 0.5 to 0.6 rad/sec. As with Configuration B, there is a low frequency phase lag which implies a conditionally stable closure, although the stability margins are large. The phase data at crossover show a time delay (τ_{θ_c}) of about 1 sec, including the pitch attitude instrument dynamics. The Pilot 2 data in Fig. 16b show a higher crossover frequency (1.2 rad/sec) and very low stability margins. The phase data show a low frequency lag. The fairing $e^{-.6j\omega}$ is not a good fit, and the phase data point at crossover indicates $\tau'_{\theta_e} = 1.3$ sec. The amplitude ratio for both pilots shows substantially less scatter about a 20 dB/decade slope than did the longitudinal-only data in Fig. 10.

The open outer loop pilot/vehicle describing function data for both pilots are shown in Fig. 17. Extrapolation of the Pilot 1 amplitude ratio data along a 20 dB/decade slope gives a crossover frequency (ω_{c_d}) of less than 0.4 rad/sec. The phase data are similar to the longitudinal-only results in Fig. 11, and indicate small stability margins. The large time delay (4 rad/sec) reflects the effective outer loop controlled element dynamics. The Pilot 2 crossover frequency is well defined at 0.2 rad/sec, and the amplitude ratio data generally follow a 20 dB/decade slope. The phase data show some scatter with a 3 sec time delay near crossover. The stability margins are large, in keeping with the low crossover frequency.

2. Pilot Describing Functions

The inner and outer loop pilot-alone describing functions are given in Fig. 18 for Pilot 1 in the all-axis (C) task, based on the spectral ratio data in Appendix C. The Y_θ data show little scatter about a gain plus time delay model form. The phase data show a time delay of about 1 sec, with a low frequency phase lag. The outer loop data in Fig. 18b are well approximated by a simple gain, $Y_d = 57$.

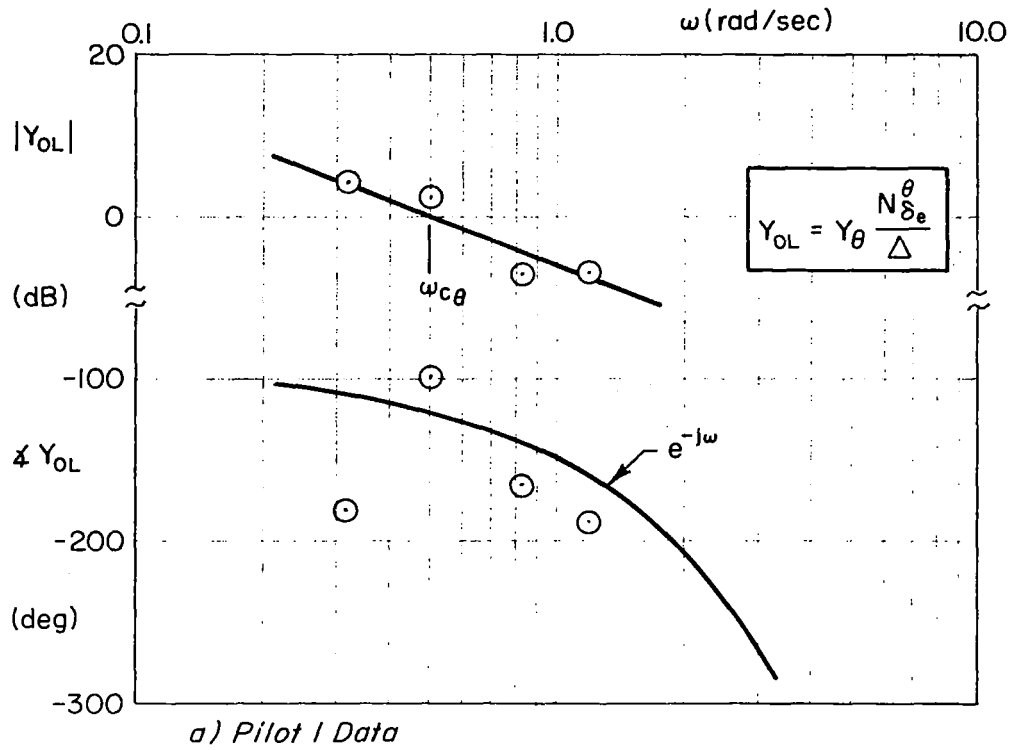

a) Pilot 1 Data

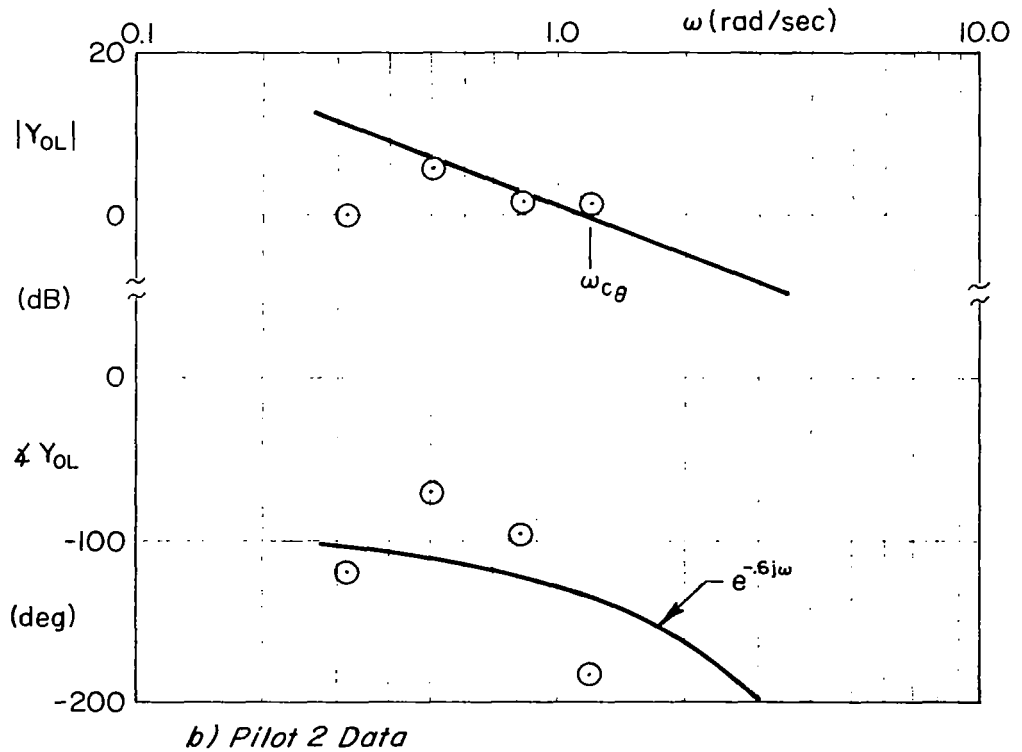

b) Pilot 2 Data

Figure 16. Inner Loop Pilot-Vehicle Describing Function for All-Axis Control

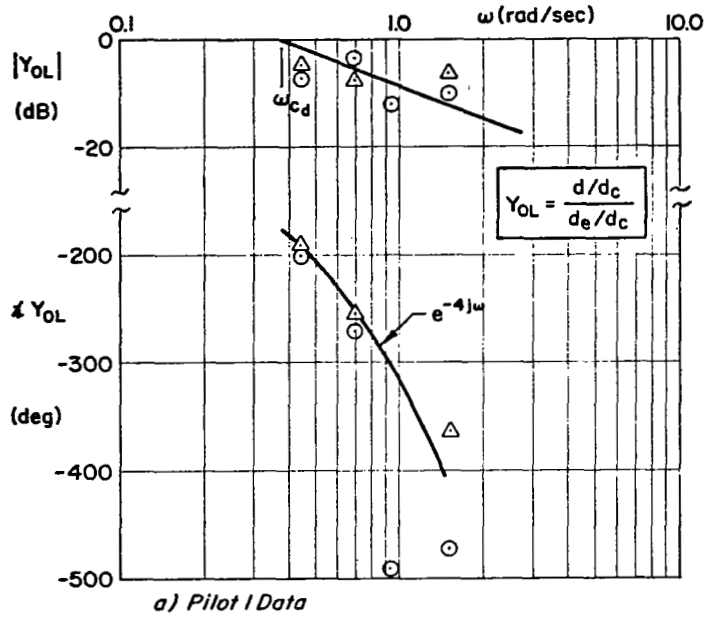

a) Pilot I Data

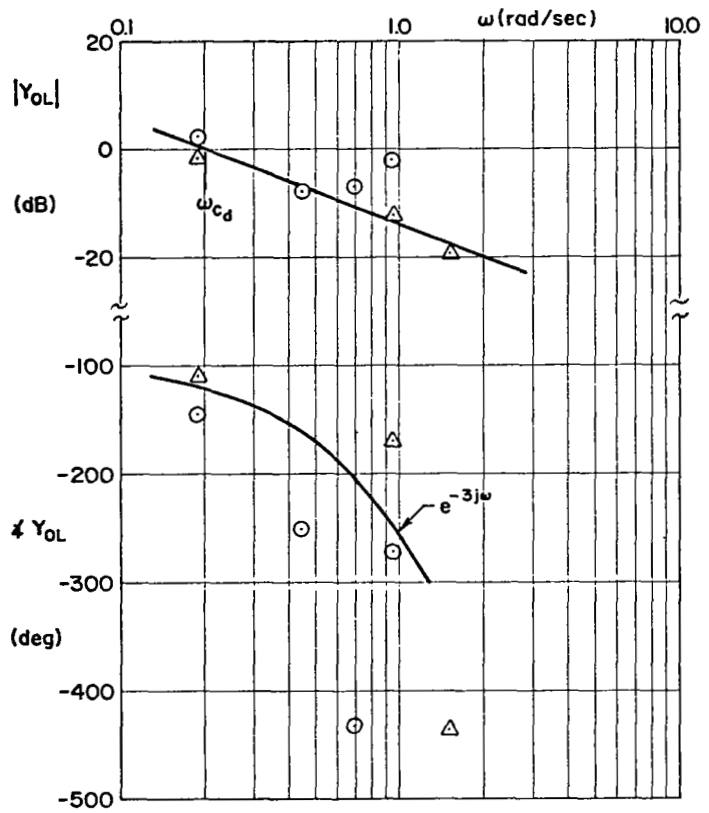

b) Pilot 2 Data

Figure 17. Open Outer-Loop Pilot-Vehicle Describing Function for All-Axis Control

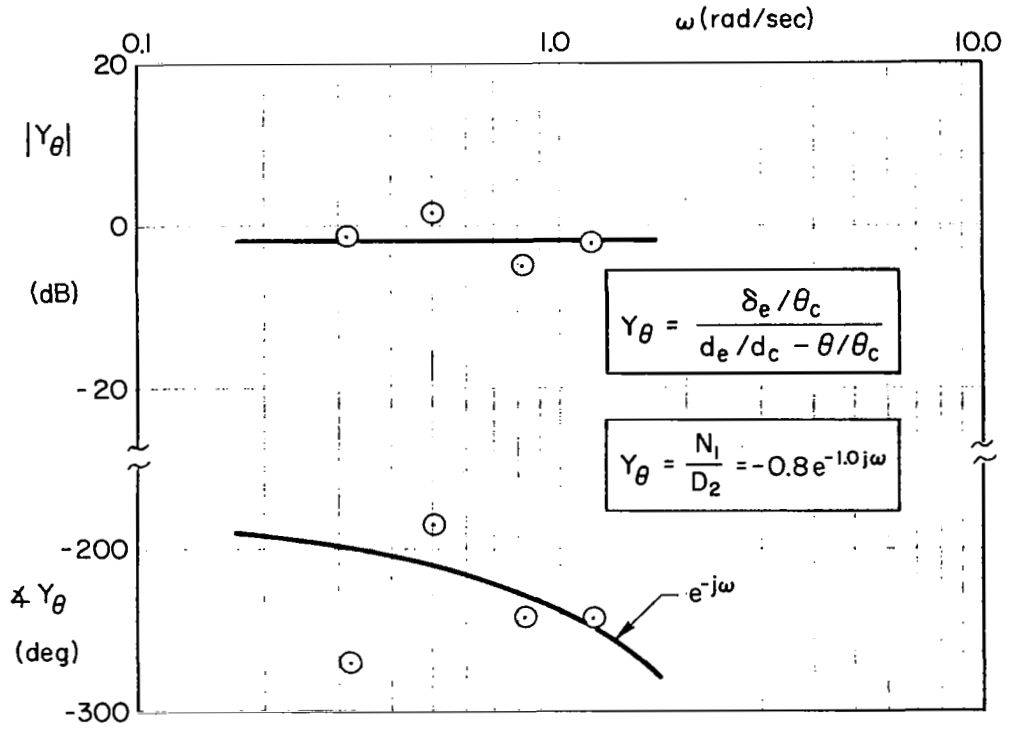

a) Inner Loop Data

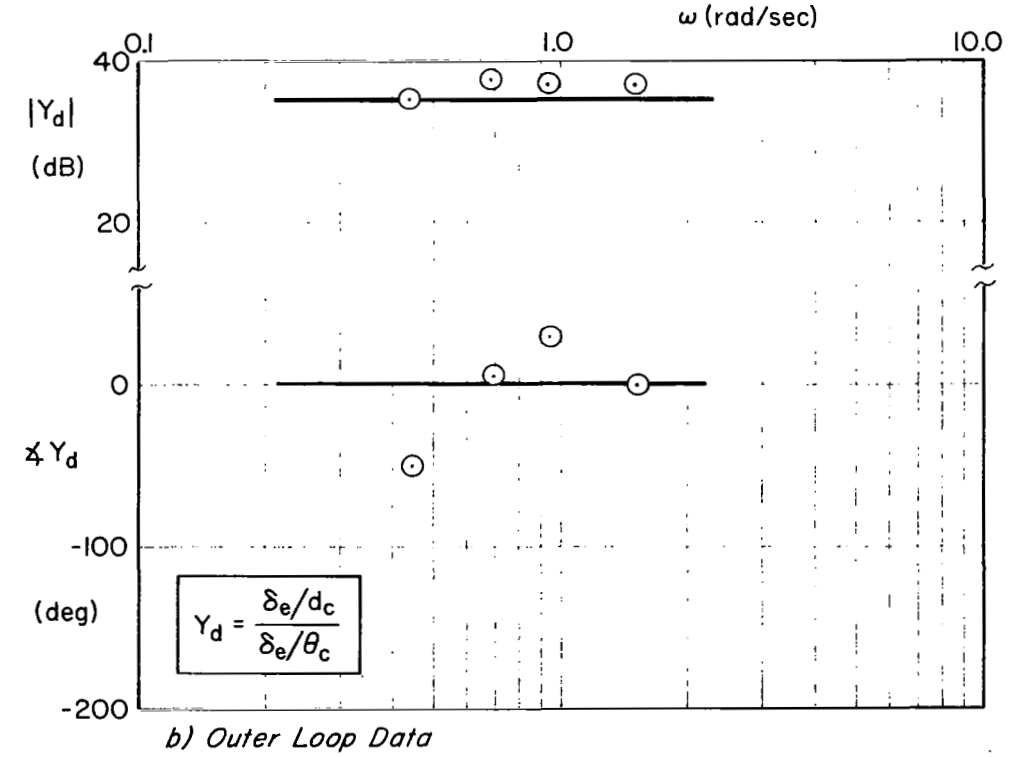

b) Outer Loop Data

Figure 18. Pilot Describing Functions for All-Axis Control, Pilot 1

The Pilot 1 fits shown in Fig. 18 were verified by closing the inner and outer loops analytically and comparing the result with the outer loop spectral ratio data. This is shown in Fig. 19, and a reasonably good comparison obtains. The inner loop crossover frequency (ω_{c_θ}) is about 0.45 rad/sec with large stability margins, while ω_{c_d} is 0.38 rad/sec with small phase and gain margin. As with the longitudinal-only task, the result is a lightly damped phugoid and well damped short period, closed-loop.

The inner and outer loop pilot describing functions for Pilot 2 are given in Fig. 20. The Y_θ data are a fair fit to a gain plus time delay model form. The phase data are variable about a time delay of 0.6 sec, and the high frequency phase point (which is near crossover) suggests a value of about 1 sec. The outer loop data (Fig. 20b) look like a simple gain with some low frequency phase lag. In general these data show substantially less variability about simple model forms than did the Pilot 2 results for the longitudinal-only task (Fig. 14).

The Fig. 20 fits were verified by comparing their closed-loop equivalent with the closed-loop spectral ratio data, and this is shown in Fig. 21. The inner loop crossover frequency (ω_{c_θ}) is 1.14 rad/sec with small stability margins, and the outer loop value is 0.39 rad/sec with moderate gain and phase margin. The comparison is poor for θ/θ_c and somewhat better for d/d_c. Both sets of data indicate that the phugoid frequency should be lower with more damping. This would imply a further reduction of outer loop gain (K_d), but the amplitude ratio fit in Fig. 20b is already at the bottom of the data. The closed-loop fit in the short period region might improve somewhat, also, with a reduction in $|K_\theta|$, but the case is not strong for this inner loop refinement.

F. DATA CORRELATIONS

The two pilots whose data are presented above demonstrate different multiloop control strategies, as noted previously. More specifically, the response measurements show that they are at either end of the "allowable" region of inner and outer loop response properties. Each could modify his gains towards the middle (e.g., lower ω_{c_θ} and higher ω_{c_d} for Pilot 2) but they were near the stability limits in the other direction of gain variation. This was evident in the preliminary data screening, and it was one reason why the data for these two subjects were selected for analysis.

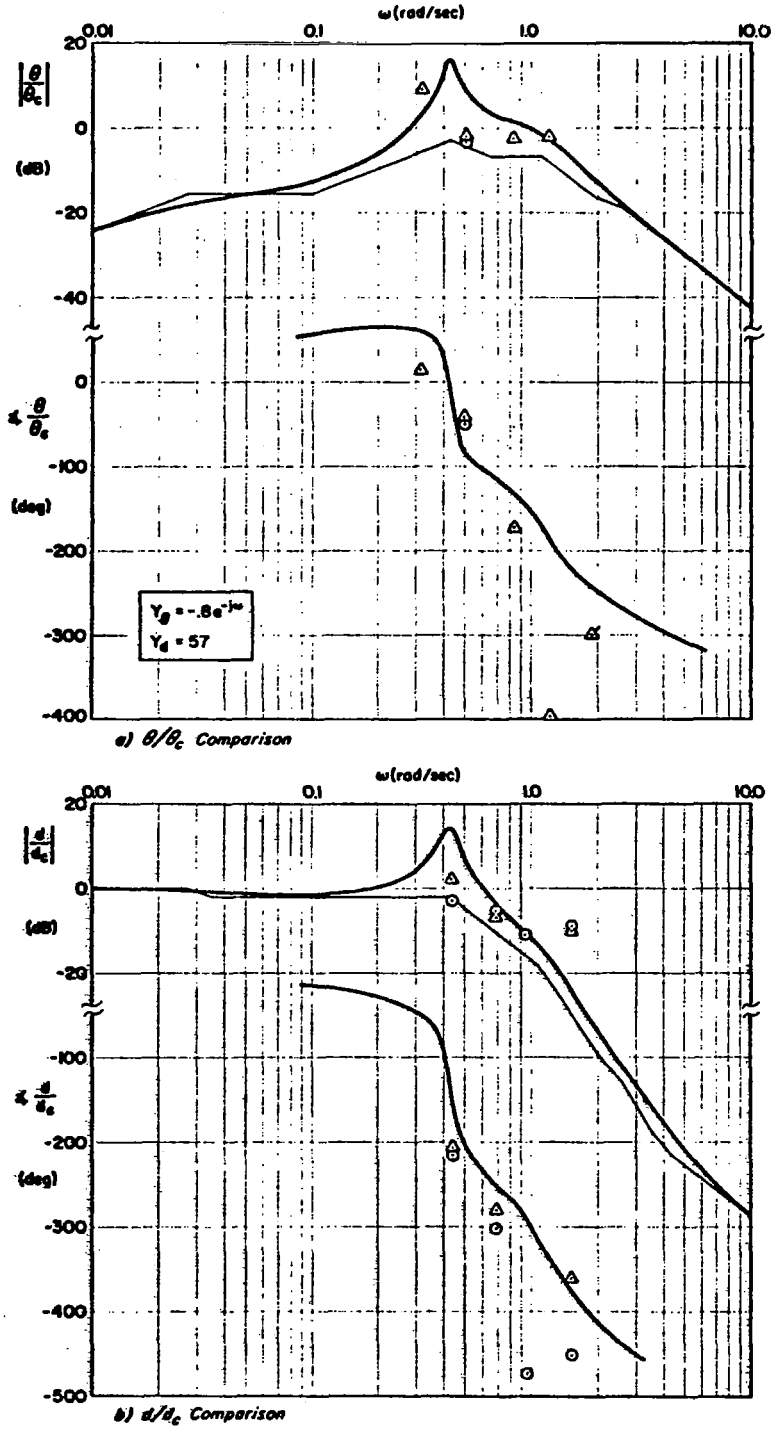

Figure 19. Closed-Loop Describing Functions for All-Axis Control, Pilot 1

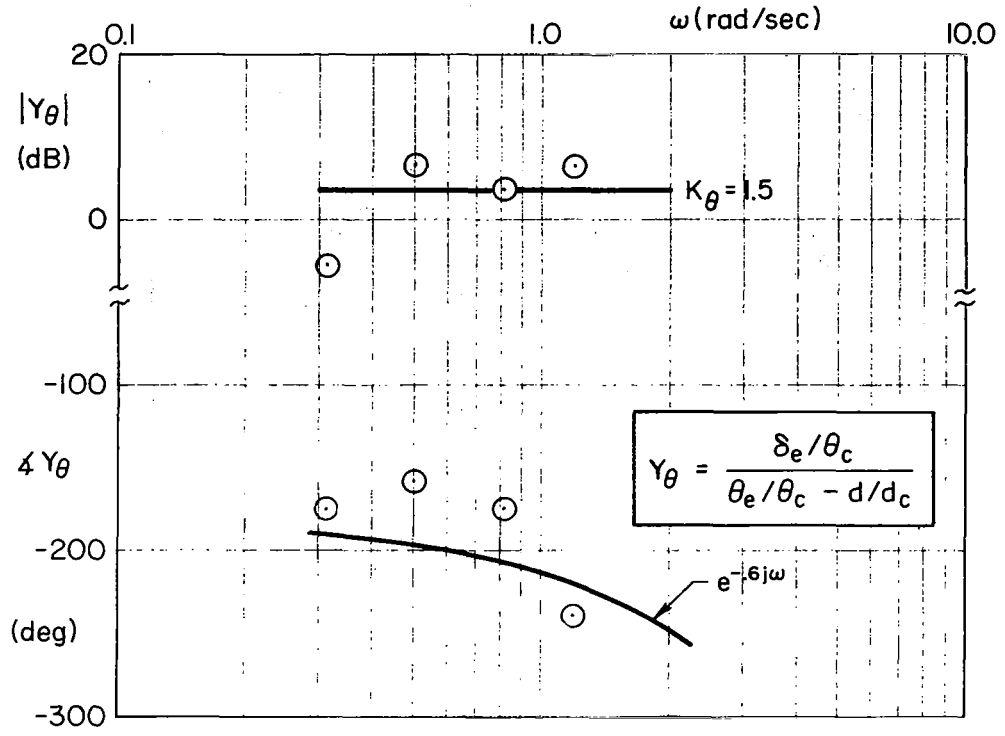

a) Inner Loop Data

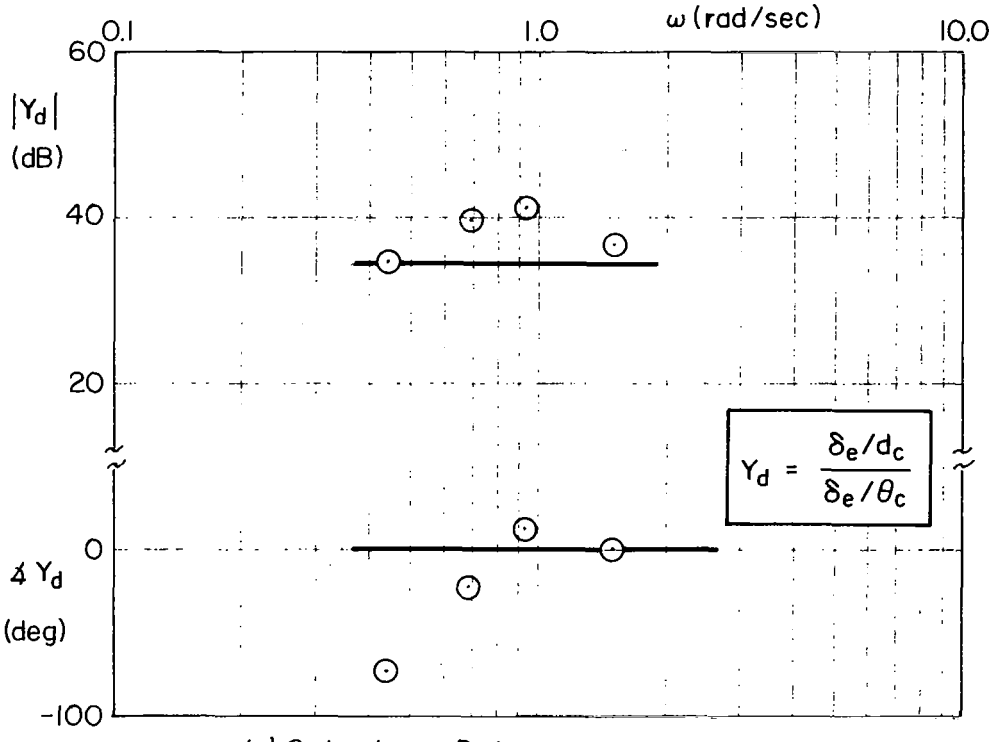

b) Outer Loop Data

Figure 20. Pilot Describing Function for All-Axis Control, Pilot 2

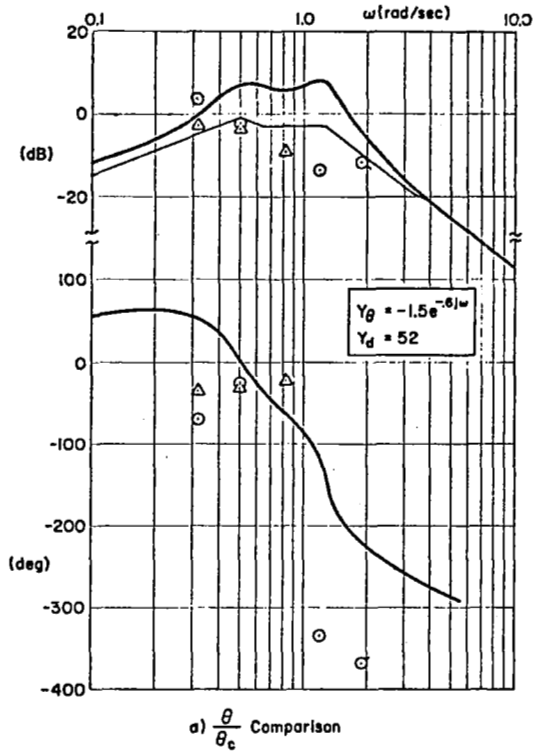

a) $\frac{\theta}{\theta_c}$ Comparison

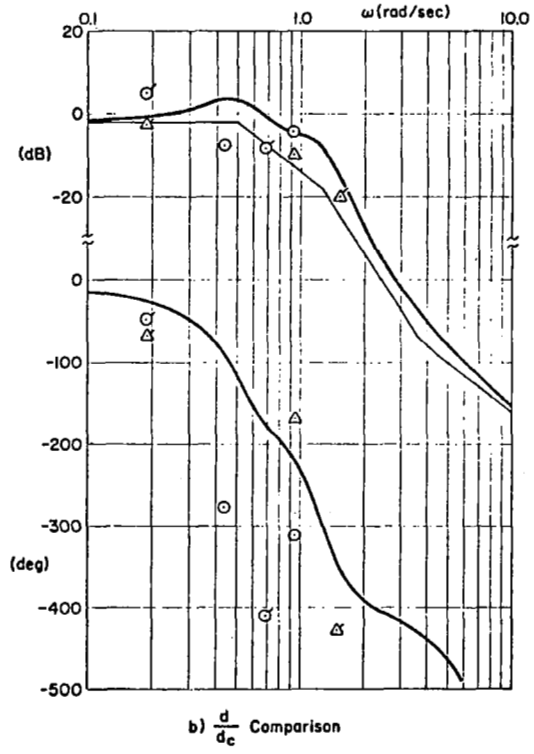

b) $\frac{d}{d_c}$ Comparison

Figure 21. Closed-Loop Describing Functions for All-Axis Control, Pilot 2

The response data shown above are generally variable about the simple model forms used. There is no clear evidence, however, in the variability of the multiloop results for alternative (perhaps higher order) model forms. Instead, the variability is due to the relatively low signal to noise quality of the multiloop data, i.e., the high levels of remnant. By contrast, the single-loop data show very little departure from well-established forms such as the crossover model.

Prior multiloop measurements which can be compared with the current data are limited, for all practical purposes, to the results of the 1238 study (Ref. 8), previously discussed. The 1238 experiments used a similar longitudinal multiloop task with two independent forcing functions. This allowed the inner and outer loop describing functions to be determined in the manner used in this study and outlined in Appendix B. As noted before, the 1238 experiments differed in display format, in the lack of multiple instrument scanning, and in the instructions to the pilot subjects.

The 1238 pilot-alone describing function data are given in Fig. 22 for Pilots A and B. The circles and triangles in Fig. 22a were taken directly from Ref. 8, and they show seemingly anomalous phase differences at low frequency. As a result, the (unpublished) basic spectral ratio data (and fairings) from the 1238 study were used to recompute the Y_θ describing function at selected points (with a computer program rather than by hand), and the resulting mean of the two pilots is shown by the X points. [The two subjects differed very little on recalculation.] The phase data now show a smooth fairing with the characteristic low frequency lag. The amplitude ratio is also reduced at low frequency. These corrections did not, however, affect the inner loop crossover frequency which occurred at a little more than 2 rad/sec.* This is substantially higher than that observed in the present data, presumably for the reasons noted. The outer loop 1238 data (Figs. 22b and c) show the characteristic simple gain nominal form, and the crossover frequency was about 1 rad/sec. The data showed low stability margins in both the inner and outer loops, and there is substantially less variability about simple model forms than in the current data.

*Obtained by taking the data of Fig. 22a and the 1238 inner loop controlled element in Fig. 8. The attitude loop crossover frequencies shown in Table IV of Ref. 8 are single loop rather than multiloop task results.

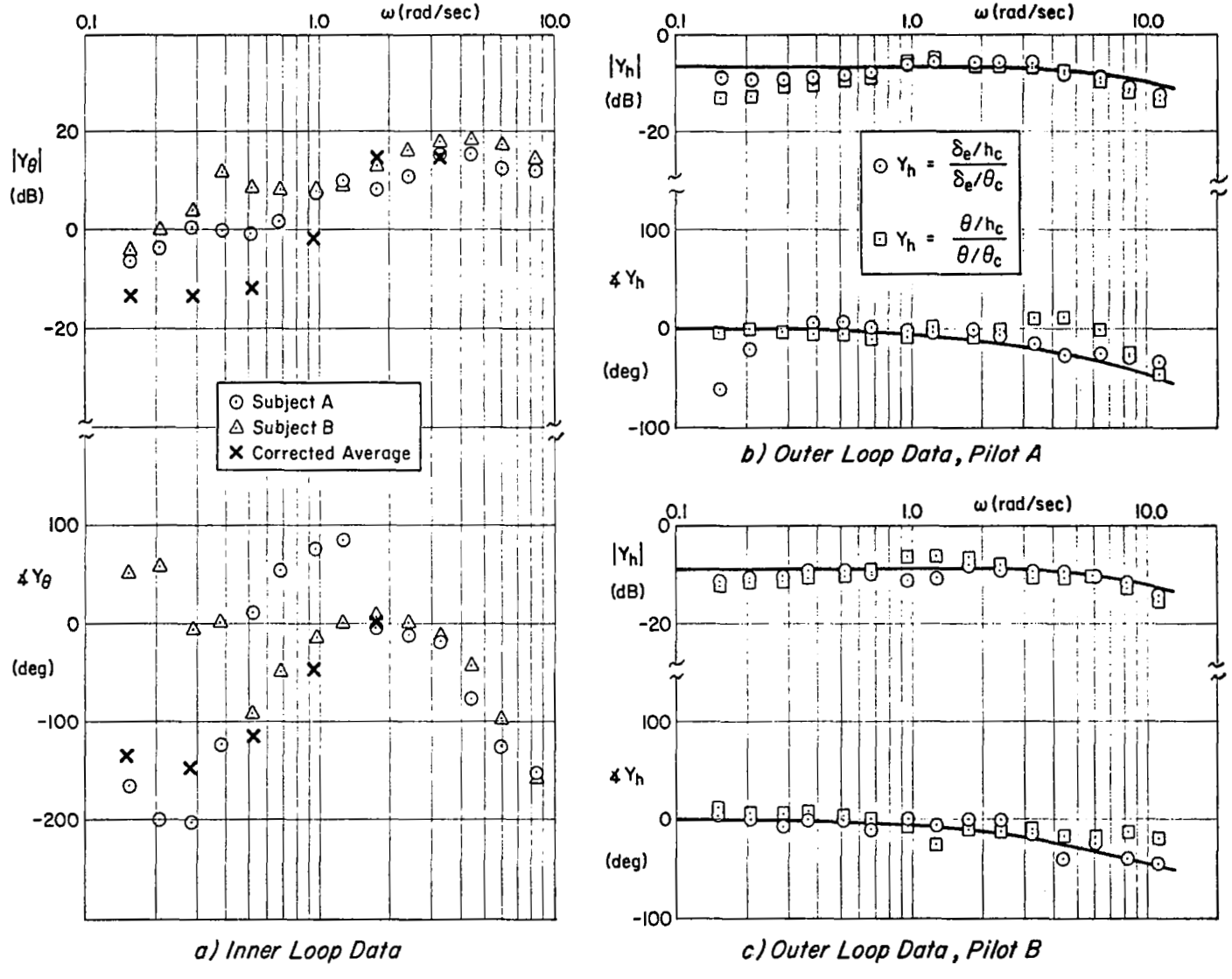

Figure 22. Pilot Describing Functions for Longitudinal Control, 1238 Study (Ref. 8)

SECTION IV

REMNANT DATA

Remnant is that portion of the pilot describing function model which accounts for his response that is not linearly correlated with the forcing function. It is generally modelled as a random noise process, injected at the pilot's input or output. In manual control tasks involving only one pilot response output, the remnant can be observed at that point as the signal power at other than forcing function component frequencies. For single loop systems with an error stimulus the remnant can be determined at this error point, also. For the multiloop tasks characterized by Configurations B and C, the inner loop error is an intangible quantity within the pilot and it is not directly observable. Since the principles and techniques for computing and modelling this multiloop error remnant have yet to be developed, attention will be restricted to remnant at the pilot's output in the multiloop case.

A. REMNANT SMOOTHING PROCEDURE

The "raw" discrete power spectral density of the pilot's output (δ_e) was computed at close-spaced frequency intervals of 0.01 Hz, corresponding to the inverse of the 100 sec data run length. The remnant consists of all the spectral points at other than forcing function frequencies.

The raw, close-spaced remnant spectra were obtained by removing the points at forcing function frequencies and replacing them with the adjacent remnant data point on the low frequency side. These remnant plots were then "smoothed" by averaging 10 adjacent spectral density points (in linear units) to obtain data points at 0.1 Hz (rather than 0.01 Hz) intervals. The smoothing used a rectangular filter which gave each point within the 0.1 Hz smoothing interval equal weight. The resulting points occurred at 0.05, 0.15, 0.25, ... etc., Hz up to a frequency of about 10 rad/sec. Above this frequency (well above the forcing function bandwidths) the smoothed remnant spectral density points were computed at 0.1 Hz intervals using a Hanning filter.

B. SINGLE LOOP REMNANT DATA

The smoothed pilot remnant power spectral densities for the pitch attitude control task are given in Fig. 23. The lower (open face) data points are the closed-loop remnant ($\Phi_{\delta_e \delta_{e_n}}$) measured at the pilot's output. The upper (solid) data points are the normalized open loop remnant injected at the operator's input, computed as follows:

$$\Phi_{nn_{\theta_e}} = \left| \frac{N^{\theta}_{\delta_e}}{1 + Y_{\theta} \frac{N^{\theta}_{\delta_e}}{\Delta}} \right|^2 \Phi_{\theta_e \theta_{e_n}} = \left| \frac{1}{Y_{CL}} \right|^2 \Phi_{\theta_e \theta_{e_n}} \tag{9}$$

In Eq. 9, $|Y_{CL}| = |(\theta/\theta_c)'|$ is obtained from the pilot/vehicle describing function data in Section II, and $\Phi_{\theta_e \theta_{e_n}}$ is the smoothed remnant power spectral density in the pitch attitude error (see the block diagram in Fig. B-1a, Appendix B). Division by the mean square error ($\sigma^2_{\theta_e}$) provides the normalization.

Pilot 2 had the higher crossover frequency, and his open loop remnant levels are higher. Opening the loop and normalizing the data, however, brings them into correspondence. The data for both pilots dip near mid-frequency then increase in amplitude at high frequency in the vicinity of the pilot's neuromuscular mode.

The smoothed remnant data for the flight director control task are given in Fig. 24. The lower points are the closed loop values at pilot's output for the four runs analyzed. The upper (solid) points are the normalized open loop remnant injected at pilot's input (see Fig. B-1b, Appendix B). They were computed using the describing function data in Section II, as follows:

$$\Phi_{nn_{FD_e}} = \left| \frac{1}{Y_{CL}} \right|^2 \left| \frac{1}{Y_{FD}} \right|^2 \Phi_{\delta_e \delta_{e_n}} \tag{10}$$

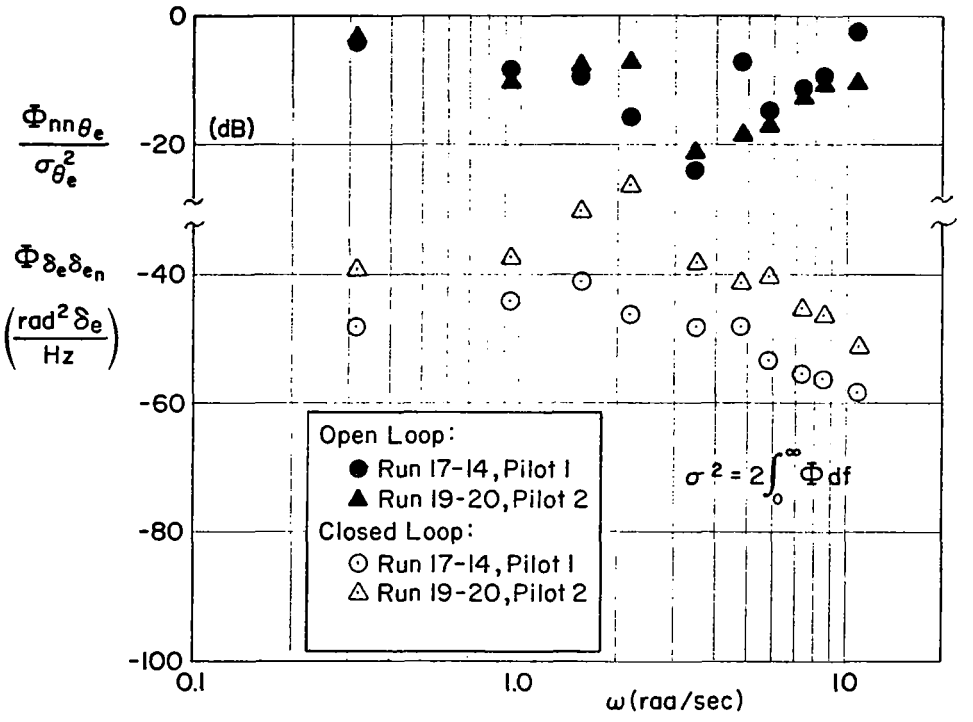

Figure 23. Remnant Spectra, Pitch Attitude Control

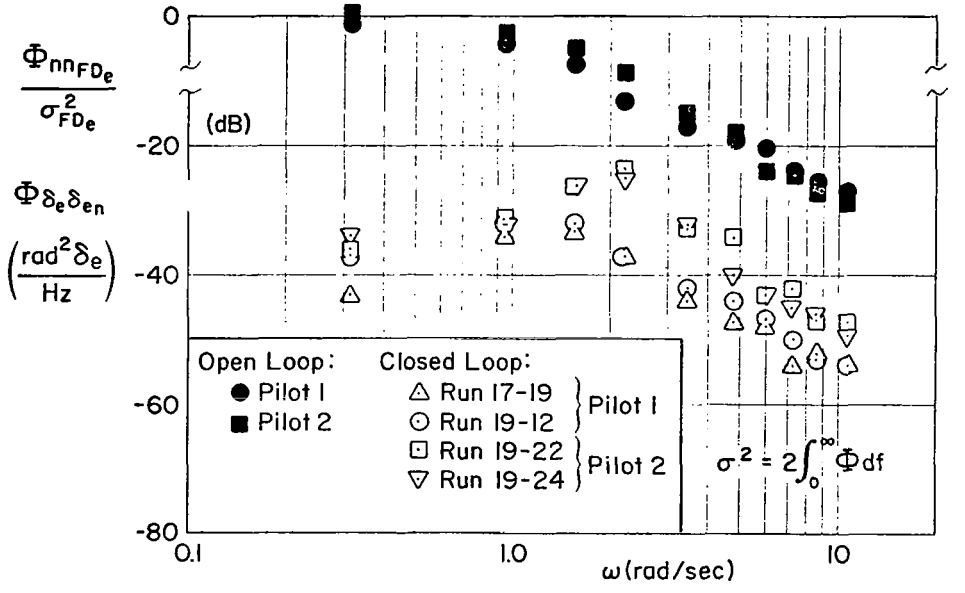

Figure 24. Remnant Spectra, Flight Director Control

The error remnant spectra were computed from

$$\Phi_{FD_e FD_{e_n}} = \left|\frac{1}{Y_{FD}}\right|^2 \Phi_{\delta_e \delta_{e_n}}$$

rather than by direct computation. The closed loop data in Fig. 24 show a higher level for the higher gain pilot, and some reduction in amplitude at low frequency. The normalized open loop remnant coalesce nicely, and roll off as a first order lag at and above the crossover frequency.

C. MULTILOOP REMNANT DATA

The closed loop remnant spectra for the multiloop longitudinal-only and all-axis tasks are given in Figs. 25 and 26. The data are quite similar, with their highest amplitude at low frequency and a steady roll off. The single and multiloop closed-loop data all have roughly the same amplitude at high frequency. The multiloop data are higher in the mid and low frequency regions. There are some detailed differences between configurations for a given pilot, and these are discussed briefly in Section VI.

The steady roll offs of about 20 dB/decade in the multiloop data are in good agreement with the form of the closed loop remnant ($\Phi_{\delta_e \delta_{e_n}}$) in the 1238 study (Ref. 8). The overall amplitude levels differ between the two studies, of course, because of the differences in the task variables and response variable scaling.

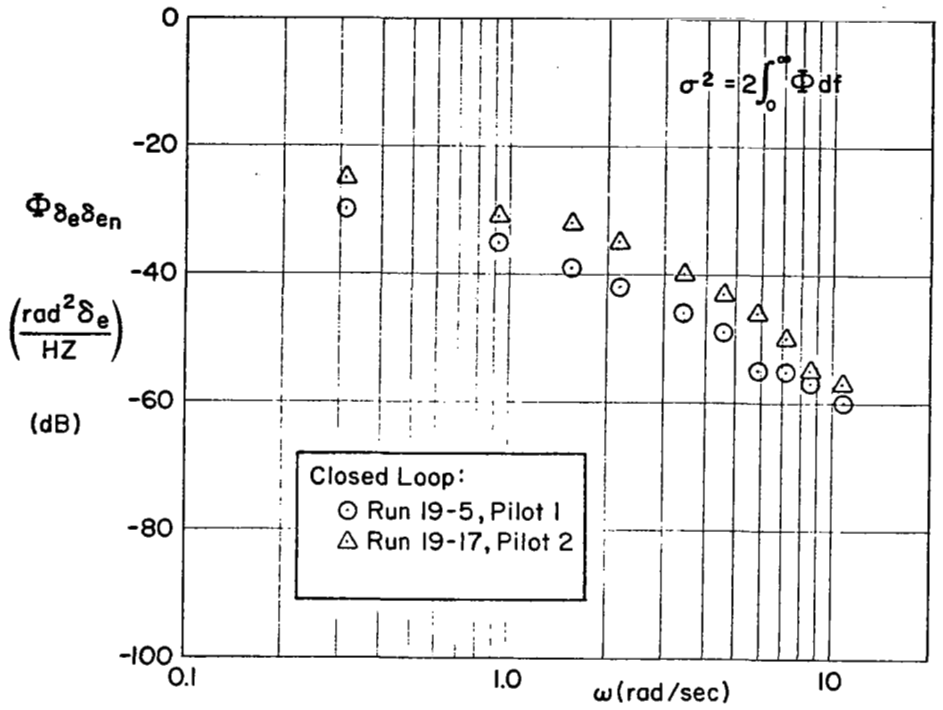

Figure 25. Remnant Spectra, Longitudinal-Only Control

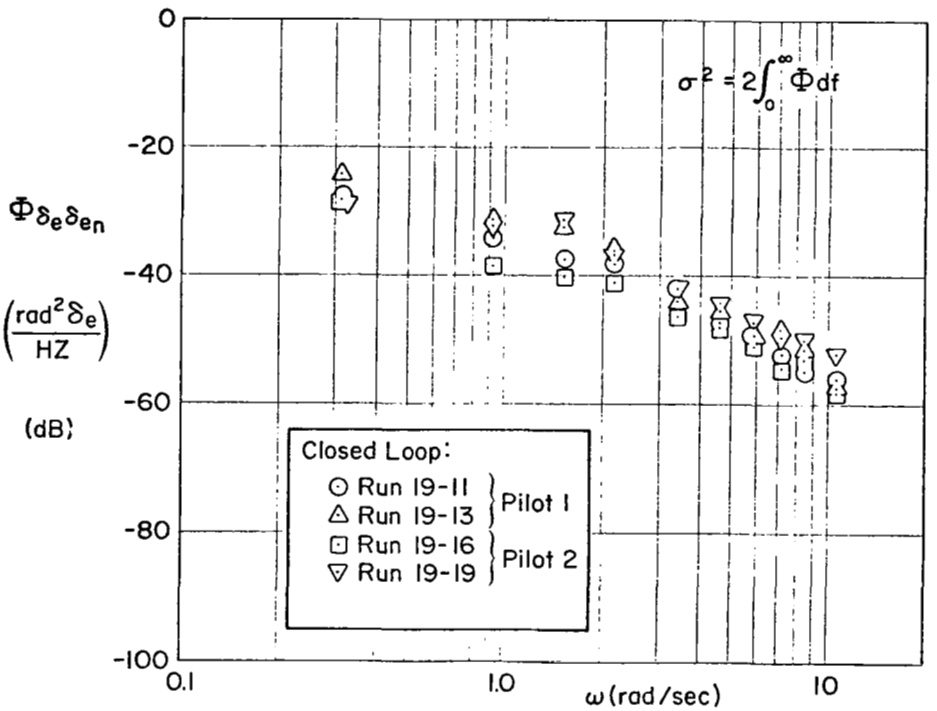

Figure 26. Remnant Spectra, All-Axis Control

SECTION V

CONNECTIONS BETWEEN RESPONSE AND SCANNING

The overall experimental data base for the response measurements presented in this report also include detailed measurements of the corresponding pilot eye scanning traffic. These data have already been reduced and the scanning traffic parameters and statistics are documented in NASA CR-1535 (Ref. 6). These reports together comprise an integrated interactive set of data and interpretations which are circumscribed by the theory of manual control displays (e.g., Ref. 3). Review and possible extension and refinement of this theory based on these new results was beyond the scope of this program. However, the key scanning statistics can be abstracted from the 1535 report and some correlations with pilot response observed, and this is accomplished in this section.

A. SUMMARY OF THE SCANNING STATISTICS

Ten of the 12 data runs analyzed in Sections II and III involved pilot scanning of various instruments on the "standard T" instrument approach panel used in the simulation. Details of the scanning traffic are given in the 1535 report, and the more important reduced parameters for the two primary instruments are given in Table 1. The mean look interval ($\overline{T}_s$) is the inverse of the mean look (or scan) rate ($\overline{f}_s$), and the variability of the look interval is given by its standard deviation (σ_{T_s}). This standard deviation was not included in the 1535 report, and it was computed subsequently and is given in Table 1 for the first time.

The following conclusions regarding the scanning traffic were reached in the 1535 report, based on all the data runs for the subject pilots:

- The scanning data were statistically stationary over the 100-sec approach time.
- The look rates on the altitude/director instrument were generally the same over all pilots and configurations.
- The look rates on the glide slope deviation instrument were significantly less for the flight director task.

TABLE 1. INDIVIDUAL RUN SCANNING STATISTICS

	CONFIGURATION	RUN	ATTITUDE/DIRECTOR INDICATOR				GLIDE SLOPE DEVIATION			
			$\bar{T}_d$	$\bar{f}_s$	η	σ_{T_s}	$\bar{T}_d$	$\bar{f}_s$	η	σ_{T_s}
PILOT 1	Flight Director (E1)	17-19	2.14	0.38	0.81	2.16	0.45	0.15	0.07	5.34
		19-12	1.26	0.52	0.65	1.05	0.58	0.27	0.16	3.38
	Longitudinal-Only (B1) (Director Bar Off)	19-5	0.71	0.50	0.35	0.85	0.72	0.65	0.47	0.44
	All-Axis (C1) (Director Bar Off)	19-11	0.71	0.49	0.35	1.03	1.05	0.50	0.53	0.73
		19-13	0.87	0.42	0.36	0.95	1.21	0.47	0.56	0.90
PILOT 2	Flight Director (E2)	19-22	2.98	0.28	0.84	3.65	0.53	0.12	0.06	5.06
		19-24	2.57	0.32	0.81	2.82	0.52	0.18	0.09	4.26
	Longitudinal-Only (B2) (Director Bar Off)	19-17	0.82	0.61	0.50	0.45	0.78	0.57	0.44	0.54
	All-Axis (C2) (Director Bar Off)	19-16	1.06	0.51	0.54	0.64	0.89	0.49	0.44	0.51
		19-19	0.92	0.48	0.44	0.64	1.12	0.48	0.54	0.52

$\bar{T}_d$ is the mean dwell time (duration of a single fixation in seconds).

$\bar{f}_s$ is the mean look rate (number of fixations per unit time).

η is the dwell fraction (fraction of total fixation time).

σ_{T_s} is the mean look interval standard deviation (in seconds, see text)

- The all-instrument scan rates were significantly less for the flight director task.
- The mean dwell times on the primary instruments were generally longer for the all-axis task than for the longitudinal-only task.
- The mean dwell times on the attitude/director instrument were much longer when the flight director was on (Configuration E).
- The mean dwell times on the glide slope deviation instrument were much longer with the flight director off (for Configurations B and C).
- The dwell fraction on the attitude/director instrument is much larger with the flight director on (Configuration E).
- The dwell fraction on the glide slope deviation instrument is greatly reduced with the flight director on, and it becomes essentially a peripheral instrument.

The results in Table 1 for the specific runs analyzed are consistent with these general conclusions. In addition, the flight director and all-axis task data are generally consistent from run to run for a given pilot, indicating that the scanning and response data can be lumped for a given pilot-configuration combination.

B. CORRELATIONS WITH PILOT RESPONSE DATA

The attitude/director instrument dwell times vary with pilot and task, and these variations seem at first to correlate with the respective crossover frequencies within a given task, i.e.,

- With the flight director task, Pilot 2 had higher crossover frequencies and longer dwell times.
- With Configurations B and C Pilot 2 had higher crossover frequencies and longer dwell times.

However, the correlation does not hold across tasks, e.g., for Pilot 2 the flight director task dwell times are more than double those for the multiloop cases (B and C) yet the respective (inner loop) crossover frequencies are about the same (1.1 to 1.4 rad/sec). Similarly, for Configurations B and C the outer loop crossover frequencies are about the same yet the dwell times differ on the glide slope deviation instrument. Thus, the variations in

dwell time that do occur appear to be related more to the degree of primacy of the instrument and the corresponding pilot scanning habits, than to the dynamic properties of the displayed variables. For example, the dwell times on truly peripheral instruments are remarkably constant across tasks and pilots (Ref. 6).

The mean look rates and dwell fractions vary sharply with the task, and they show minor interpilot differences in some cases. In the longitudinal-only (B) and all-axis (C) configurations where scanning between two primary instruments was required, the allocations of look rates and dwell fractions are closely related to the respective inner (θ) and outer (d) loop crossover frequencies. The ratio of inner and outer loop look rates is seen to be monotonically related to the ratio of crossover frequencies in Fig. 27. Note that the individual look rates ($\bar{f}_s$) alone in Table 1 do not correlate with the corresponding crossover frequencies across pilots, and taking the ratios removes the variability due to minor differences in pilot scan patterns. Similar results occur for the relation between dwell fraction (η) and crossover frequency, and the correlation of the ratios is shown in Fig. 28.

Variations in remnant levels between tasks are related to the pilot scanning activity. The normalized open-loop remnant injected at the pilot's input is higher with the flight director task (which involved some status scannings) than for the single instrument pitch attitude control task (see Fig. 23 and 24). Similarly the closed-loop remnant at pilot's output ($\Phi_{\delta_e \delta_{e_n}}$) was higher in the flight director case due to a combination of status scanning and increased crossover frequency. The closed-loop remnants at pilot's output in the multiloop tasks (B and C) are substantially higher at mid- and low-frequency than are the flight director remnants, despite a reduction in crossover frequencies. Hence, this must reflect an increase in pilot remnant which is associated with the requirement for scanning between the two primary instruments in the multiloop tasks. The closed-loop-multiloop remnant (especially for the all-axis task) shows little difference between pilots despite their pronounced difference in dynamic response properties, which suggests that the scanning related remnant may be a relatively invariant injected noise peculiar to the eye scanning process.

SECTION VI

CONCLUSIONS

A. SINGLE-LOOP DESCRIBING FUNCTIONS

The investigation included two single loop tasks: pitch attitude control and flight director control. In attitude control only one instrument was operating. For the flight director the primary display was again a single instrument, but the total task included some scanning of other panel instruments. In addition the flight director had: different controlled element dynamics at frequencies much less than the crossover region, more sensitive display scaling, and larger amplitude forcing function. Conclusions on describing function results are given below.

1. Pitch Attitude Control

- The pitch attitude control task describing function data are consistent with the results of CR-1238 (Ref. 8), except that the crossover frequencies are lower. The display scaling was about the same in both studies, as were the pilot gains; thus the major difference in the crossover region is the mid frequency amplitude ratios of the controlled elements. (N.B., if the two controlled elements were used in the same experiment this result would be unexpected. Instead, the crossover frequencies would tend to be unchanged, with the pilot making up any controlled-element gain differences.)

- The amplitude ratio and phase data show relatively little scatter, and there is no low frequency phase lag (α effect). The effective neuromuscular-manipulator subsystem lag may be larger than for simple manipulators, due to the dynamics of the transport-type control column.

- The two pilots exhibited their different styles by adopting different crossover frequencies. The lower gain pilot (1) had a crossover frequency which may be regressive.

- The open-loop pilot-vehicle properties correspond to a crossover model interpretation.

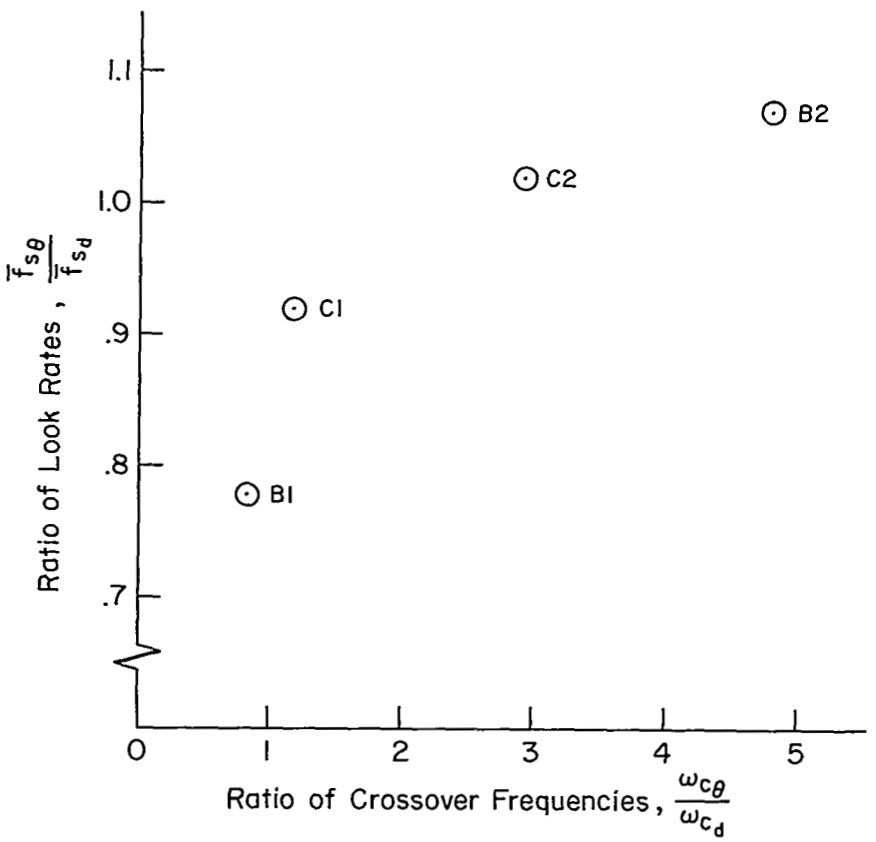

Figure 27. Relation Between Scanning and Crossover Frequency

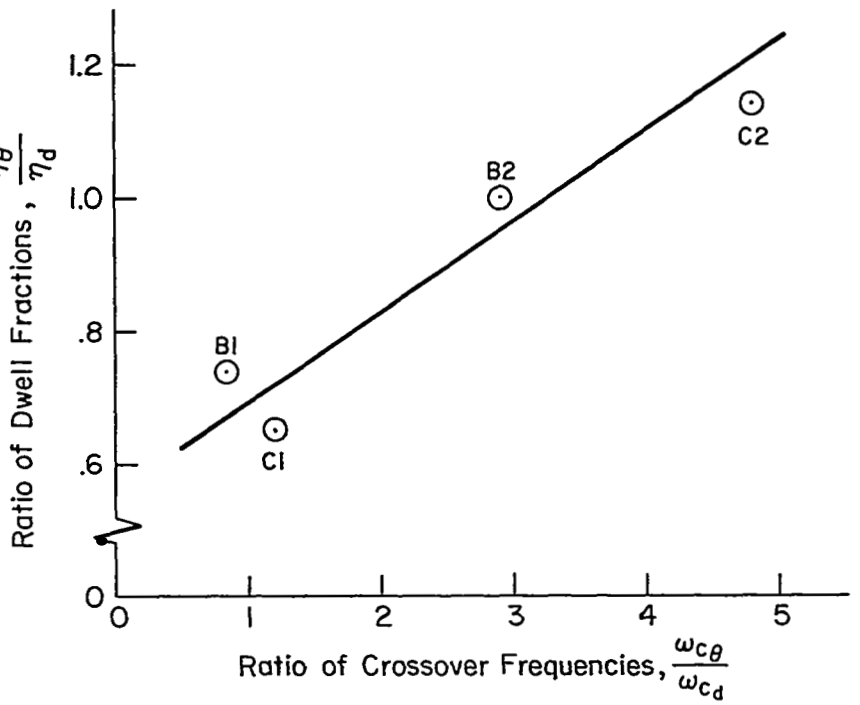

Figure 28. Relation Between Dwell Fraction and Crossover Frequency

2. Flight Director Control

- The flight director data differ somewhat from the pitch attitude control results:
  - Crossover frequencies with flight director are higher for both pilots.
  - Phase data with flight director have more scatter and indicate a low-frequency phase lag (α effect). This phase lag is below the attitude control measurement bandwidth, so it may not reflect a true difference.
  - Phase data for Pilot 2 indicate a mid-frequency phase lead, similar to the phase properties seen for this pilot in some of his multiloop results.
- The flight director describing function data in the crossover region are very similar to the single loop results in the CR-1238 study; more so in fact than are the pitch attitude control results.
- The association of higher gain with an increase in disturbance magnitude (for the flight director task compared with pitch attitude control) has precedent in the Ref. 9 results.
- The two pilots again exhibited their different styles by adopting different crossover frequencies (and gains), although these were closer (ratio 1.75) than for pitch attitude (ratio about 2.5). These may be associated with differences in scanning behavior. The lower gain Pilot 1 had a lower dwell fraction (74%) on the primary flight director instrument than did Pilot 2 with 82%.
- The flight director data are adequately described by the crossover model form in the mid-frequency region.

B. MULTILOOP DESCRIBING FUNCTIONS

Two multiloop control tasks were used: longitudinal-only (with lateral autopilot), and an all-axis longitudinal and lateral task with response measurements made for the longitudinal control loops only. Of the seven pilot subjects, data for two were analyzed in detail. Conclusions on describing function results are given below.

- The two pilots whose data were reduced in detail differed in their control style and overall strategy. Pilot 1 used a relatively low-gain inner (attitude) loop and high-gain outer (beam deviation) loop. This gave a well-damped closed-loop short period and a lightly damped phugoid. Pilot 2, on the other hand, adopted a high-gain inner loop and a relatively low-gain outer-loop characteristic; the short period was consequently lightly damped and the closed-loop phugoid well damped.

- The spectral ratio data were generally consistent for a given pilot across his longitudinal-only and all-axis runs. An exception occurred for Pilot 2, whose longitudinal-only spectral ratio data are somewhat different from the other multiloop results. The inner-loop data for this case show large low-frequency lead and a high crossover frequency which appears to be connected with a higher fractional scanning workload on the attitude instrument. The Pilot 2 all-axis data are to some extent similar, although the effects are not so prominent.

- In general, the response data were compatible with a simplistic view of what the describing function forms should be to satisfy the pilot/vehicle system guidance and control requirements. The data were also consistent with a "series" multiloop structure, comprising a pitch attitude inner loop driven by a beam deviation outer-loop reference. The pilot describing function forms in this interpretation are a gain and time delay for Y_θ, and a gain for Y_d.

- When compared with the CR-1238 results for the longitudinal task, both K_θ and K_d were smaller. This is associated with fundamental differences between the tasks in display and instructions. The CR-1238 experiment had a combined display, whereas a full panel (with scanning required) was used for the current data. Both disturbance signal levels and the experimenter's instructions and coaching of the subjects tended to induce high gains in the CR-1238 series. For the present results, great care was taken to instruct the pilots to exhibit their normal instrument approach behavior. Though still subjectively large, the disturbance levels were reduced as much as possible. Consequently, the crossover frequencies and associated system dynamic characteristics in the current study are felt to be closely representative of actual transport approach tasks.

- Some of the describing function data points deviate from simple model forms, even in the mid-frequency region. Nevertheless, these deviations are generally in the direction to improve system response, e.g., a lead "bump" in the phase near crossover.

- The derived pilot describing function parameters and closure criteria are summarized in Table 2. These show:

  - The inner-loop time delays (τ_θ) are larger for the all-axis (C) task than for longitudinal-only (B).

  - The inner-loop crossover frequencies for the all-axis (C) task are consistently higher than those for the longitudinal-only (B) situation.

  - The outer-loop crossover frequencies (ω_{c_d}) are about the same across all multiloop tasks and pilots.

TABLE 2

SUMMARY OF PILOT DESCRIBING FUNCTIONS RESULTS

	CONTROL CONFIGURATION	Y_θ OR Y_{FD}							Y_d					
		K_θ (LINEAR)	K_θ (LINEAR)	τ_θ† (SEC)	EQUALI-ZATION	ω_{c_θ} (RAD/SEC)	ϕ_{m_θ} (DEG)	K_{m_θ} (dB)	K_d* (LINEAR)	K_d (dB)	τ_d† (SEC)	ω_{c_d} (RAD/SEC)	ϕ_{m_d} (DEG)	K_{m_d} (dB)
PILOT 1	Pitch Attitude (A1) $\theta \rightarrow \delta_e$	2.1	.63	.43	$\frac{j\omega + 1.2}{j\omega + 4}$	.37	85	10						
	Flight Director (E1) FD $\rightarrow \delta_e$	5.5	2.6	.45	$\frac{j\omega + 1.2}{j\omega + 2.5}$	.8	55	5						
	Longitudinal-Only (B1) $\theta, d \rightarrow \delta_e$ Lateral Autopilot	.5	.5	.4	—	.33	77	14	84	38.5	0	.40	3	1.5
	All-Axis (C1) $\theta, d \rightarrow \delta_e$ Lateral Manual	.8	.8	.9	—	.45	62	6.8	57	35	0	.38	18	1.8
PILOT 2	Pitch Attitude (A2) $\theta \rightarrow \delta_e$	4.9	1.1	.43	$\frac{j\omega + 1.2}{j\omega + 5.4}$	.9	74	6						
	Flight Director (E2) FD $\rightarrow \delta_e$	6.5	3.1	.43	$\frac{j\omega + .82}{j\omega + 1.7}$	1.2	45	3						
	Longitudinal-Only (B2) $\theta, d \rightarrow \delta_e$ Lateral Autopilot	1.7	1.7	.7	—	1.2	6	1.5	38	31.5	0	.25	73	10
	All-Axis (C2) $\theta, d \rightarrow \delta_e$ Lateral Manual	1.5	1.5	.5-.9	—	1.14	26-0	4-0	52	34.5	0	.39	43	6.8

*Units of K_d are rad θ_c/rad glide slope deviation. Multiply K_d by .002 to get deg θ_c/ft d_e.

†Lags due to instrument dynamics have been removed.

- A major difference in behavior between the two pilots is exhibited by their crossover frequencies (ω_{c_θ}) on both the single-loop (A and E) tasks and the inner loop of the multiloop (B and C) tasks.

- As the differences between pilots in time delays on a given task are fairly small, the stability margins (φ_m and K_m) in the loop (inner loop for Pilot 2 and outer loop for Pilot 1) for which a pilot has the relatively higher gain are smaller.

- The multiloop pilot/vehicle describing function data interpreted in terms of crossover model forms are summarized in Table 3. They show that:

  - The inner-loop effective time delays (τ_{θ_e}) are about the same, except for C2 which shows a larger τ_{θ_e} in the data point near crossover. The effective inner-loop time delay shown includes some controlled element contributions.

  - Pilot 1 has a lower gain inner loop and higher gain outer loop than Pilot 2.

  - For each pilot, the all-axis (C) data show higher crossover frequencies (ω_{c_θ}) than the longitudinal-only (B) task.

TABLE 3

SUMMARY OF RESULTS BASED ON
CROSSOVER MODEL INTERPRETATION

	CONTROL CONFIGURATION	INNER LOOP				OUTER LOOP			
		ω_{c_θ} (RAD/SEC)	$\tau^*_{\theta_e}$ (SEC)	φ_m (DEG)	K_m (dB)	ω_{c_d} (RAD/SEC)	$\tau'^*_{d_e}$ (SEC)	φ_m (DEG)	K_m (dB)
PILOT 1	Longitudinal-Only (B1) $\theta, d \rightarrow \delta_e$ Lateral Autopilot	.3-.35	1	30-80	10-15	.25	3.6	30	8
	All-Axis (C1) $\theta, d \rightarrow \delta_e$ Lateral Manual	.5-.6	1	50-60	7-10	<.4	4	0+	0+
PILOT 2	Longitudinal-Only (B2) $\theta, d \rightarrow \delta_e$ Lateral Autopilot	1-1.1	1	30-35	4-6	.2	2.5-3.2	80	8-11
	All-Axis (C2) $\theta, d \rightarrow \delta_e$ Lateral Manual	1.2-1.4	.6-1.3	0+	0+	.2	3	30-60	5-9

*Instrument dynamic lag included.

- The effective outer-loop time delays (τ'_{de}) for Pilot 1 are greater than for Pilot 2, which is consistent with the differences in their inner-loop closure properties.

- The crossover model form is a reasonably good fit to the data in most cases for the all-axis results, and for one longitudinal-only case. Where it is not, the variations in the data from the model are generally such that system response is improved, hence the crossover model interpretation provides a conservative basis for estimation and analysis.

C. PERFORMANCE MEASURES

The performance measures are summarized in Table 4. Key comparisons and conclusions are listed below.

TABLE 4

PERFORMANCE MEASURES

	CONTROL CONFIGURATION	RUN	σ_{δ_e} (DEG)	σ_{θ_e} (DEG)	σ_{d_e} (FT)	σ_{FD_e} (DEG θ)	σ_θ (DEG)	$\sigma_{\dot{d}}$ (FT/SEC)	$\sigma_{\dot{d}}/\sigma_\theta$
PILOT 1	Pitch Attitude (A1) $\theta \rightarrow \delta_e$	17-4	.84	1.03					
	Flight Director (E1) FD $\rightarrow \delta_e$	17-19	1.73	1.67	21.7	.56	1.93		
		19-12	1.82	1.84	22.9	.59	2.08		
	Longitudinal-Only (B1) $\theta, \dot{d} \rightarrow \delta_e$ Lateral Autopilot	19-5	1.52	2.22	32.1		2.57	9.14	3.55
	All-Axis (C1) $\theta, \dot{d} \rightarrow \delta_e$ Lateral Manual	19-11	1.26	2.56	33.8		2.25	7.95	3.53
		19-13	2.40	3.22	38.0		3.51	10.9	3.11
PILOT 2	Pitch Attitude (A2) $\theta \rightarrow \delta_e$	19-20	2.4	.99					
	Flight Director (E2) FD $\rightarrow \delta_e$	19-22	3.17	1.90	24.8	.69	2.31		
		19-24	3.01	1.88	23.0	.65	2.22		
	Longitudinal-Only (B2) $\theta, \dot{d} \rightarrow \delta_e$ Lateral Autopilot	19-17	1.99	2.30	27.2		2.31	7.94	3.43
	All-Axis (C2) $\theta, \dot{d} \rightarrow \delta_e$ Lateral Manual	19-16	1.16	1.24	30.7		1.31	8.18	6.24
		19-19	1.95	1.87	43.8		1.91	11.1	5.82
Analog Pilot $\rightarrow$		17-8	4.2	2.18	15.3		2.41	7.86	3.26

- The overall beam deviation performance of the two pilots is not markedly different on any given task.

- The quality of beam-following task performance for the three cases is in the order: flight director; longitudinal-only; all axis.

- With the flight director, Pilot 2 has significantly larger (95% conf.) mean square elevator control response ($\sigma_{\delta_e}^2$) than Pilot 1; this is consistent with their differences in crossover frequency.

- The mean square elevator activity between the two pilots on the all-axis task is not much different, nor are the all-axis measures different from the longitudinal-only.

- Although the two pilots show marked differences in their dynamic response in the multiloop tasks, their overall control activity and outer-loop path errors are about the same.

- The mean square beam rate (rate of climb) values ($\sigma_{\dot{d}}^2$) do not differ between the two pilots for the multiloop tasks, nor do they differ significantly from the longitudinal analog pilot result.

- The $\sigma_{\dot{d}}/\sigma_\theta$ ratios for both pilots on three of the four multiloop conditions (excepting only the C2 runs) are very similar, indicating that the closed-loop modal response ratio relating $\dot{d}$ to θ for the dominant path mode is about the same across the board, despite differences in their control strategy.

D. LINEAR CORRELATIONS

The average linear correlations at pilot output ($\rho_{a_c}^2$) and at the error point ($\rho_{a_e}^2$) for the single-loop cases are given in Table 5. For the flight director configuration (E), $\rho_{a_e}^2$ is calculated for the displayed flight director error.

- For each pilot, the respective $\rho_{a_c}^2$ are generally about the same in both the multiloop tasks and the flight director tasks.

- The linear correlations at pilot's output ($\rho_{a_c}^2$) are larger for Pilot 1 than Pilot 2 in all tasks; this correlates with the greater single loop and inner multiloop crossover frequencies for Pilot 2.

TABLE 5

LINEAR CORRELATIONS

CONTROL CONFIGURATION	PILOT 1			PILOT 2		
	RUN	$\rho_{a_c}^2$	$\rho_{a_e}^2$	RUN	$\rho_{a_c}^2$	$\rho_{a_e}^2$
Pitch Attitude (A) $\theta \rightarrow \delta_e$	17-4	.78	.95	19-20	.18	.43
Flight Director (E) FD $\rightarrow \delta_e$	17-19	.76	.90	19-22	.39	.70
	19-12	.65	.76	19-24	.40	.68
Longitudinal-Only (B) θ, d $\rightarrow \delta_e$ Lateral Autopilot	19-5	.77		19-17	.44	
All-Axis (C) θ, d $\rightarrow \delta_e$ Lateral Manual	19-11	.35		19-16	.40	
	19-13	.64		19-19	.55	

E. REMNANT

The remnant data include power spectral densities of the uncorrelated components of the error and the pilot output. Normalized open-loop remnant, injected at the error point, were computed for the single-loop pitch attitude and flight director tasks.

- The flight director remnant is flat at low frequencies, and rolls off as a first-order lag at about the crossover frequency.
- The pitch attitude remnant is similar in shape to the flight director data at low frequencies, but peaks up at high frequency in the vicinity of the closed-loop neuromuscular mode.
- The flight director remnant (which includes the effects of status scanning) are somewhat higher at low and mid-frequency than the single-loop pitch attitude results.
- There is little difference in remnant between pilots in a given task, despite the differences in their detailed response properties (noted earlier).

For the multiloop cases basic remnant measurement at the pilot's output is in a closed-loop form, $\Phi_{\delta_e \delta_{e_n}}$, which cannot be uniquely converted to

open-loop form without specific assumptions. Therefore, the remnant comparisons are based on this closed-loop form without arbitrary conversions. Smoothed closed-loop remnant at pilot's output, $\Phi_{\delta_e \delta_{en}}$, shows little variation from run to run for a given pilot and task. Comparisons between tasks within pilots show differences which must be related to differences in response and performance. In general, the following occurs in the closed-loop remnant with both pilots:

- The single-loop and flight director data both roll off to low amplitude below 1 rad/sec, peaking up near crossover; while
- The longitudinal-only and all-axis data have their largest amplitude at the lowest frequency and roll off steadily.
- The flight director remnant data are generally greater than or equal to the multiloop (B and C) results.

For Pilot 1:

- The single-loop (A) and longitudinal-only (B) results are about equal, and they have the lowest amplitude.
- The flight director (E) and all-axis (C) data are about equal, and approximately 5-10 dB larger than the other two except (as noted above) at low frequency A is less than B, and E is less than C due to their different shape.

For Pilot 2:

- The longitudinal-only (B) and all-axis (C) data have about the same shape and amplitude.
- The flight director (E) and single-loop results (A) have about the same shape and amplitude; and the amplitudes are higher than for B and C, except for the low frequency roll-off.

Referring to the describing functions in Table 2, the remnant amplitudes in the mid-frequency are seen to relate generally to the crossover frequency of the inner (or dominant) loop, as the case may be. This is not unexpected, since the closed-loop remnant are being examined at the pilot output.

F. CONNECTIONS BETWEEN RESPONSE AND SCANNING

Differences in the individual pilot response properties are reflected in the corresponding scanning statistics (detailed in Ref. 6). Comparisons of these scanning data with the dynamic response data of this report leads to the following conclusions.

- Some scanning properties are insensitive to response and performance variations. Though variable, average dwell times on individual instruments don't change with changes in crossover frequency in the control loop for that instrument. There are differences between instruments, as noted in Ref. 6.

- Differences in the dwell fraction (i.e., the fractional scanning workload) do correlate with differences in the inner- and outer-loop crossover frequencies on the respective instruments. As the ratio of crossover frequencies increases, so does the ratio of dwell fractions.

- Similar positive correlations occur between ratios of look rates (average fixations per unit time) and ratios of crossover frequencies on the inner- and outer-loop instrument pairs.

G. OVERALL REMARKS

A new pilot response data base has been obtained, reduced, and interpreted. It contains response, performance, and eye scanning data for a range of single and multiloop instrument approach control tasks. The data are generally consistent with prior data for similar task conditions; and differences with prior data that are present can usually be attributed to differences in instructions, simulator configuration, and other experimental details.

The response data and pilot commentary show the expected result that the pilot "workload" increases with scanning requirements and control task complexity. This resulted in subjective pilot stress and significantly reduced system performance. The data reveal the causal details of the change in dynamic response and eye scanning between tasks and pilots.

Individual pilot style is a dominant feature of these data. It is evidenced by differences in loop closing strategy, response technique, and

corresponding panel scan patterns. For example, the two pilots had similar responses with the flight director, but they differed for the scanned multiloop control case, which involved the use of raw data from separated instruments. The differences between the two subjects generally span the useful range of control parameters for adequate stable system performance; the data when compared therefore provide a useful index to parameter variation in design and synthesis problems.

The pilot/vehicle system crossover model interpretations for both the inner- and outer-loop response more often than not correlate well with the consequences and interpretations of the significant properties of the pilot-alone describing functions. Hence, the crossover model approach (as updated by these data) with its several advantages can be extended to these kinds of multiloop situations as a very useful tool for estimation and prediction of pilot/vehicle response and performance properties.

REFERENCES

1. McRuer, Duane, Henry R. Jex, Warren F. Clement, and Dunstan Graham, A Systems Analysis Theory for Displays in Manual Control, Systems Technology, Inc., Tech. Rept. No. 163-1, Oct. 1967 (Revised June 1968).

2. Clement, Warren F., and Lee Gregor Hofmann, A Systems Analysis of Manual Control Techniques and Display Arrangements for Instrument Landing Approaches in Helicopters. Volume I: Speed and Height Regulation, Systems Technology, Inc., Tech. Rept. No. 183-1, July 1969.

3. Clement, Warren F., Henry R. Jex, and Dunstan Graham, "A Manual Control Display Theory Applied to Instrument Landings of a Jet Transport," IEEE Trans. on Man-Machine Systems, Vol. MMS-9, No. 4, Dec. 1968, pp. 93-110.

4. Allen, R. W., W. F. Clement, and H. R. Jex, Research on Display Scanning, Sampling, and Reconstruction Using Separate Main and Secondary Tracking Tasks, NASA CR-1569, July 1970.

5. Senders, John W., Jaime R. Carbonell, and Jane L. Ward, Human Visual Sampling Processes: A Simulation Validation Study, NASA CR-1258, Jan. 1969.

6. Weir, David H., and Richard H. Klein, The Measurement and Analysis of Pilot Scanning and Control Behavior During Simulated Instrument Approaches, NASA CR-1535, June 1970.

7. Klein, R. H., Description of STI Master Tape I Containing Pilot Response and Scanning Data for Instrument Approach Tasks, Systems Technology, Inc., Tech. Rept. No. 195-1, May 1970.

8. Stapleford, Robert L., Samuel J. Craig, and Jean A. Tennant, Measurement of Pilot Describing Functions in Single-Controller Multiloop Tasks, NASA CR-1238, Jan. 1969.

9. Schweizer, G., Pilot Behavior in VTOL Aircraft, AGARD Rept. 521, Oct. 1965.

10. Weir, David H., Compilation and Analysis of Flight Control System Command Inputs, AFFDL-TR-65-119, Jan. 1966.

11. Bullard, E. C., F. E. Oglebay, W. H. Munk, and G. R. Miller, A User's Guide to BOMM — A System of Programs for the Analysis of Time Series, Univ. of Calif., La Jolla, Inst. of Geophysics and Planetary Physics, Jan. 1966.

12. McRuer, Duane, Dunstan Graham, Ezra Krendel, and William Reisener, Jr., Human Pilot Dynamics in Compansatory Systems — Theory, Models, and Experiments with Controlled Element and Forcing Function Variations, AFFDL-TR-65-15, July 1965.

APPENDIX A

DESCRIPTION OF THE EXPERIMENTS

The experiments involved pilot control during a conventional Category II-like instrument approach in a six degree of freedom fixed-base simulation of a DC-8 aircraft. The experiments were performed at the NASA Ames Research Center. The panel layout was typical of a subsonic jet transport, with some configurations employing a flight director (FD). The subjects were airline pilots and copilots. The task was to fly an ILS (Instrument Landing System) approach from the outer marker (30,000 ft from threshold) to the middle marker in the presence of vertical gusts, θ_c, and glide slope beam bends, d_c. Aircraft motions, displayed signals, pilot response, and eye point of regard were recorded. Complete details of the experimental setup and procedures are given in Ref. 6, which also documents the scanning traffic. This appendix summarizes only those experimental details which are pertinent to interpreting the pilot/vehicle dynamic response data.

CONTROL CONFIGURATIONS AND PILOT INSTRUCTIONS

The experimental configurations are described in Table A-1. Configuration A was a pitch attitude tracking task designed to provide single-loop response data for correlation with other data and models. Configurations B and C involved a "raw presentation" of localizer and glide slope deviation, pitch and roll attitude, and peripheral instruments, but no flight director display.* Configuration E employed all the displays of C plus a lateral and longitudinal flight director display superimposed on the artificial horizon.

Other tasks used in the experimental program (but not included here) involved range varying versions of Configurations C and E. The range variation results in an increasing instrument display sensitivity and nonstationary controlled element dynamics. Hence, the pilot response must be nonstationary, and conventional describing functions are inappropriate. Range varying dynamics were studied for reference. Details are given in Ref.

*Called "All-axis" here; Configuration C was termed "Manual ILS" in Ref. 6.

TABLE A-1

EXPERIMENTAL CONFIGURATIONS

CONTROL CONFIGURATION	DESCRIPTION	PURPOSE	INSTRUCTIONS TO SUBJECTS
A Pitch Attitude	Single axis tracking task with pitch attitude display and forcing function. Other instruments masked. Other axes controlled by autopilot. No flight director.	Tie in with single loop tracking data.	Simulates a portion of the approach task. Control pitch attitude only, and try to keep pitch error equal to zero. There is some turbulence. The lateral autopilot is ON.
B Longitudinal-only	Three degree of freedom longitudinal task. Lateral axes under autopilot control, but instruments visible. No flight director.	Provide longitudinal scanning task, and basis for validating multiloop pilot response model.	Simulates a split-axis manual approach under Category II conditions. Control only the longitudinal motions. An autopilot is controlling the lateral motions. There is some turbulence. Try to keep the glide slope needle centered at all times.
C All-axis	All axis approach task. The glide slope deviation computer range was fixed at 30,000 ft from threshold; however the altimeter and rate of climb meters appeared normal (showed a varying range). No flight director.	Provides all axis task. Reference case for comparison with split axis, range varying, and flight director cases.	Simulates a Category II manual ILS approach. There is some turbulence. Try to keep the glide slope and localizer needles centered at all times.
E Flight Director	All axis approach task with flight director on, and driven by forcing functions. Same as Configuration C plus flight director.	Provides equalized, integrated display and all axis task. Typical of modern approach practice.	Simulates a Category II FD approach. There is some turbulence. Use the Director to follow the approach path, keeping the glide slope and localizer needles centered. Pitch commands must be obeyed immediately to avoid a standoff. The glide slope and localizer needles must be monitored.

In addition to the instructions in Table A-1, each of the pilot subjects was given an overall briefing on the program and its research goals. The following points were covered:

- Simulated airplane is a DC-8
- The task involves a Category II-like approach using conventional instruments up to the point of visual runway acquisition, flare, and landing. There will be no surprises or unexpected emergencies.
- A set of sensors mounted on eyeglass frames will be used to monitor eye scanning.
- Pitch attitude and glide slope beam deviation inputs are used to make the task difficult. It will look like severe turbulence and it may seem a little artificial, but try and fly it as you would an actual approach.
- This study is considering "limiting cases" which are the ones which govern designs. Assume that you have to make this approach and that you can't abort. The only alternative is to bail out or crash land.

This was followed by an informal discussion of the simulation layout and general procedures.

After becoming settled in the left seat in the simulator the pilots were given general instructions regarding the initial conditions and cockpit procedures. These instructions were:

> "The task is to fly the approach from outside the outer marker to inside the middle marker. You will begin stabilized on the 3 deg glide slope. Beam acquisition is not required. The 'bug speed' is 135 kts. Both gear and flaps are down and all check-lists are completed. The initial altitude is 2,000 ft and the field elevation is 312 ft. The problem will end prior to runway visual range and there is no need to flare or look for the runway. The experimenter will announce the end of the run. Try to keep the glide slope and localizer needles centered at all times.
>
> Due to the simulation setup and limitations we would like you to try to follow these additional conditions:

- Retrim pitch attitude ball at start of run.
- Don't use the trim button or trim wheels.
- Full flap all the way down the glide slope.
- There should be no need for throttle movements (it's initially trimmed)."

These general instructions were not given to the pilot more than once or twice, but the appropriate instructions in the right hand column of Table A-1 were given to the pilot prior to each individual run. The need to try to keep the glide slope and localizer needles centered at all times was reemphasized continuously.

FORCING FUNCTIONS

Command inputs in pitch angle and glide slope deviation provided the forcing functions and the basis for describing function measurements. They were shaped to represent a vertical gust disturbance and glide slope beam deviation noise, respectively. Gusts actually enter the system through the airframe, not as commands, but a true gust input results in poor measurements since the signal/noise ratio can be low at high frequency. An equivalent pitch attitude command was used to avoid these measurement problems.

The equivalent power spectrum of the random-appearing pitch attitude forcing function is shown by the solid line in Fig. A-1. The circles indicate the sine wave components which are summed to generate the spectrum. The effective forcing function bandwidth was about 0.8 rad/sec. The high frequency "shelf" provided some measurement power at and beyond the expected crossover region. The input had an rms pitch deviation of about 1.2 deg, equivalent to a vertical gust with an rms amplitude of about 5 ft/sec. This forcing function is roughly consistent with that used in Ref. 8 which had a bandwidth of 1 rad/sec and an rms of 8 ft/sec.

The glide slope beam deviation forcing function is shown in Fig. A-2. The circles represent the sine wave input components. The effective forcing function bandwidth is about 0.3 rad/sec with a second-order rolloff and a -20 dB shelf. The relative amplitude was set to have an rms of 0.04 deg

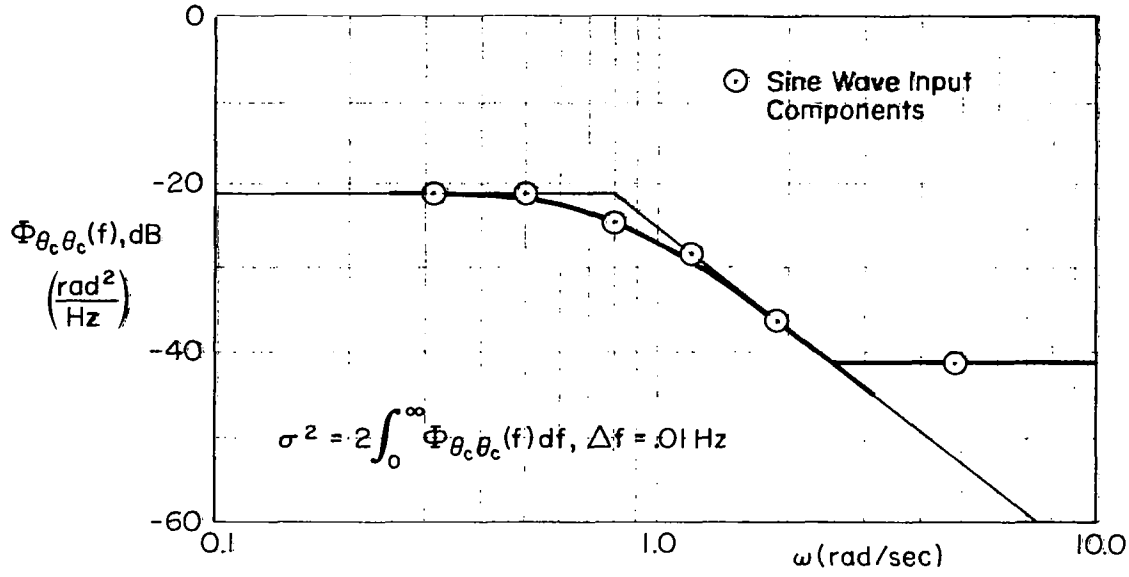

Figure A-1. Power Spectral Density of Pitch Angle Forcing Function

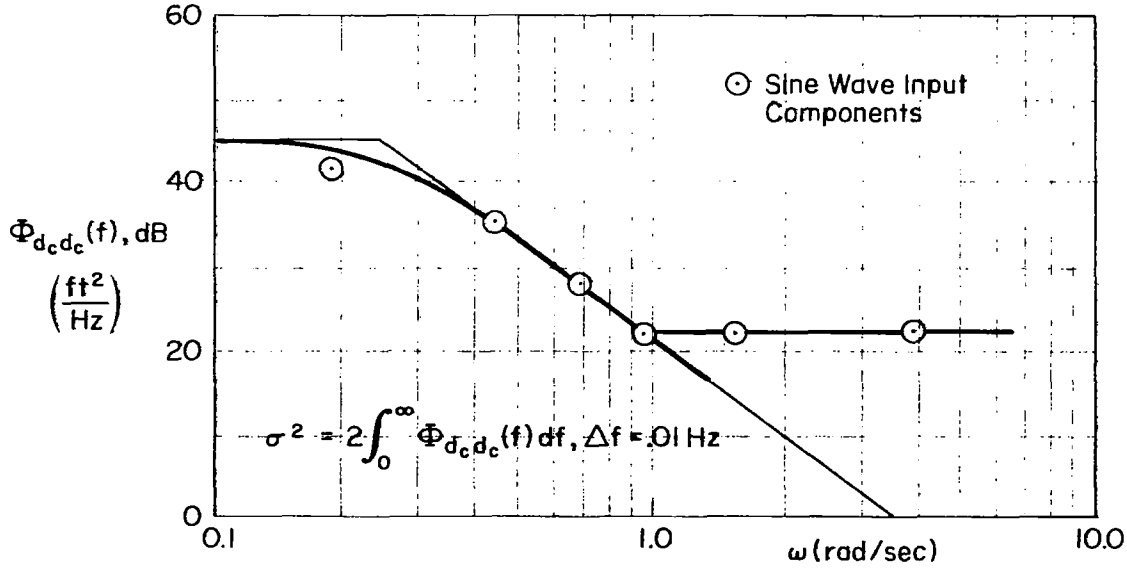

Figure A-2. Power Spectral Density of Beam Deviation Forcing Function

glide slope angle (21 feet at 30,000 ft range), or about 0.2 dots of rms needle deflection. This forcing function is consistent with beam bend data of Ref. 10.

The forcing functions drove the flight director (as well as the basic instruments) when that configuration was used.

INSTRUMENT DYNAMICS

Frequency response measurements were made for all the cockpit instrumentation (panel layout is shown in Ref. 6. This was done using a photocell and calculating the phase shift from the zero axis crossings. Amplitude ratios were taken subjectively by the experimenter. Figures A-3 to A-5 present these results. The phase data were fit in the region of crossover by the pure time delays shown, which were removed from the overall human pilot describing function measurements.

MANIPULATOR

A transport-type wheel and control column were used. Static force-displacement data were obtained for the simulator elevator system (Fig. A-6). Although dynamic responses were not measured, an estimate of the system's frequency and damping may be obtained from Fig. A-7 for releases from a given displacement.

CONTROLLED ELEMENTS

One landing approach flight condition was used for the simulated DC-8, with an approach speed of 135 kt, gross weight of 180,000 lb, flaps 50°, and gear down. The yaw damper was assumed on. No other augmentation, such as autothrottle, was used. For the frozen range configurations analyzed, the aircraft was trimmed straight and level at a range of 30,000 ft and 1,650 ft altitude above ground level in order to define its dynamic properties. The rate of climb and pitch attitude meters were appropriately biased, and the altimeter was driven by an integrator to make the display represent descent along the 3° glide slope. All prelanding checklists were assumed complied with.

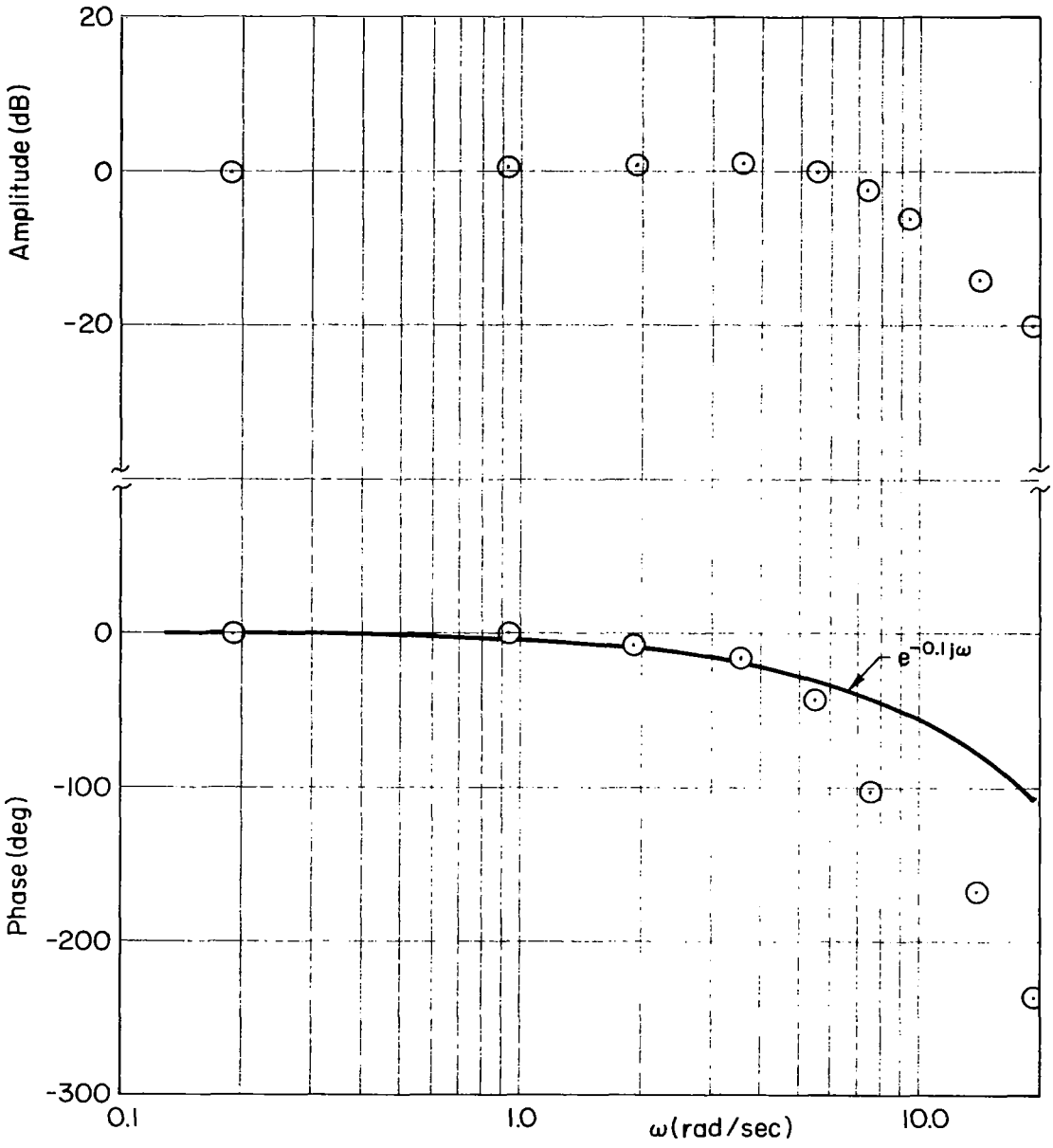

Figure A-3. Pitch Attitude Instrument Frequency Response

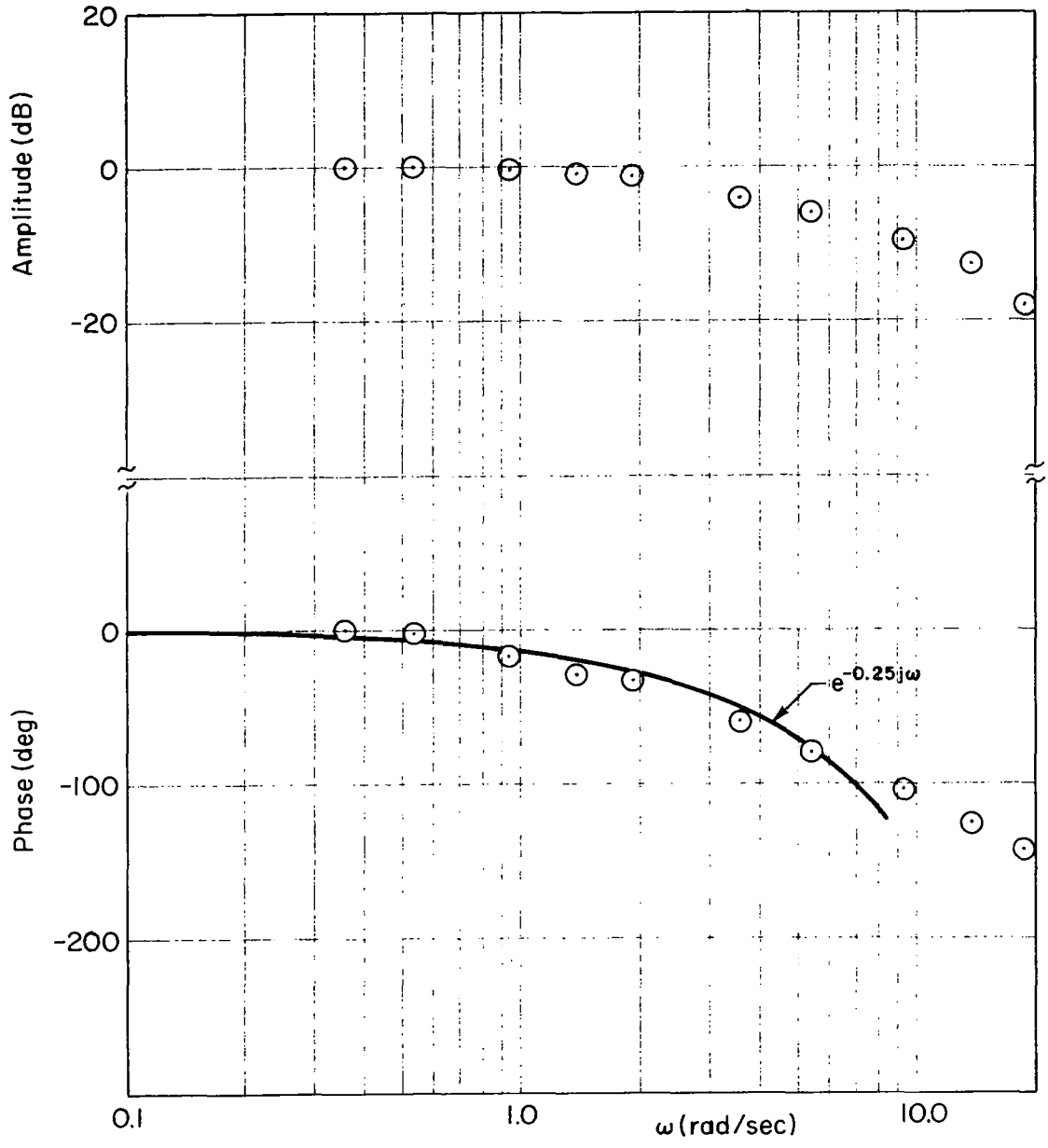

Figure A-4. Glide Slope Instrument Frequency Response

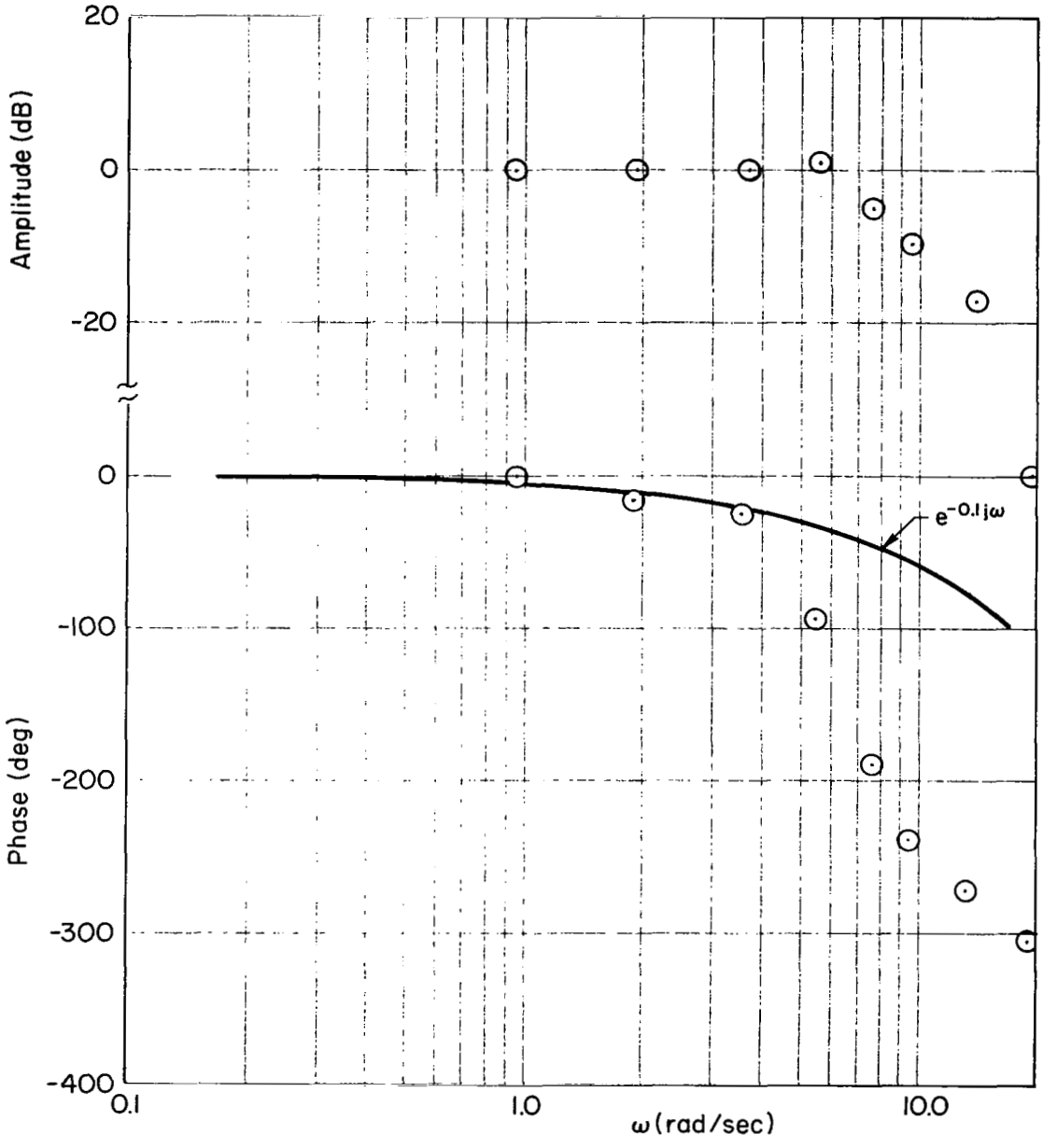

Figure A-5. Longitudinal Flight Director
Instrument Frequency Response

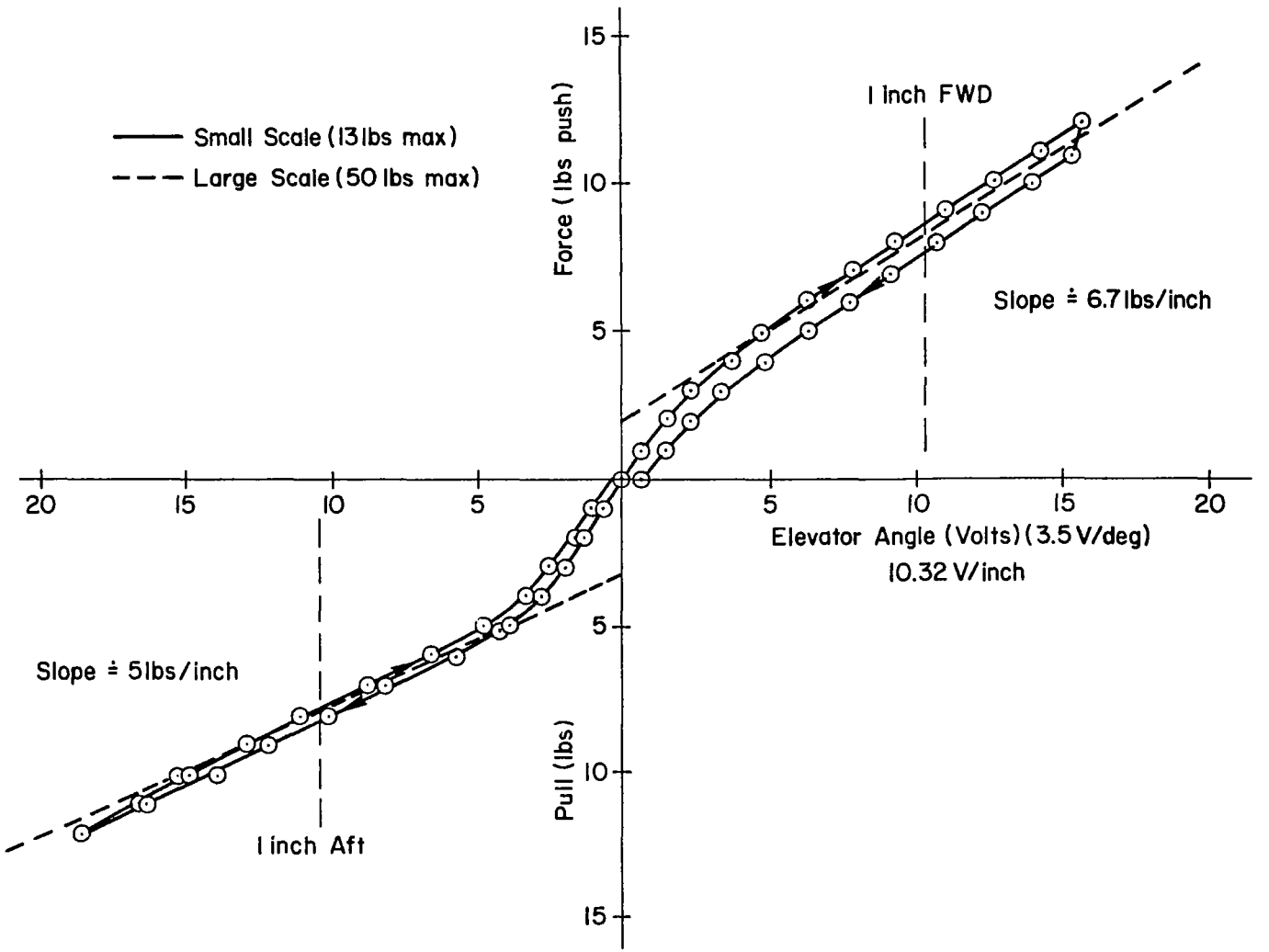

Figure A-6. Longitudinal Control Column Force Characteristics

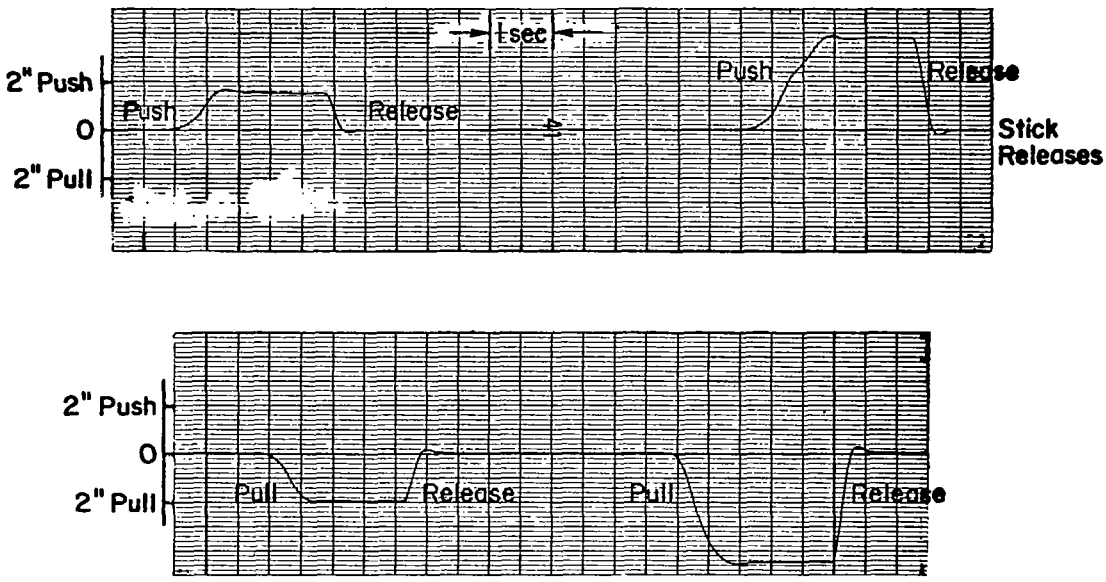

Figure A-7. Longitudinal Control Column Response from a Displacement Release

The equations of motion and stability derivatives are detailed in Ref. 6. The linearized perturbation equations gave the following longitudinal transfer function denominator and numerator polynomials:*

$$\Delta = [0.0865\,;\,0.166][0.627\,;\,1.23]$$

$$N^{\theta}_{\delta_e} = -0.915(0.101)(0.646)$$

$$N^{\dot{a}}_{\delta_e} = 9.25(-3.63)(0.0352)(4.42)$$

The resulting controlled element; $j\omega$-Bode plots for pitch attitude and beam deviation to elevator control are given in Figs. A-8 and A-9, respectively. The curves and asymptotes correspond to the factors shown above. The over-plotted frequency response points were obtained from the reduced analog pilot data.

*For brevity, the polynomial factors $A[s^2 + 2\zeta\omega s + \omega^2]$ are written $A[\zeta\,;\,\omega]$, and $A(s + a)$ is written $A(a)$.

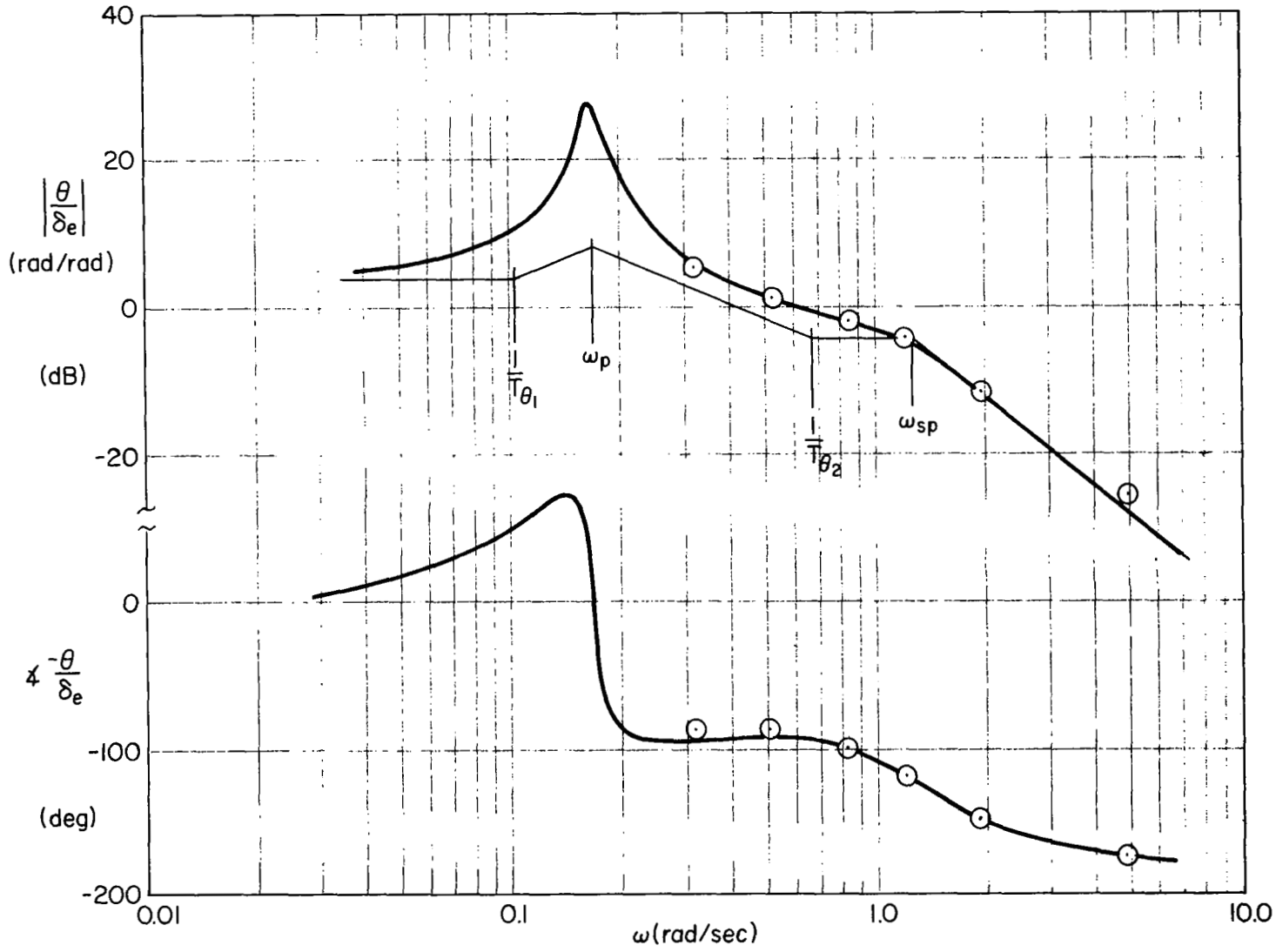

Figure A-8. Open-Loop Pitch Attitude to Elevator Response

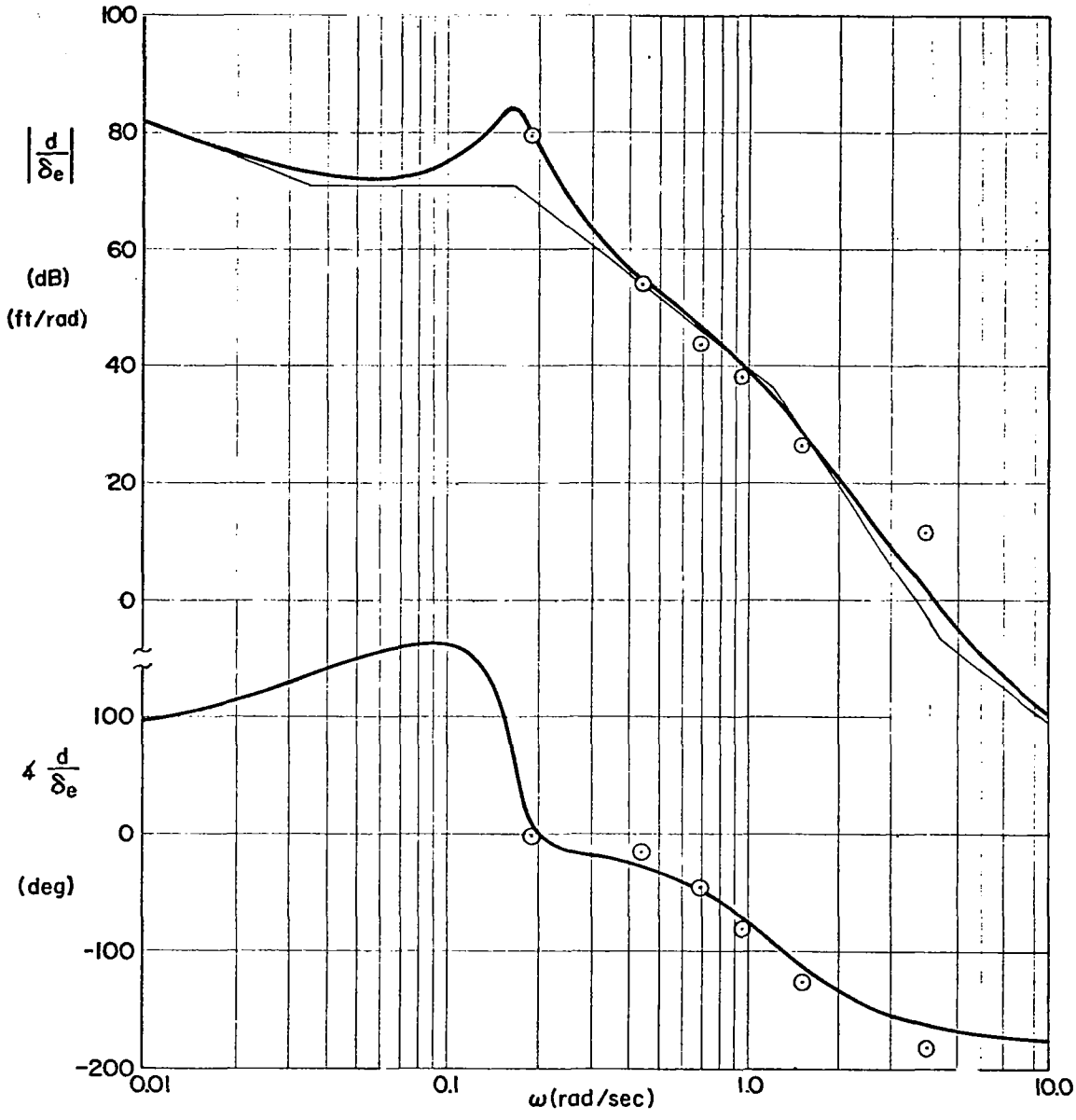

Figure A-9. Open-Loop Beam Deviation to Elevator Response

The longitudinal flight director computer equation was

$$FD = 0.0005d_e + 0.5\theta_e \frac{s}{s + 0.082}$$

The beam deviation error, d_e is in feet, and the pitch attitude error, θ_e, is in radians. The open-loop longitudinal flight director transfer function for a glide slope range of 30,000 ft becomes:

$$\frac{FD}{\delta_e} = \frac{-0.453(0.048)(0.065)[0.8\ ;\ 0.4]}{(0)(0.082)[0.087\ ;\ 0.166][0.63\ ;\ 1.23]}$$

The units are arbitrarily selected to be pitch angle. The $j\omega$-Bode plot is shown in Fig. A-10. The overplotted data points are a direct measure of the effective controlled element dynamics obtained from the reduced analog pilot data. The additional lag in the points at high frequency is due to filtering in the flight director computer.

PILOT-SUBJECT CHARACTERISTICS

Of the seven pilots used altogether in the experimental program, the data for two were selected for the detailed dynamic response analysis presented in this report. The pilots were volunteers who had an interest in the program and its eventual outcome, and their selection was based on the following factors:

- Interest, motivation, and availability
- Experience and current flight assignment
- Acceptance of the simulation
- Quality of eye point of regard data (minimum saccade artifacts, eyelid lag, drift, etc.)
- No need for corrective glasses, since it interfered with the eye movement device.

These qualities were also considered in selecting the data for detailed analysis. The pilots were paid a modest hourly rate.

The pilots reflected a cross section of age and background. Pilot 1 was a senior instructor captain with multiengine piston and jet bomber experience. Pilot 2, a younger copilot, transitioned to commercial flying via the general aviation/light aircraft route. Pertinent biographical details are given in Table A-2.

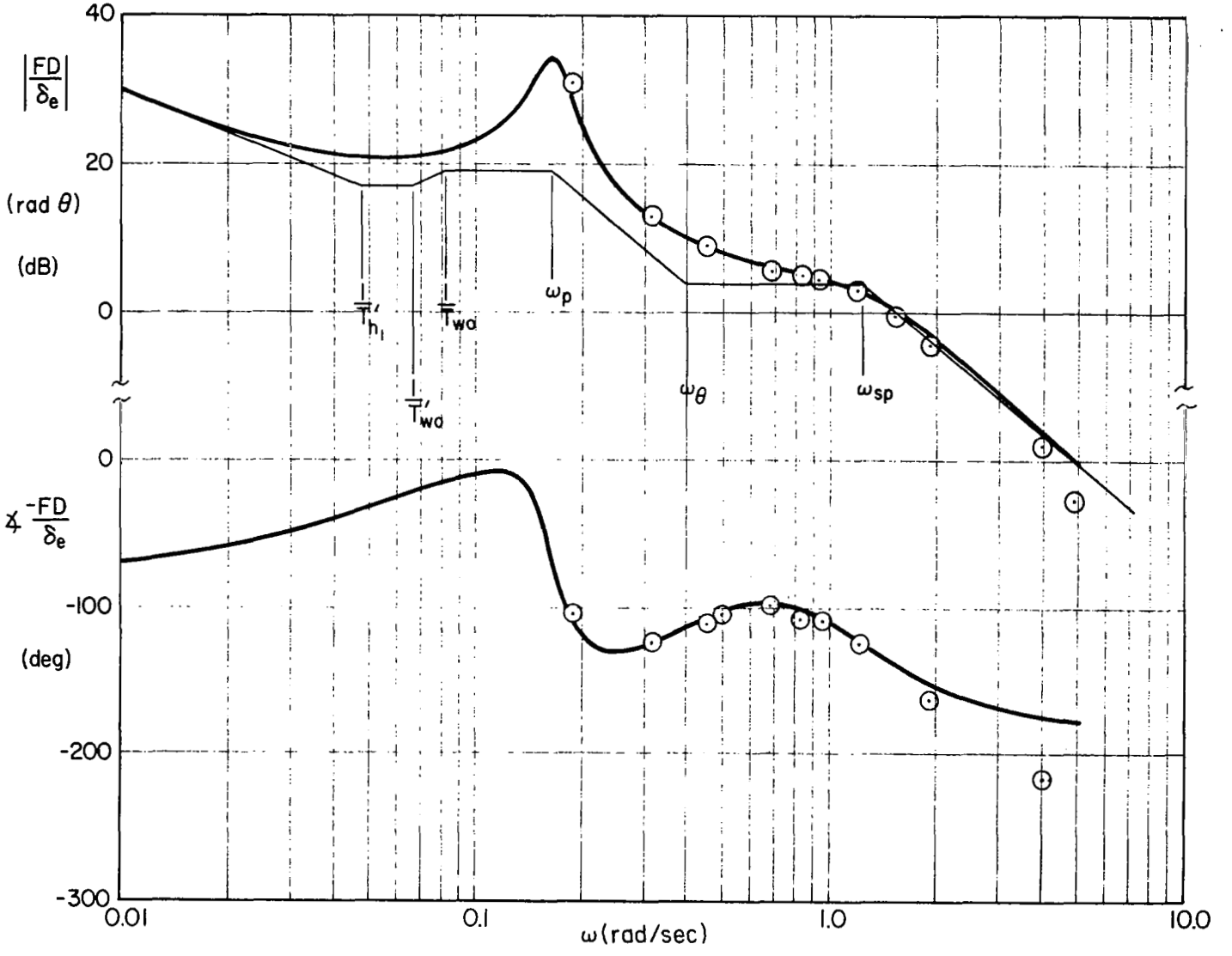

Figure A-10. Open-Loop Longitudinal Flight Director to Elevator Response

TABLE A-2

BIOGRAPHIC SUMMARY OF PILOT SUBJECTS

CURRENT EQUIPMENT	EXPERIENCE
Aircraft: B-707 Flight Director: Sperry Panel Configuration: 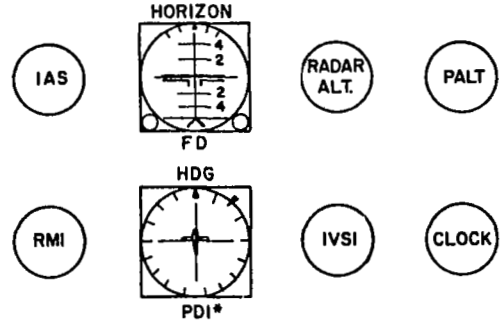 *Glide slope and localizer	Pilot No. 1 Age: 50 Position: Training Captain (PAA) Total Hours: 14,500 Commercial Flight Experience: 1,600 hrs jet (707, 720) 10,800 hrs recip. (DC-3, DC-4, Convair 340, 240) Military Flight Experience: 1,300 hrs recip. (B-25, C-121, Bristol) 300 hrs fighter (P-51) Private Flight Experience: None Number of ILS Approaches: 500 Hours Last 6 Months: 230 Number of Category II Landings: 55 Last Category II Landing Within: 1 week
Aircraft: B-720B Flight Director: Collins FD-108 Panel Configuration: 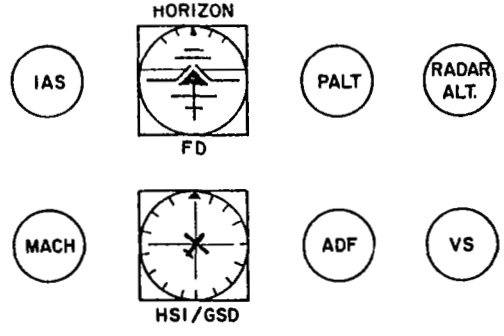 	Pilot No. 2 Age: 26 Position: Copilot (Western) Total Hours: 3,400 Commercial Flight Experience: 1,200 hrs jet (707) 145 hrs simulator Military Flight Experience: None Private Flight Experience: 2,500 hrs (Cessna 120, 310) Hours Last 6 Months: 200 Number of ILS Approaches: 100 (est.) Last Category II Landing Within: None

APPENDIX B

DATA REDUCTION PROCEDURES AND ANALOG PILOT

DATA REDUCTION

The pilot/vehicle response data were digitized at 40 samples/sec and reduced digitally using the BOMM Program for Time Series Analysis (Ref. 11). The reduced data include:

- Mean, mean square, amplitude, histograms, and higher order moments for the system variables.
- Close-spaced (Δf = 0.01 Hz) and smoothed (Δf = 0.1 Hz) power spectra for the system variables.
- Smoothed remnant (Δf = 0.1 Hz) at pilot's control output, $\Phi_{\delta_e \delta_{e_n}}$.
- Spectral ratios between response variables and forcing functions; the ratios of Fourier coefficients at the respective component input frequencies.

The statistical and remnant results are given in the main text, and the multiloop spectral ratios for the subject pilots are in Appendix C.

Open and closed loop describing functions were computed for the single loop and multiloop tasks, using the spectral ratios. The block diagram forms assumed for data reduction and interpretation are shown in Fig. B-1. The "series" form for the multiloop case (Fig. B-1c) was selected for computational convenience and simplicity of model form, as reflected in prior results (Ref. 8). An equivalent "parallel," or other, structure could have been used. The remnant is shown injected at the error point for the pitch attitude and flight director tasks, and corresponding data interpretations are given in the main text. Though present, the remnant is not shown explicitly in the multiloop case, and only the closed loop remnant at pilot's output was considered in this study.

The single loop describing function for the pitch attitude task is computed from the following relation of the spectral ratios:

$$Y_\theta = \frac{\delta_e/\theta_c}{\theta_e/\theta_c} \qquad \text{(B-1)}$$

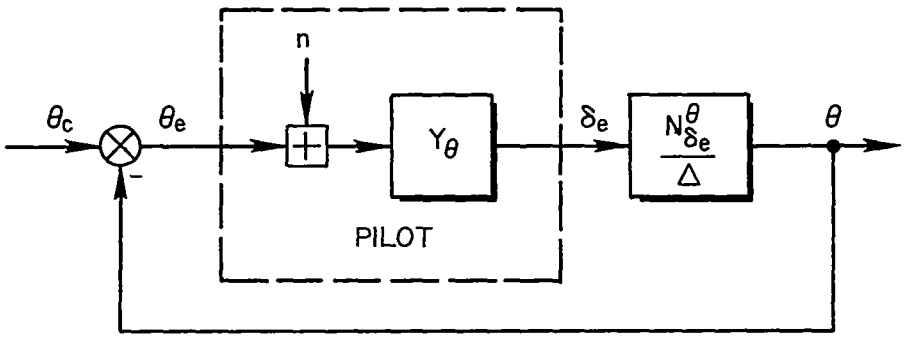

a) Pitch Attitude Task, Configuration A

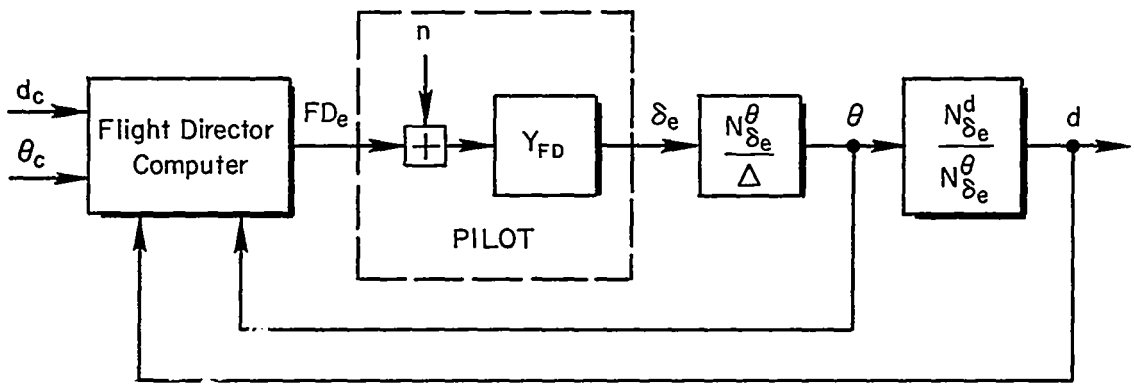

b) Flight Director Task, Configuration E

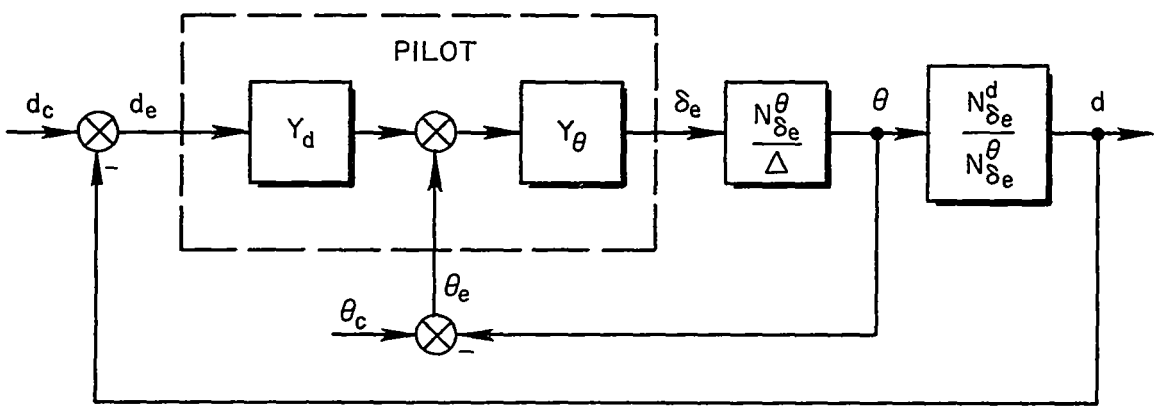

c) Longitudinal Only and All Axis Tasks, Configurations B and C

Figure B-1. Pilot/Vehicle System Models for Data Reduction

It is defined only at the discrete frequencies corresponding to the sine wave components in the random-appearing θ_c forcing function (see Appendix A). The flight director task pilot describing function is equally simple, i.e.,

$$Y_{FD} = \frac{\delta_e/(d + \theta)_c}{FD_e/(d + \theta)_c} = \frac{\delta_e/FD_c}{FD_e/FD_c} \tag{B-2}$$

This is defined only at the combined discrete forcing function frequencies, which acts like a single forcing function denoted by $(d + \theta)_c = FD_c$.

Calculation of the multiloop describing functions, Y_θ and Y_d, is more involved. Using the series structure of Fig. B-1c, several alternative forms have been derived (Ref. 8). The pitch attitude inner loop describing function has the general form

$$Y_\theta = \frac{N_i}{D_j} \tag{B-3}$$

with alternative numerators and denominators given by

$$N_1 = \frac{\delta_e}{\theta_c} \tag{B-4}$$

$$N_2 = \frac{\theta}{\theta_c} \frac{\Delta}{N^\theta_{\delta_e}} \tag{B-5}$$

$$N_3 = \frac{d}{\theta_c} \frac{\Delta}{N^d_{\delta_e}} \tag{B-6}$$

$$D_1 = \frac{\theta_e}{\theta_c} - \frac{d}{d_c} \tag{B-7}$$

$$D_2 = \frac{d_e}{d_c} - \frac{\theta}{\theta_c} \tag{B-8}$$

Because of the prewhitening effect of the aircraft dynamics, N_1 generally has the best signal to noise properties at high frequency (relative to

crossover), while N_2 and N_3 are better at mid- and low frequency, respectively. The subsequent analog pilot results illustrate these points, while it is less evident in the human pilot response (Appendix C). Both denominators involve the difference of two terms, and this difference can be small at low frequency. Thus, small errors in measuring the spectral ratios are amplified, and there is a lower limit on the frequency range for which meaningful measurements can be obtained. Equally important is the fact that the two terms in each denominator form are referenced to a different forcing function, hence interpolation of the spectral ratios between input frequencies is required before the sum can be computed. The practice in this study has been to interpolate d/d_c and d_e/d_c to the θ_c input frequencies, since the inner loop describing function is being computed.

The outer loop beam deviation describing function, Y_d, has several alternative forms, also, i.e.

$$Y_{d_1} = \frac{\delta_e/d_c}{\delta_e/\theta_c} \tag{B-9}$$

$$Y_{d_2} = \frac{\theta/d_c}{\theta/\theta_c} \tag{B-10}$$

$$Y_{d_3} = \frac{d/d_c}{d/\theta_c} \tag{B-11}$$

Ideally, as with the Y_θ numerators, these have their peak amplitude ratio in different frequency regions. Best signal to noise ratio should be obtained at high, medium, and low frequency with Eqs. (B-9) to (B-11) respectively. This is the case with the analog pilot, but it is less true with the less ideal human pilot spectral ratios (Appendix C). Interpolation to the common input frequency components is also required here, and the practice has been to estimate the θ_c spectral ratios at the d_c frequencies for these outer loop calculations.

Fitting and interpreting the multiloop data is an artistic but crucial step. It depends on an understanding of the system guidance and control requirements, previous data, etc.; and requires a fairly intensive iteration

and aggregation of the results. Attempts were made in this study to compute the multiloop describing functions numerically using fairly elaborate model forms and optimization criteria. The results were generally unsuccessful; because critical features of the data could not be distinguished from variability in some of the points, and the rules and criteria were not sufficiently elaborated to prescribe and constrain the result.

LONGITUDINAL ANALOG PILOT

Pre-experimental analyses were made to estimate pilot/vehicle response and performance in the multiloop longitudinal control task. The results were used in experimental planning and data interpretation, and they were mechanized as an analog pilot during the simulation experiments. The longitudinal analog pilot provided the following, among other things:

- A low noise, linear controller element for checking simulator operation and data reduction procedures, and for calibrating residual error levels in the data.
- A basis for on-line assessment of human pilot response properties; to monitor learning and proficiency and to compare subject with the model or other subjects.
- A reference example of spectral ratios, describing functions, and performance measures useful in data interpretation.

The analog pilot did not include remnant.

The longitudinal analog pilot block diagram has the mechanization shown in Fig. B-1c. The form of the inner loop pitch attitude describing function was assumed to be

$$Y_\theta = K_\theta \frac{(T_L s + 1)}{(T_I s + 1)} \frac{\left(-\frac{\tau s}{2} + 1\right)}{\left(\frac{\tau s}{2} + 1\right)} \qquad \text{(B-12)}$$

The beam deviation describing function was

$$Y_d = K_d \qquad \text{(B-13)}$$

The vehicle dynamics are given in Appendix A. The values assumed for the analog pilot parameters were:

$$K_\theta = -2.8$$

$$T_L = .667 \text{ sec}$$

$$T_I = .1 \text{ sec}$$

$$\tau = .35 \text{ sec}$$

$$K_d = +.00265 \text{ rad } \theta/\text{ft (for 30,000 ft range)}$$

$$= .15 \text{ deg } \theta/\text{ft}$$

$$= 79.5 \text{ rad } \theta/\text{rad } d_e; \ (d_e = \text{beam deviation error})$$

The pilot/vehicle response properties for pitch attitude control are summarized with the Bode and root locus plots in the system survey of Fig. B-2. The amplitude ratio shows a broad K/s region in the neighborhood of 1 to 2 rad/sec, good mid-frequency gain, acceptable low frequency response, and good dipole suppression. The crossover frequency is about 2.1 rad/sec. The loop closure is sensitive to lead, and the inverse lead time constant cannot be much smaller without lowering the mid-frequency gain. This would also be reflected in the pilot rating and commentary.

The beam deviation (outer) loop was closed using the series structure of Fig. B-1c. The open outer-loop transfer function is given by

$$\left(\frac{d}{d_e}\right)_{\theta \rightarrow \delta_e} = \frac{Y_d Y_\theta N^d_{\delta_e}}{\Delta'} \qquad \text{(B-14)}$$

where $\Delta' = \Delta + Y_\theta N^\theta_{\delta_e}$ (roots of inner loop closure).

The beam deviation loop system survey is given in Fig. B-3. Due to the series construction, the inner-loop pilot time delay and lead equalization are effectively part of the outer-loop describing function also. Additional low frequency outer-loop lead would be detrimental by producing a nuisance mode at the closed-loop short-period frequency yet not increasing the maximum crossover frequency. A pilot gain of 0.15 deg θ per foot beam deviation error results in a crossover frequency of 0.5 rad/sec with good phase and gain

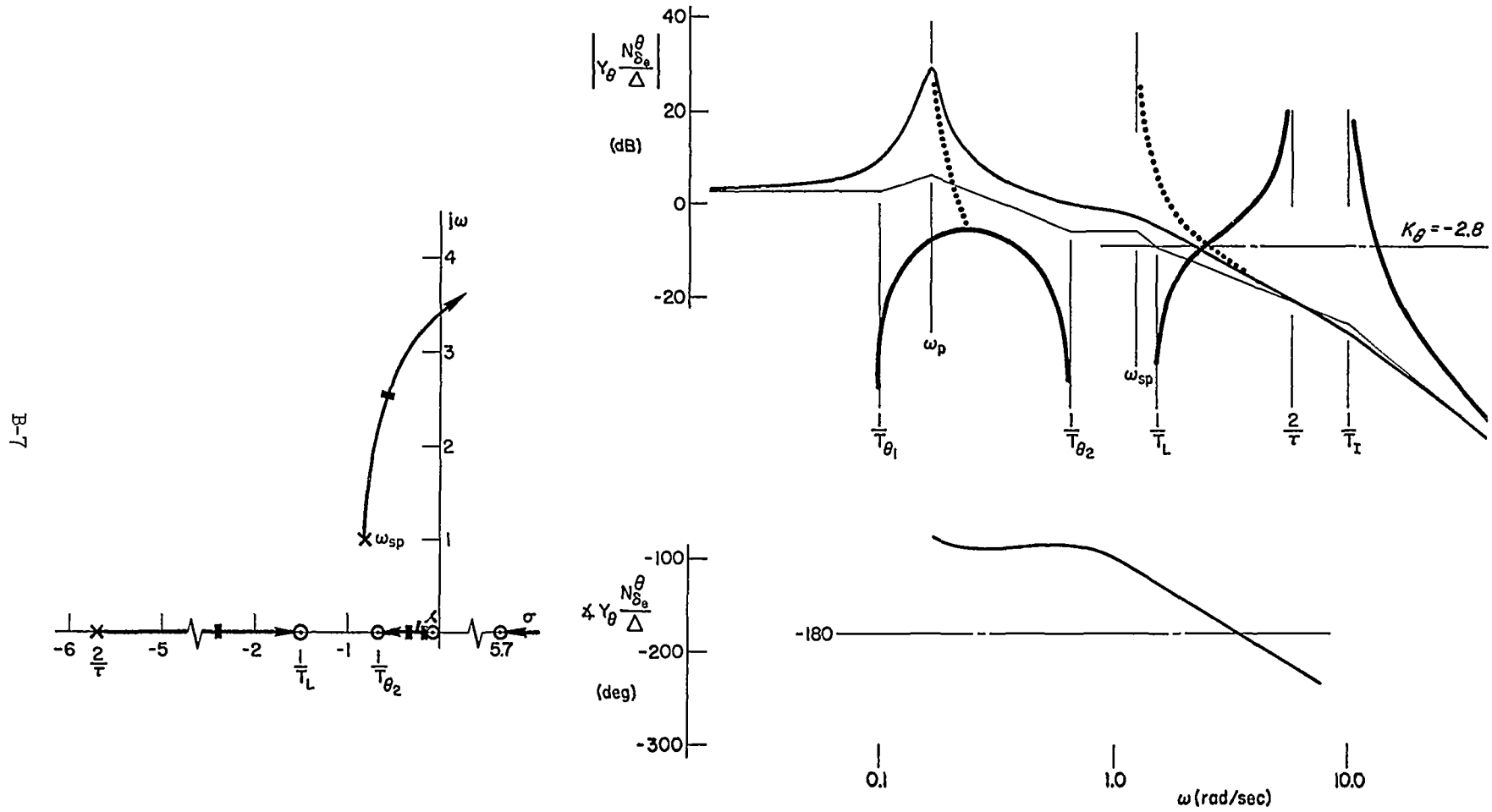

Figure B-2. Pitch Attitude System Survey for Analog Pilot

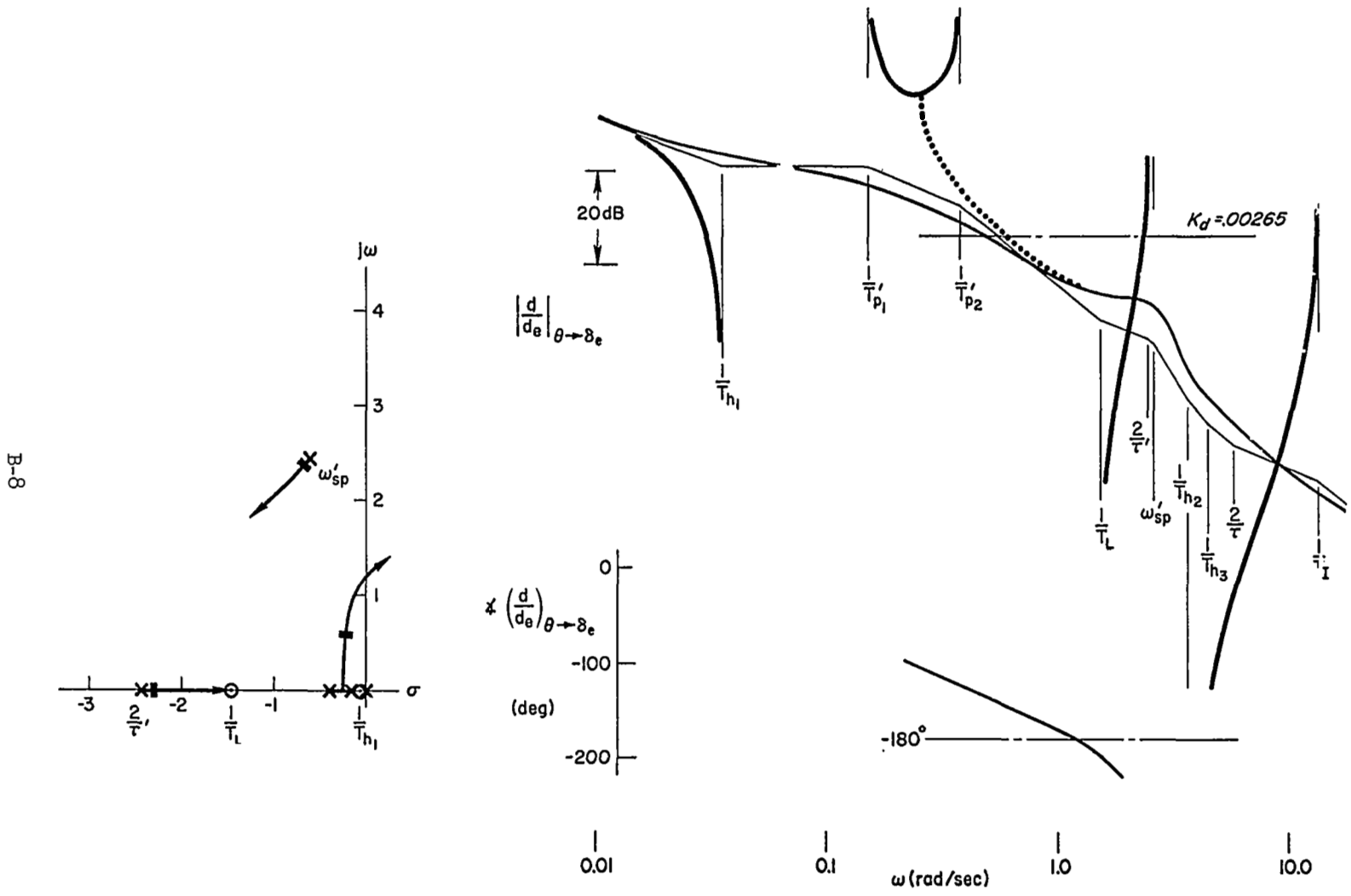

Figure B-3. Beam Deviation System Survey for Analog Pilot

margins (45 deg and 10 dB, respectively). The open-loop amplitude ratio is not much greater than K/s in the vicinity of 0.5 rad/sec and is insensitive to changes in pilot gain.

For the describing functions given in Eq. (B-12) and (B-13), the closed-loop characteristic equation of the multiloop pilot/vehicle system is:

$$\Delta'' = \frac{(s + .031)(s + 2.33)(s + 13.1)[s^2 + 2(.37)(.62)s + (.62)^2][s^2 + 2(.28)(2.48)s + (2.48)^2]}{s(s + 10)(s + 5.7)}$$

This is used in computing the "spectral ratios" for the analog pilot.

The analog pilot spectral ratios are shown in Figs. B-4 and B-5. These spectral ratios are for both feedback loops closed, of course, although the double prime (") notation has been deleted. The solid lines are the analytical result of the analog pilot loop closures described above. The amplitude ratio and phase angle points plotted are the "data" reduced from the recorded pilot/vehicle system response variables in the corresponding analog pilot simulation. They show the inherent fidelity of the data reduction process, and indicate the minimum overall levels of variability. The θ_e/θ_c spectral ratio plot in Fig. B-4 has the several closed loop poles and zeroes identified, and on this figure a single prime denotes the effect of closing the $d \rightarrow \delta_e$ loop alone.

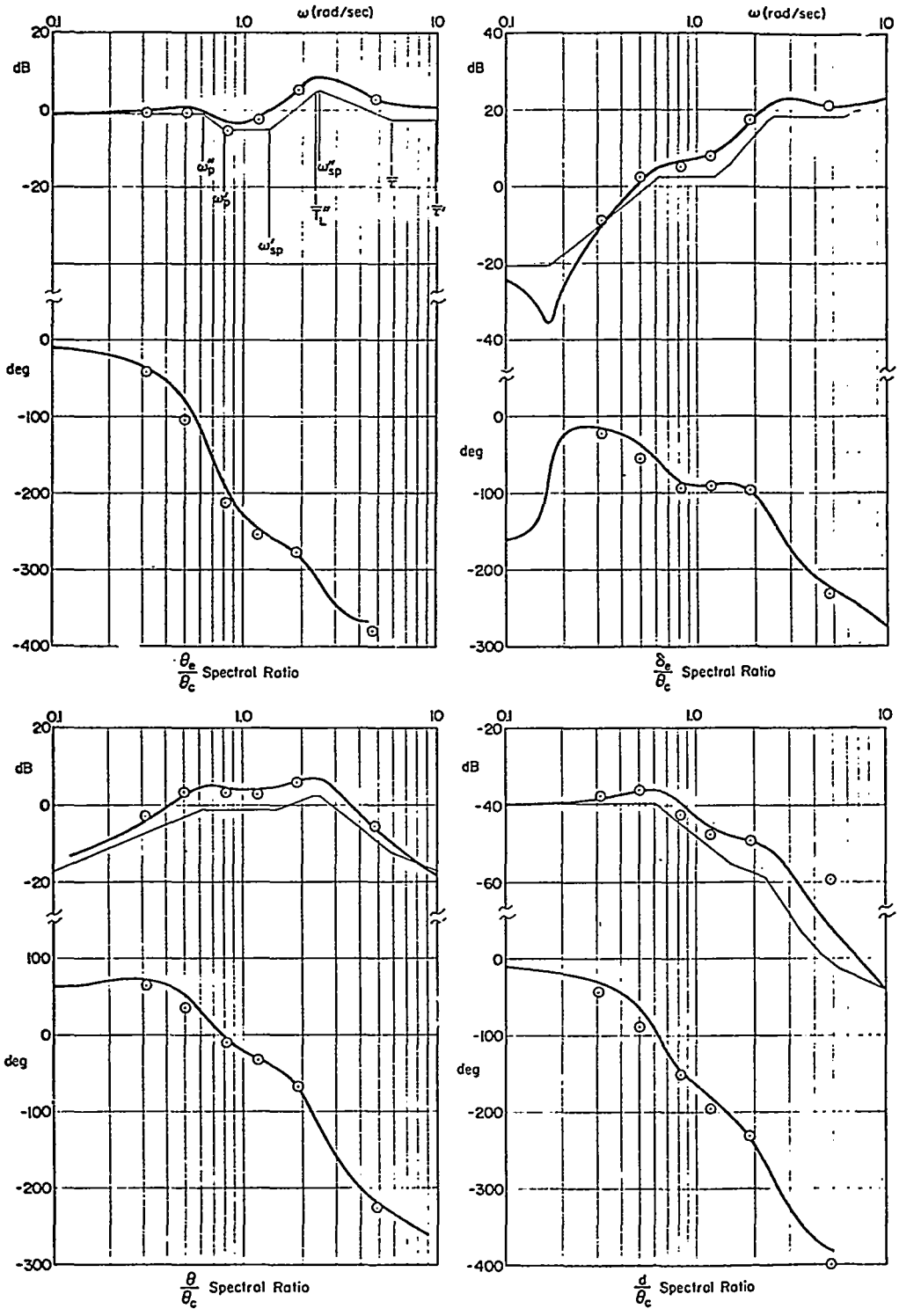

Figure B-4. Multiloop Spectra, Analog Pilot

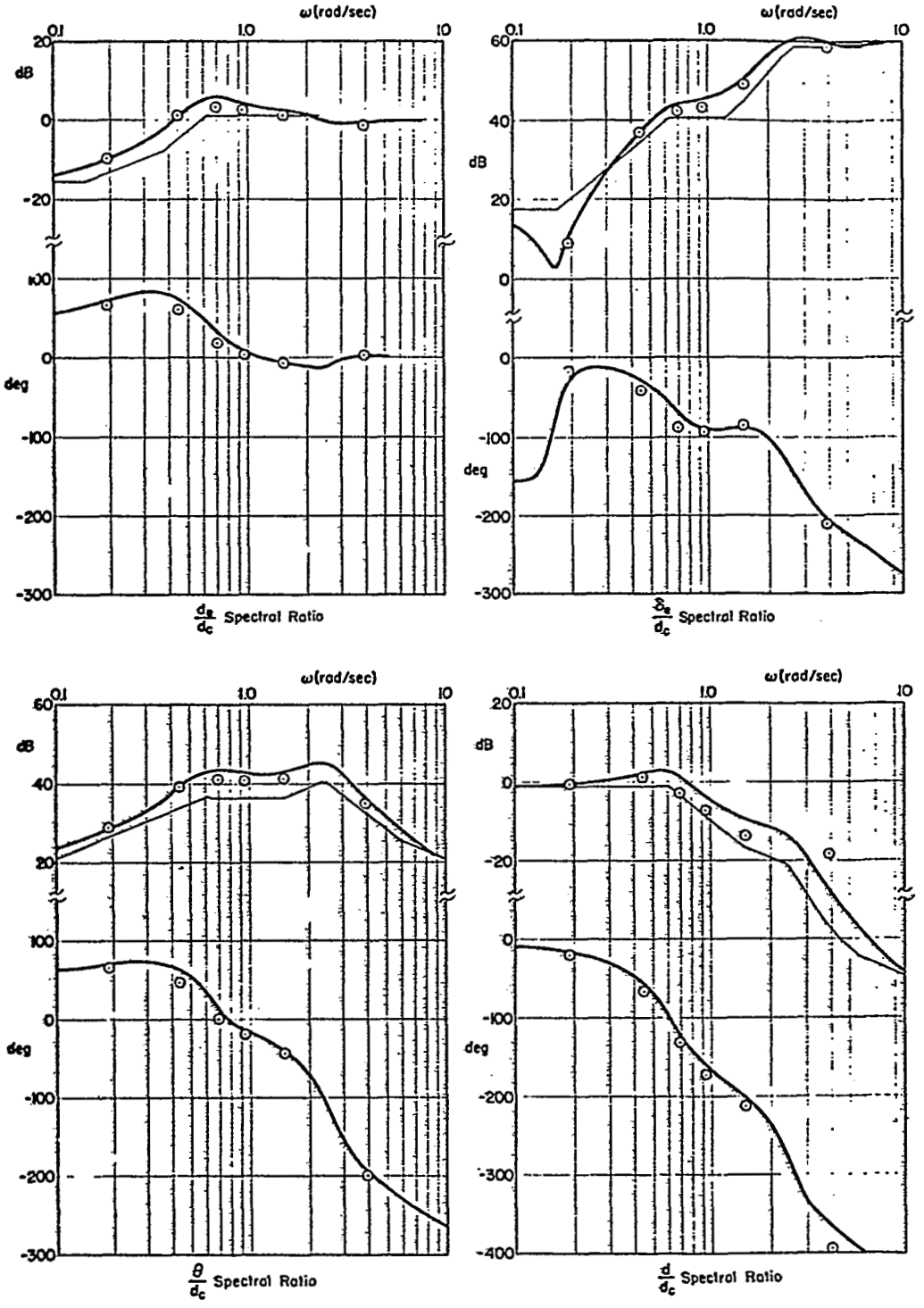

Figure B-5. Multiloop Spectra, Analog Pilot

APPENDIX C

BASIC MULTILOOP SPECTRAL RATIO DATA

The basic pilot and vehicle response time histories were Fourier analyzed at both sets of input frequencies to obtain the spectral ratios used in the describing function calculations. The general method and computation forms are summarized in Appendix B. The particular computation forms used are shown in Table C-1. The detailed data are shown in Figures C-1 through C-8.

The expressions shown in Table C-1 were chosen on the basis of best signal to noise properties and as being most appropriate to the response strategy employed by a given pilot. For example; the forms were selected such that the dominant denominator term was the spectral ratio with best signal to noise and least variability with respect to known model forms. This varies somewhat from the combinations noted as theoretically best in Appendix B, for the following reasons. The actual pilot data do not show the extreme variations in amplitude ratio seen for the analog pilot, hence there is less prewhitening advantage. For the Y_θ numerator, all the N_i are about the same at low and mid frequency and they only differ at high frequency where N_1 is the best estimate. Hence, it is convenient to use N_1 across the board. The same result occurs for Y_d; and Y_{d_1} is the best estimate at high frequency and equally good elsewhere. Furthermore, using N_1 and Y_{d_1} allows the δ_e/θ_c spectral ratio interpretation to simultaneously satisfy the inner and outer loop iteration. As a final remark, some of the spectral ratios should differ only by a known aircraft transfer function and the data in Figs. C-1 through C-8 generally reflect this with only minor variability.

Not all data points are plotted in Fig. C-1 to C-8. The data were screened at the outset, and the spectral ratio points at input frequencies were retained when their amplitude was at or above the adjacent remnant power. Only these good points are plotted. Analysis showed that the rejected points would have given misleading results, in general.

Two replications of the all-axis (C) runs were available for each pilot. These were lumped and averaged at the spectral ratio level for a given pilot; because the scanning data showed no differences, the response data showed no

TABLE C-1

DESCRIBING FUNCTION COMPUTATION FORMS

CONFIGURATION	Y_θ	Y_d	REMARKS
Pilot 1: Longitudinal only (B) All axis (C)	$\frac{N_1}{D_2} = \frac{\delta_e/\theta_c}{a_e/a_c \doteq \theta/\theta_c}$	$Y_{d_1} = \frac{\delta_e/a_c}{\delta_e/\theta_c}$	• Mainly a d-loop closer • Faired d spectra accurately, and smoothed θ spectra
Pilot 2: Longitudinal only (B) All axis (C)	$\frac{N_1}{D_1} = \frac{\delta_e/\theta_c}{\theta_e/\theta_d \doteq d/a_c}$	$Y_{d_1} = \frac{\delta_e/a_c}{\delta_e/\theta_c}$	• Mainly a θ-loop closer • d spectra are scattered • Faired θ spectra accurately, and smoothed d spectra • Used N_1/D_2 at 1.89 rad/sec

clear differential trends, and the total number of data points were not large for a single run.

As noted above, only certain spectral ratios were used in the describing function calculations of Table C-1. These are identified in the data plots by the addition of solid faired lines showing the actual values used at the various input frequencies. Some spectral ratios were interpolated at the other set of input frequencies (e.g., δ_e/θ_c at the d_c component frequencies) and this interpolation is indicated on the fairings by a short vertical line. Computation of the inner and outer loop describing functions was accomplished with the resulting spectral ratio fits using a Fortran computer program. This allowed the analyst to iterate between the fairings and the describing function fits, in order to obtain reasonable model forms.

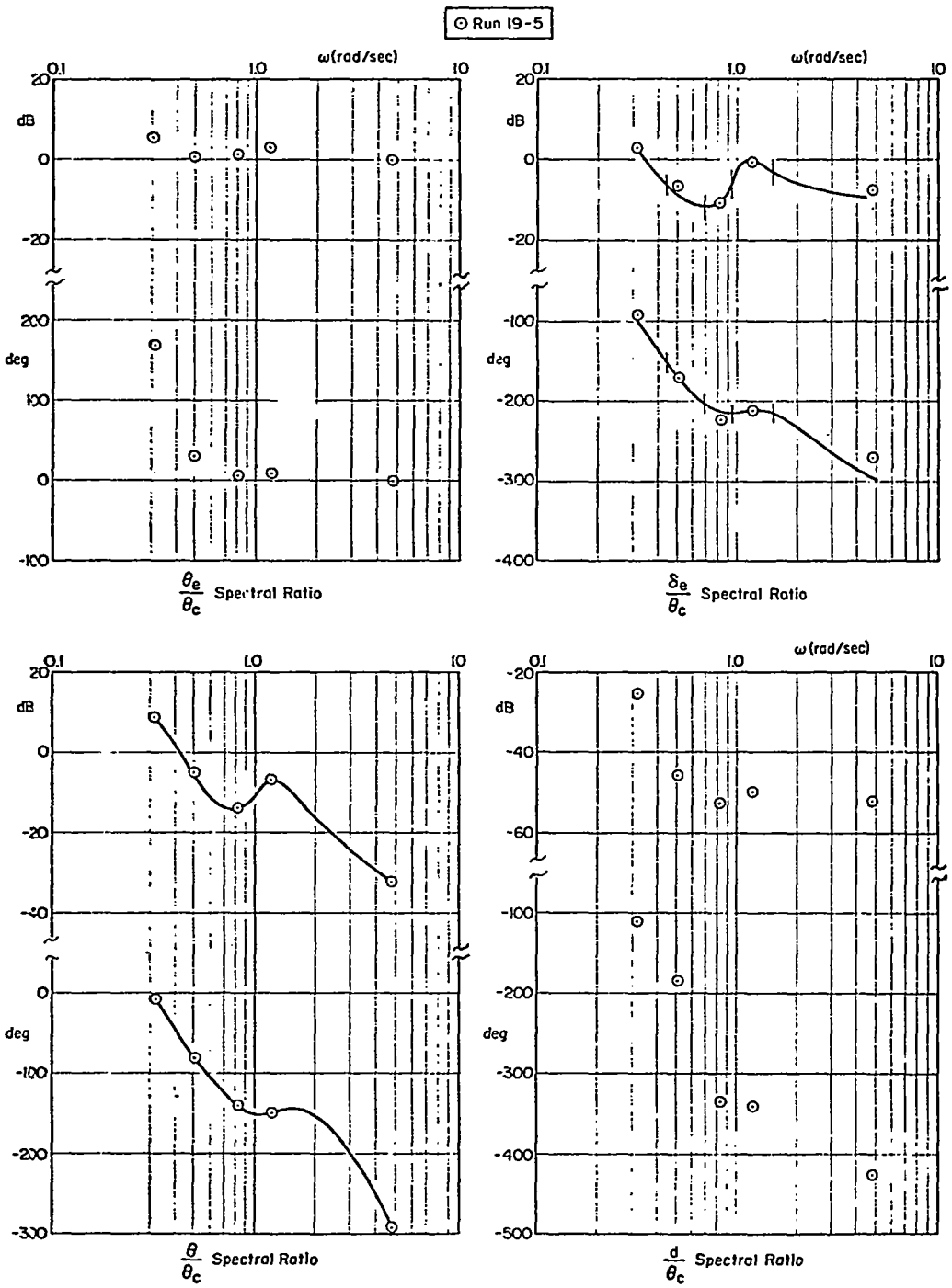

Figure C-1. Multiloop Spectra, Configuration B, Pilot 1

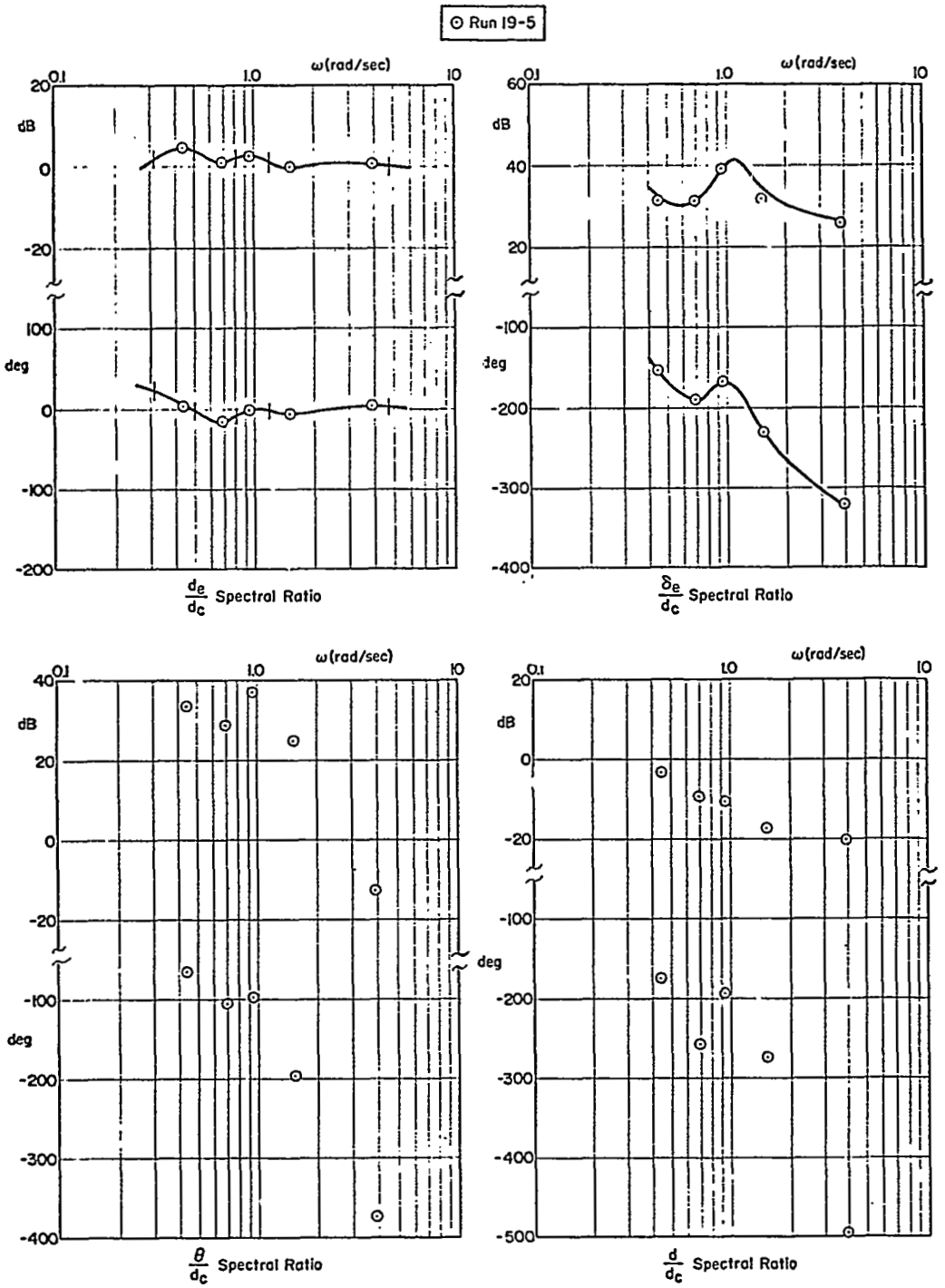

Figure C-2. Multiloop Spectra, Configuration B, Pilot 1

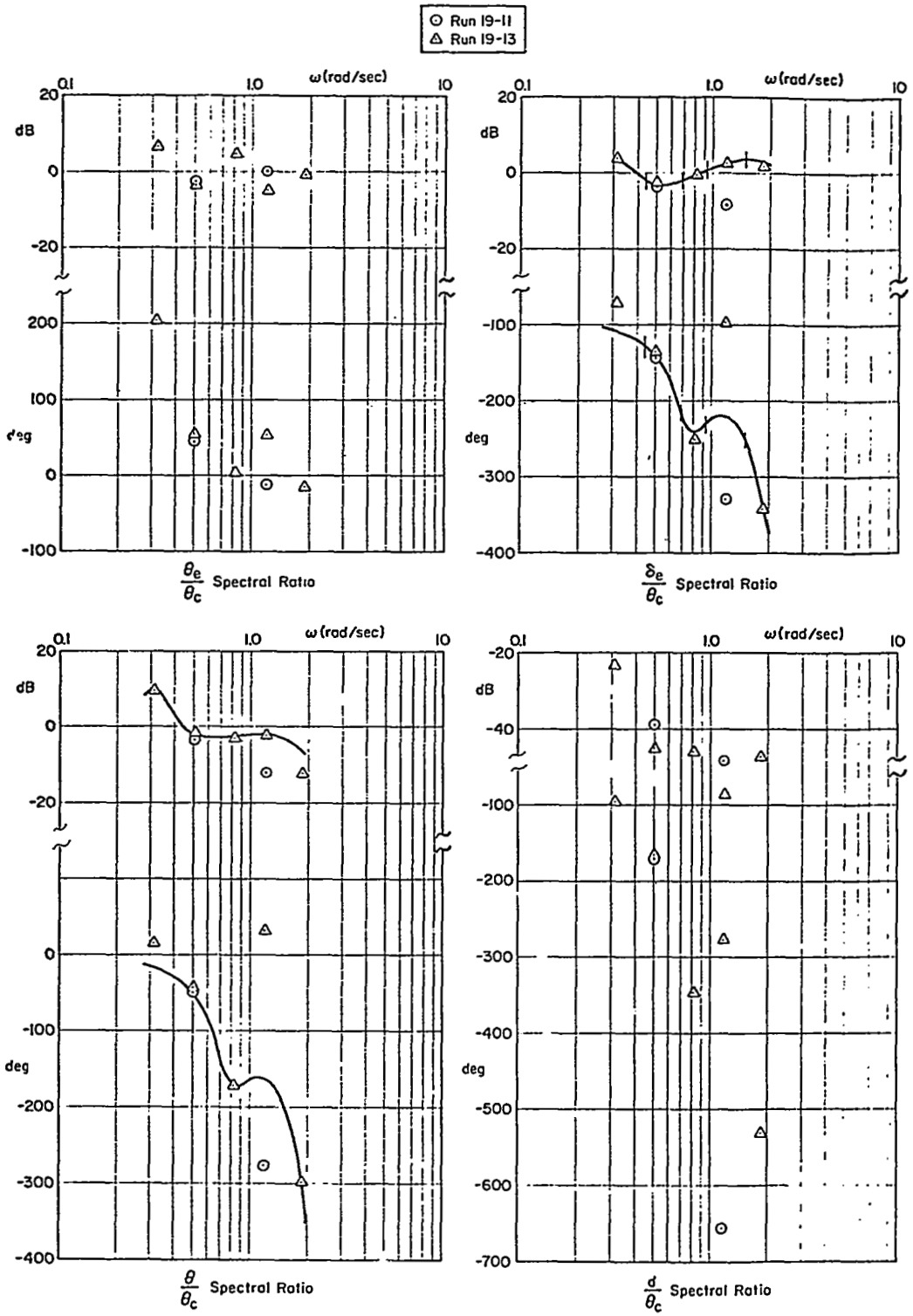

Figure C-3. Multiloop Spectra, Configuration C, Pilot 1

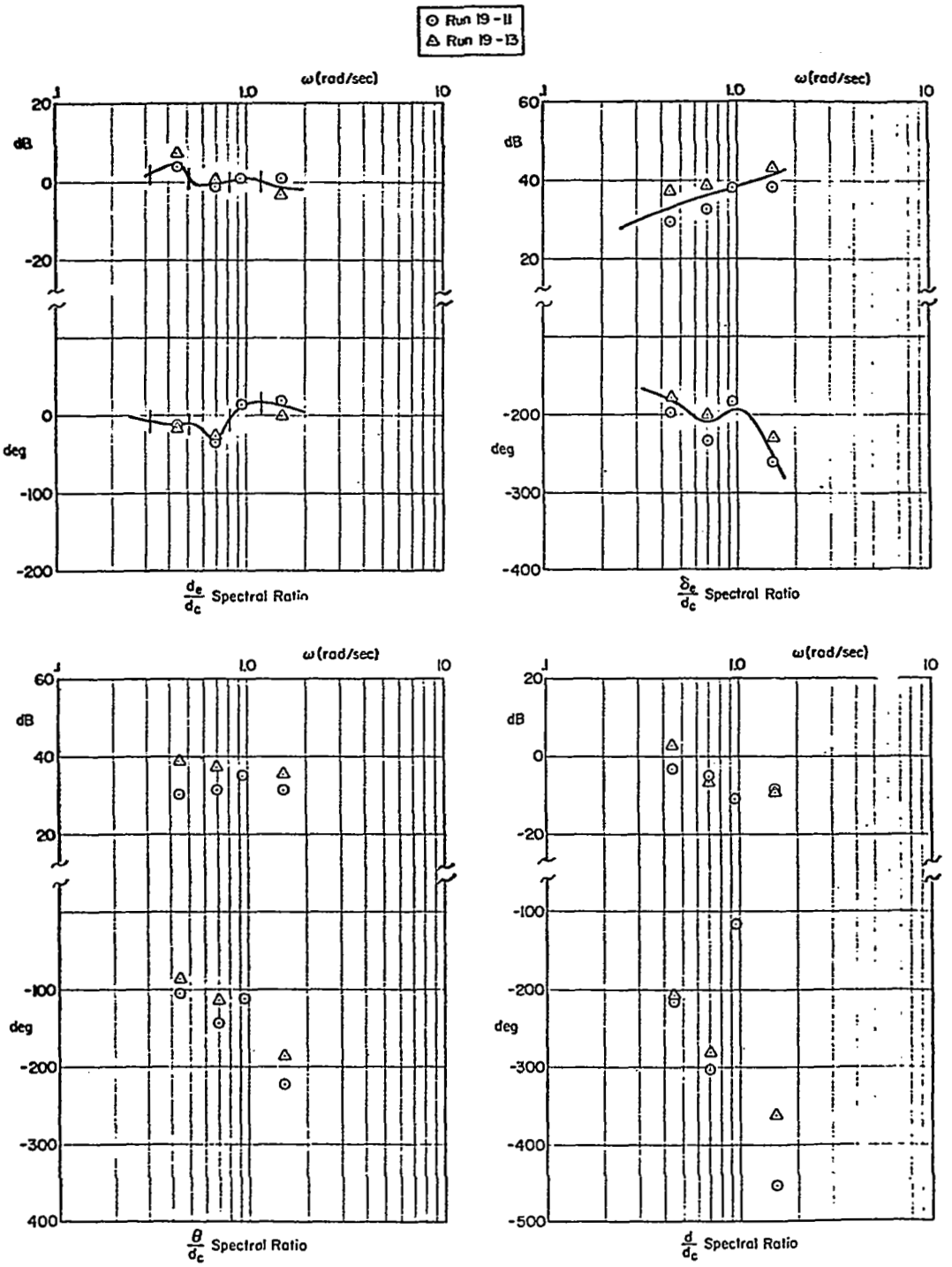

Figure C-4. Multiloop Spectra, Configuration C, Pilot 1

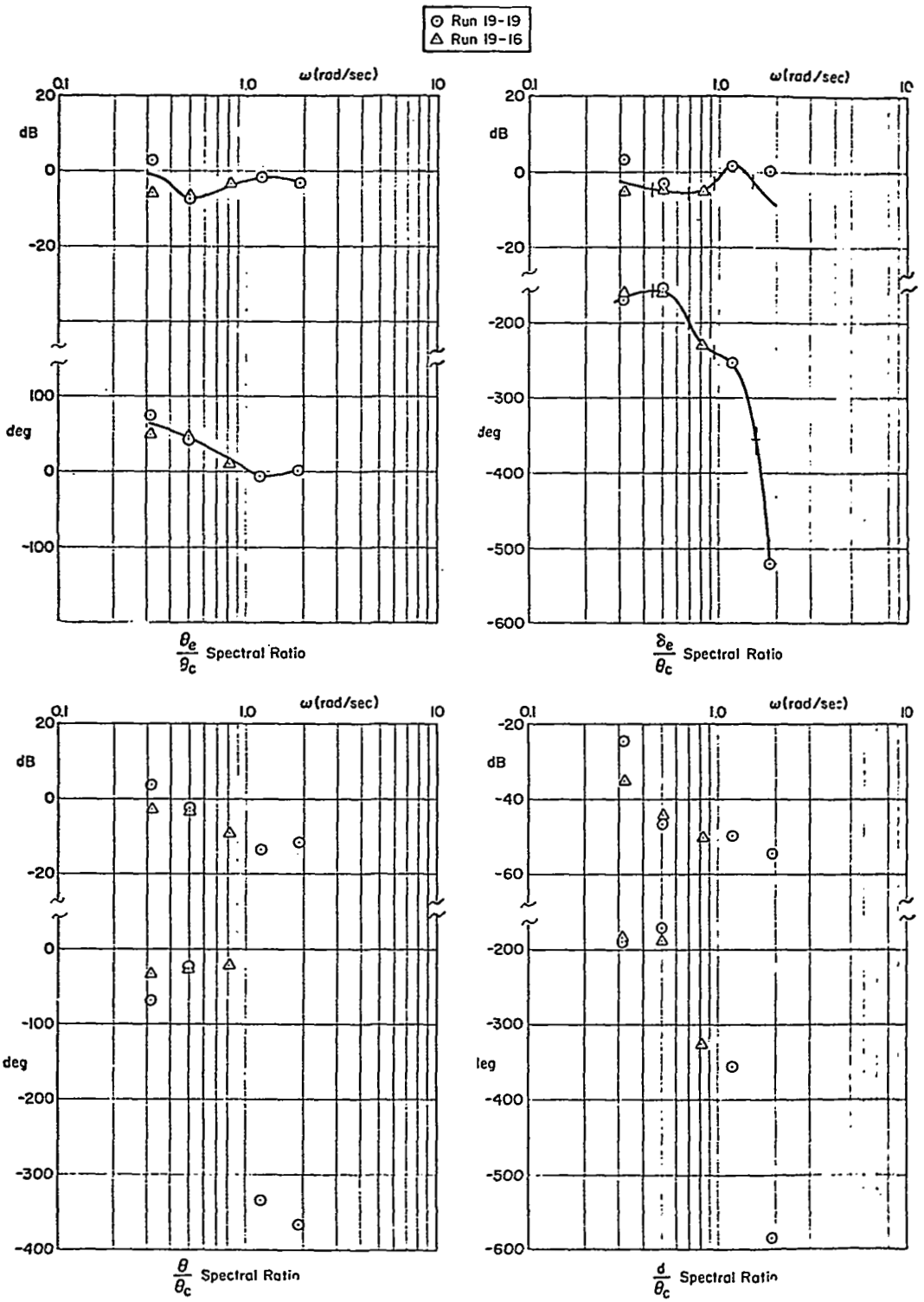

Figure C-5. Multiloop Spectra, Configuration B, Pilot 2

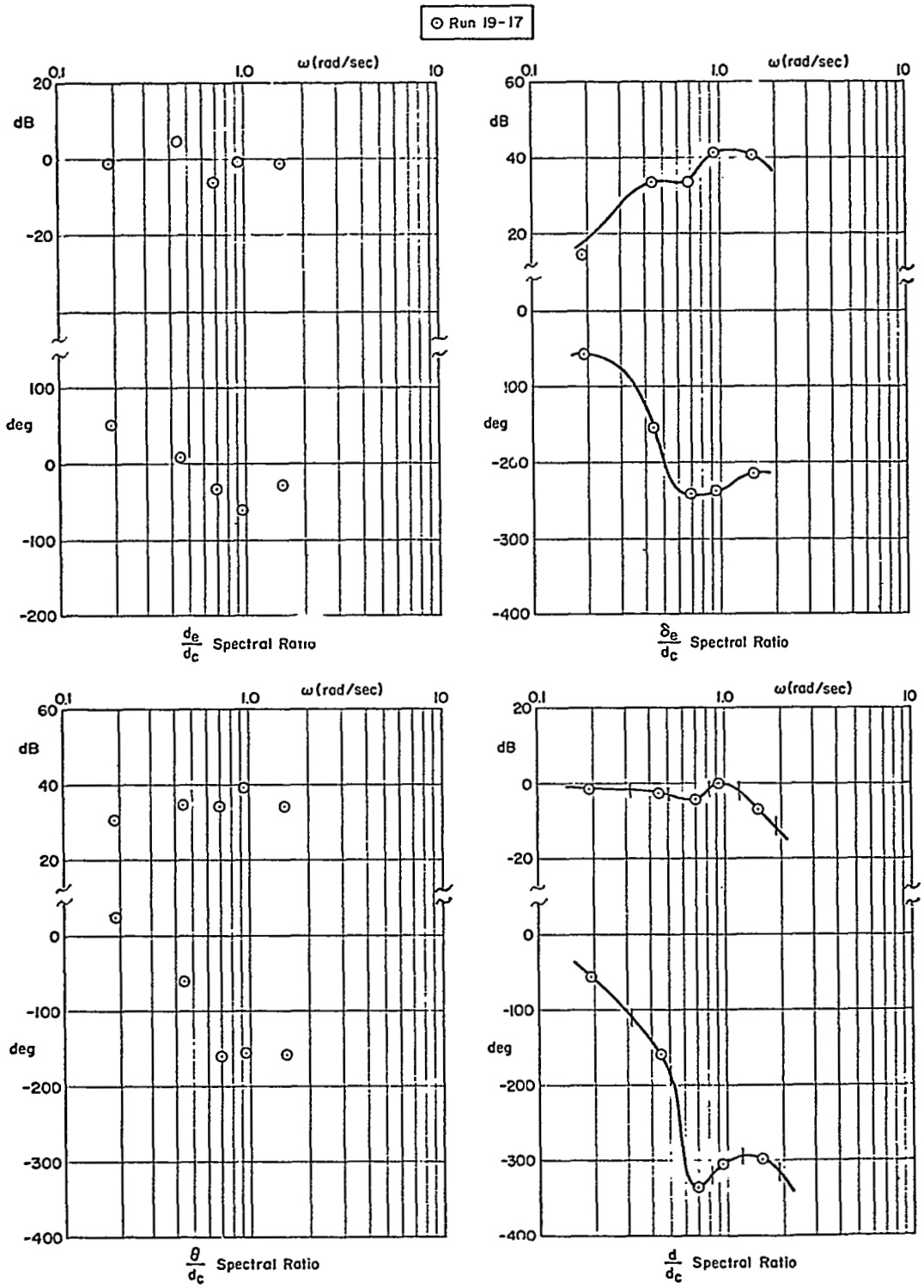

Figure C-6. Multiloop Spectra, Configuration B, Pilot 2

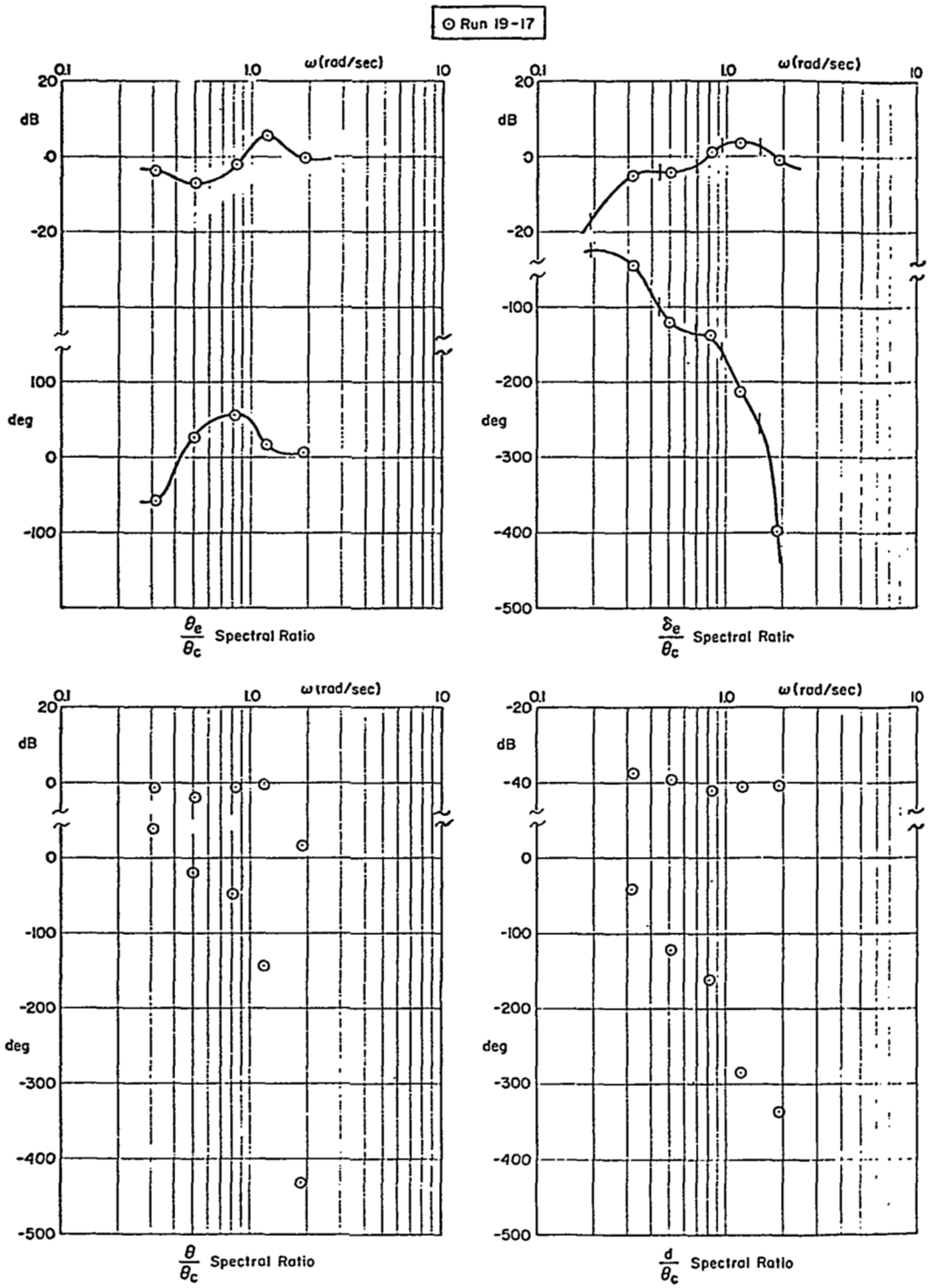

Figure C-7. Multiloop Spectra, Configuration C, Pilot 2

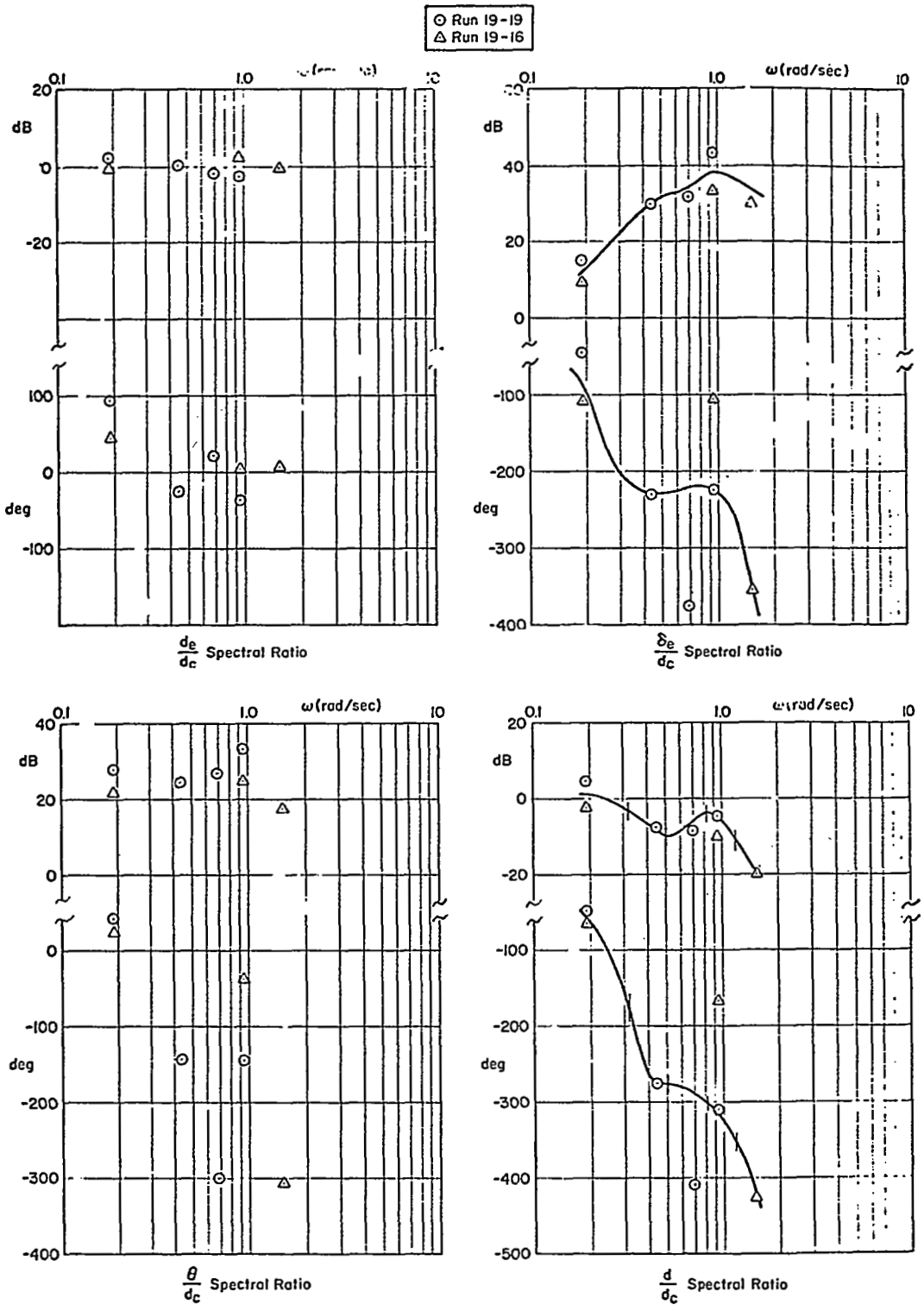

Figure C-8. Multiloop Spectra, Configuration C, Pilot 2